GREEN SYNTHESIS AND CHARACTERIZATION OF GOLD NANOPARTICLES USING GREEN ALGA *Ulva lactuca* AND EVALUATION OF THEIR CATALYTIC ROLE

UNIVERSITY *of the*
WESTERN CAPE

BY

OFHANI CHRISTOPHER MUKHORO

B.Sc. Biochemistry and Microbiology, B.Sc. Honours Microbiology

A thesis submitted in partial fulfilment of the requirement for the Degree of *Magister Scientiae* in Nanoscience in the Department of Biotechnology
University of the Western Cape, South Africa

Supervisor

Dr. Edith Antunes

Co-supervisors

Prof Denzil Beukes and Prof Mervin Meyer

February 2016

Declaration

I, Ofhani Christopher Mukhoro, hereby declare that this mini dissertation is my own work and effort and that it has not been submitted anywhere for any award. Where other sources of information have been used, they have been acknowledged and referenced.

Student Mukhoro O.C **Date** 23 February 2017

Supervisor **Date** 23 February 2017

Co-supervisor **Date** 23 February 2017

Co-supervisor **Date** 23 February 2017

Acknowledgements

A warm and grateful thank you to all those who contributed in their own invaluable way to the completion of this dissertation

In particular, I would like to thank:

- My wonderful and God-sent supervisor Dr Edith Antunes without whom this work would have been impossible. Your guidance, your patience and your invaluable words of wisdom are the very foundation of the success of this project!
- The collaborators of this project, in particular Prof Denzil Beukes my co-supervisor.
- Prof Wiets Roos at University of the Free State (for XPS analyses).
- Ms Natasha Peterson at University of the Western Cape (for TEM, EDX and SAED)
- Mr Mohamed Jaffer at University of Cape Town (for TEM of the biological samples).
- Ms Riana Roussouw at Stellenbosch University (for ICP-AES analyses).
- Dr Remy Bucher at iThembaLabs (for XRD analyses).
- Ms Valencia Jamalie for taking care of the bursary and also purchasing all the necessary reagents and materials required for the project.
- The financial support of this project from the National Nanoscience Postgraduate Teaching and Training Platform (NNPTTP), Department of Science and Technology (DST) and University of the Western Cape, without your financial contribution this project would have not been feasible and my finances would have been a constant source of worry!
- My family and friends, your encouragement and prayers helped me all the way through.
- All my friends and colleagues from the Marine Biodiversity Research Group (University of the Western Cape) for their continuous support, encouragement, words of advice and help.

Dedication

This work is dedicated to my caring mom Mrs Azwifaneli Salmina Mukhoro

Academic Output

The following section lists technology transfer activities (posters, conference) derived from the results obtained from this research work.

Conferences:

- Ofhani Christopher Mukhoro, Wiets D. Roos, John Bolton, Denzil R. Beukes and Edith M. Antunes, Gold nanoparticles stabilized on *Ulva lactuca* as an active catalyst for the reduction of 4-nitrophenol in aqueous media at room temperature, MSc Nanoscience Symposium 2016, Hotel Verde at the Cape Town airport; 03 October 2016. *Oral* presentation.

- Ofhani Christopher Mukhoro, Wiets D. Roos, John Bolton, Denzil R. Beukes and Edith M. Antunes, Green syntheses and characterization of gold nanoparticles using the green alga *Ulva lactuca* and evaluation of their catalytic role, 2016 All Africa Congress on Pharmacology and Pharmacy, Misty Hills Hotel and Conference Centre, Gauteng; 5 – 8 October 2016. *Poster* presentation.

Publication:

- Ofhani Christopher Mukhoro, Wiets D. Roos, John Bolton, Mervin Meyer, Denzil R. Beukes and Edith M. Antunes. Supported gold nanoparticles synthesised by living *Ulva lactuca* to catalyse the reduction of 4-nitrophenol. Manuscript submitted for review (2017).

Abstract

Nanoparticles synthesized using typical chemical procedures have associated environmental risks because of the use of hazardous chemicals. With the ever-increasing potential application for nanomaterials, there is a growing need to develop new synthetic procedures for nanomaterials which are non-toxic and eco-friendly.

This study presents, as a first step, the screening of the aqueous extracts of several seaweeds in order to assess their ability to produce gold nanoparticles (AuNPs). Eleven aqueous extracts were screened for the synthesis of AuNPs and where AuNPs were formed, these were further characterized using UV-vis spectroscopy and HRTEM primarily. Three of the eleven aqueous extracts shown to produce AuNPs were extracts obtained from brown algae. The total antioxidant and total reducing power contents, as well as the DPPH radical scavenging abilities for these extracts were determined and related to their ability to produce the NPs. The AuNPs were found to be of various shapes and sizes including spheres, rods and triangles, with sizes ranging from 20 nm to 200 nm.

The serendipitous discovery of a green synthetic method for AuNP synthesis using a live marine green seaweed *Ulva lactuca* followed this study. The formation of AuNPs was at first visually observed with a change in solution colour from yellow and to a deep pink colour, and confirmed by monitoring with UV-vis spectroscopy. UV-vis spectroscopy showed that the production of AuNPs commenced in solution after 30 min as observed by an increase in absorbance at the surface plasmon resonance (SPR) band of AuNPs at 550 nm, and a shoulder at 660 nm, up until 120 min, when a decrease in the maximum absorbance was observed at both wavelengths. The amount of gold remaining in the solution after addition of *Ulva* was quantified using ICP-AES, revealing that *Ulva* rapidly depletes the heavy metal from solution (> 50% in 10 min). HRTEM coupled to energy dispersive X-ray (EDX) spectroscopy and selected area electron diffraction (SAED) was used to determine average particle size, morphology, elemental composition and crystallinity of the AuNPs. The images revealed AuNPs which were mostly spherical, with the occasional triangular shape, with sizes ranging between 9 and 30 nm. Additionally, HRTEM was also used to determine the site of formation of the AuNPs on and in the *Ulva* leaf and cells. HRTEM, FESEM and XPS revealed that the AuNP formation takes place on the surface of the *Ulva* thallus, while the TEM images further revealed that the AuNPs were located in the chloroplasts and around the cell walls.

The oxidation state of the Au on the surface of the *Ulva* thallus was determined to be in its metallic state (i.e. Au(0)) using XPS, while diffraction patterns in the XRD spectra showed the AuNPs embedded in the *Ulva* to be in an fcc crystalline phase, with an average particle size of ~10 nm. The catalytic ability of the as-synthesized AuNPs supported on the *U. lactuca* seaweed were subsequently assessed using the reduction of 4-nitrophenol (4-NP), a common environmental pollutant, as a model reaction. The AuNPs supported on *Ulva* were successful in reducing the toxic 4-nitrophenol to the less toxic, industrially useful intermediate, 4-aminophenol (4-AP). The AuNPs supported on *Ulva lactuca* demonstrated excellent catalytic activity in the reduction of 4-NP by $NaBH_4$ especially at lower concentrations of 4-NP, as shown by the rapid decrease in the nitrophenolate absorption band at 400 nm and the appearance of new absorption band at 298 nm, revealing formation of the 4-aminophenol.

Keywords: Green nanotechnology, *Ulva lactuca*, gold nanoparticles, marine seaweeds, catalysis, 4-nitrophenol, reduction, nitrophenolate ion, sodium borohydride, 4-aminophenol.

Table of Contents

List of Figures

List of Tables

List of Abbreviations and Symbols

4-NP	4-nitrophenol
4-AP	4-aminophenol
AgNPs	Silver nanoparticles
AAE	Ascorbic acid equivalent
ATR–FTIR	Attenuated total reflection Fourier transform infrared spectroscopy
AuNPs	Gold nanoparticles
BE	Binding energy
BSE	Back scattered electrons
BHT	Butylated hydroxytoluene
CCD	Charge-coupled device
CNT	Carbon nanotube
CTAB	Cetyltrimethylammonium bromide
DLS	Dynamic light scattering
DPPH	2,2-diphenyl-1-picrylhydrazy
EDX	Energy dispersive X-ray spectroscopy
EGFR	Epidermal growth factor receptor
EMs	Electron microscopes
EPA	Environmental Protection Agency
eV	Electron volt
F-C	Folin-Ciocalteu reagent
fcc	Face centered cubic
FDA	Food and Drug Administration
FEG	Field-emission gun
FESEM	Field emission microscope
FTIR	Fourier transform infrared spectroscopy
GAE	Gallic acid equivalents
h	Hour
hrs	Hours
HER-2	Human epidermal growth factor receptor 2

HRTEM	High resolution transmission electron microscopy
HSA	Hemispherical analyser
ICP-AES	Inductively coupled plasma atomic emission spectroscopy
ICP-OES	Inductively coupled plasma optical emission spectrometry
IR	Infrared
IRE	Internal reflection element
K	Kelvin
KeV	Kilo electron volt
KeV/s	Kilo electron volt per second
M^+	Metal ion
mA	Milliamperes
Min	Minutes
mM	Millimolar
mm^2	Square millimetre
$mol.L^{-1}.min^{-1}$	Mole per litre per minute
MTX	Methotrexate
mV	Millivolts
$NaBH_4$	Sodium borohydride
NIR	Near infra-red
NIST	National Institute of Standards and Technology
nm	Nanometer
NMs	Nanomaterials
NPs	Nanoparticles
OHC	Oil holding capacity
PBS	Phosphate-buffered saline
PdNPs`	Palladium nanoparticles
PEG	Polyethylene glycol
ppm	Parts per millions
PtNPs	Platinum nanoparticles
QELS	Quasi-elastic light scattering
QDs	Quantum dots

rpm	Revolutions per minute
SAED	Selected area electron diffraction
SE	Secondary electrons
SEM	Scanning electron microscopy
SERS	Surface enhanced Raman spectroscopy
SPION	Superparamagnetic iron oxide NPs
SPR	Surface plasmon resonance
SWC	Swelling capacity
TCA	Trichloroacetic acid
TEM	Transmission electron microscopy
TGA	Thermal gravimetric analysis
TiO_2	Titanium dioxide
TOAB	Tetraoctylammonium bromide
TNF-α	Tumour necrosis factor-alpha
TPP	Triphenylphosphine
U. fasciata	*Ulva fasciata*
U. intestinalis	*U*lva *intestinalis*
U. lactuca	*Ulva lactuca*
U.S.	United States
UV-vis	Ultra Violet - Visible spectrophotometry
WHC	Water holding capacity
XPS	X-ray photoelectron spectroscopy
XRD	X-ray powder diffraction spectroscopy
ZnO	Zinc oxide
T	Absolute temperature
Θ	Bragg diffraction angle (Theta)
Δ	Delta
λ_{max}	Maximum wavelength
ζ	Zeta potential

Chapter 1 Introduction

Summary

The chapter gives some background to the study, including a brief discussion on the conventional methods used for metallic nanoparticle synthesis, issues encountered using conventional methods, applications of these nanoparticles, the importance of green synthetic methods in addition to a brief background on the green seaweed *Ulva lactuca.* The research problem and its importance, the study's aim and objectives, research questions as well as the outline of the thesis are also presented.

1.1. Background

In recent years, the discovery of nanometre-sized technologies has led to the development of a relatively new field known as nanotechnology, which focuses on the synthesis, fabrication and application of nanoparticles (NPs) in different fields (Goodsell, 2004; Shah *et al.,* 2015). It is the small size of these nanomaterials as well as their large surface-area-to-volume-ratio which gives them their remarkably different properties (e.g. biological, catalytic function, mechanical properties, melting point, optical absorption, thermal and electrical conductivity) as compared to the same material in bulk form (Perez *et al.,* 2005).

Due to the exceptional physicochemical, optical and electronic characteristics, NPs are of great interest for several applications including catalysis, as sensors, in electronic components, in medical diagnostic imaging, pharmaceutical products as well as in various medical treatment protocols. For instance, metallic NPs of coinage metals such as gold, silver, platinum and palladium, have been extensively utilised in an assortment of areas from the cosmetic to medical and pharmaceuticals fields (Shah *et al.,* 2015).

Gold nanoparticles (AuNPs) have been widely employed in numerous areas such as biomedical applications (Puvanakrishnan *et al.,* 2012), separation sciences (Sykora *et al.,* 2010), disease

diagnosis (Torres-Chavolla *et al.*, 2010), pharmaceuticals (Cai *et al.*, 2008; Bhumkar *et* al., 2007) and catalysis (Sharma *et al.*, 2007; Haruta *et al.*, 1987). Silver nanoparticles (AgNPs) in particular have been found to possess effective anti-bacterial and anti-inflammatory properties that can additionally promote rapid wound healing. Since AgNPs possess such advantageous properties, they have been incorporated into commercially available products such as wound dressings, pharmaceutical preparations and medical implant coatings (Li *et al.*, 2011b; Pollini *et al.*, 2011).

Platinum nanoparticles (PtNPs) have also been extensively utilised in biomedical applications, in either a pure form or in combination with other NPs (Hrapovic *et al.*, 2004), while palladium nanoparticles (PdNPs) have been shown to be effective in catalytic and electro-catalytic applications (Akhtar *et al.*, 2013), chemical sensors (Coccia *et al.*, 2012), optoelectronics (Chen *et al.*, 2007) and anti-bacterial applications (West *et al.*, 2010). Furthermore, non-noble metal NPs such as iron (Fe) (Njagi *et al.*, 2011), copper (Cu) (Lee *et al.*, 2011), zinc oxide (ZnO) (Brayner *et al.*, 2006) and selenium (Se) (Prasad *et al.*, 2012) have also been widely used in medical treatments, cosmetic formulations and in anti-bacterial treatments.

Consequently, in recent years, several chemical and physical procedures have therefore been developed for the synthesis of NPs with different sizes, shapes and compositions, because of the high demand for these nanomaterials (Shah *et al.*, 2015). NPs have conventionally been produced and stabilized through a variety of physical and chemical methods. Physical procedures include techniques such as laser ablation (Mafune *et al.*, 2001), lithography (Zhang and Wang, 2008) and high-energy irradiation (Treguer *et al.*, 1998), whereas chemical methods include chemical reduction, as well as electrochemical and photochemical reduction procedures (Chen *et al.*, 2001; Eustis *et al.*, 2005; Rodríguez-Sanchez *et al.*, 2002).

Traditional synthetic procedures involve the use of toxic chemicals and physical processes that are expensive due to the high-energy consumption demands and the frequent utilization of harmful materials which pose potential threats such as environmental toxicity, cytotoxicity and carcinogenicity (Ai *et al.*, 2011). Problems associated with toxicity arise due to the use of

hazardous materials as reducing agents and stabilizers for avoiding NP agglomeration. There are also reports that the NP toxicity can also be due to the NP's inherent properties such as composition, size, shape and surface chemistry (Shah *et al.,* 2015). Aggravating the situation further is also the fact that the reagents used in these procedures are present in excess, not in stoichiometric quantities, resulting in unnecessary wastage. Thus, the associated hazardous reagents used in synthesizing the NPs, has often prevented their use in clinical and biomedical applications, despite their remarkable properties and considerable potential (Kulkarni and Muddapur, 2014).

There is therefore a growing need to develop green synthetic methods for NP production which is clean, reliable, biologically compatible, benign and environmentally friendly (Kulkarni and Muddapur, 2014; Jain *et al.*, 2011; Ai *et al.,* 2011). In recent years, the use of biological materials has emerged as an ideal substitute for traditional synthetic techniques. Biosynthetic methods employ eco-friendly green chemistry based procedures that utilize unicellular and multicellular biological materials or natural substances such as bacteria (Hulkoti and Taranath, 2014), fungi (Visha *et al.,* 2015), yeast (Moghaddam *et al.,* 2015), viruses (Dujardin *et al.,* 2003), whole plants (Makarov *et al.,* 2014), plant tissues (Kuppusamy *et al.,* 2014), fruits (Jain *et al.,* 2009), plant extracts (Jain *et al.*, 2013, Kuppusamy *et al.*, 2015), marine algae (Asmathunisha and Kathiresan, 2013; Singaravelu *et al.,* 2007) and micro–fluids (Zhang *et al.,* 2015) for the reduction and stabilization of NPs.

NPs synthesized using biological methods possess numerous advantages over chemical methods. They produce NPs which are biocompatible, have broad size distributions, the processes are readily scalable, the organisms are easily available (thus resources are renewable), the materials are safe to handle and the overall production process is less expensive in terms of materials used and energy efficiency (Allafchian *et al.*, 2016). Aquaculture of marine seaweeds, for example, provide a highly renewable resource and their incorporation into the synthesis of nanomaterials reveals single-step production processes in which NPs are produced quickly and efficiently (Hinrichsen, 2007; Singaravelu *et al.,* 2007).

Seaweeds incorporate several metabolites that may aid the reduction of the metal salt (Vijayan *et al.,* 2014) and they are low maintenance which eliminates the need for elaborate cell culture maintenance processes such as those needed in maintaining microorganisms. Several algal extracts have been successfully used in the synthesis of AuNPs for example, including the brown marine algae (*Sargassum wightii* and *Sargassum incisifolium*) which were used to produce AuNPs with a size range of 8–12 nm (Singaravelu *et al.,* 2007; Mmola *et al.* 2016), *Turbinaria conoides* (Vijayan *et al.,* 2014; Rajeshkumar *et al.,* 2013) and *Fucus vesiculosus* (Mata *et al.,* 2009). Green (Sangeetha and Saravanan, 2014) and red seaweeds (Priyadharshini, 2014) have also been used, but to a much lesser extent.

Few terrestrial plants that are capable of uptaking heavy metals such as *Sesbania drummondii*) and *Arabidopsis* (Parker *et al.,* 2014) have been successfully employed in the synthesis of AuNPs (Sharma *et al.,* 2007 and PdNPs (Parker *et al.,* 2014) respectively using the whole organisms. There reports on *Ulva*'s ability to accumulate heavy metals such as mercury (Costa *et al.,* 2011; Kumar *et al.,* 2009) and cadmium (Muse *et al.,* 2005). Therefore, it was cosidered necessary to investigate the live *Ulva's* ability to produce AuNPs. The use of a live marine green seaweed, *Ulva lactuca*, remains unexplored in the synthesis of AuNPs, which is not surprising given that it is mostly the brown algae that have been successfully employed in the synthesis of NPs. Although *U. lactuca* has been used in the synthesis of AgNPs, only crude aqueous extracts of the seaweed were used (Sangeetha and Saravanan, 2014).

U. lactuca, commonly found throughout the Pacific and Indian Oceans, is known for its robustness and high growth rate which allows them to be cultivated on a large scale for commercial purposes (Troell *et al.,* 2006). This makes this seaweed, a highly desirable and reliable, renewable resource. In addition, the *U. lactuca* macrostructure, with its large, very simple two cell layer structure, would facilitate an easy study of the fate of the NPs once it has been accumulated or produced within the seaweed.

Seaweeds have previously been assessed for their potential in the bioaccumulation of heavy metals (Giusti, 2001) and their ability to produce NPs (including Au, Ag NPs, *etc*.). However, to the best of our knowledge, no studies have been conducted on the fate of the AuNPs produced once it has been accumulated by the seaweed or the potential application of these NPs as catalysts for example

in the reduction of 4-nitrophenol (4-NP). 4-NP is a common environmental pollutant frequently present in wastewater through the degradation of pesticides such as parathion and nitrofen (Marais *et al.*, 2006), industrial plants used in paper manufacturing processes, in pharmaceutical companies and dye industries (Li *et al.*, 2007; Gupta *et al.*, 2014). The catalytic reduction of 4-NP by $NaBH_4$ to form 4 aminophenol (4-AP) is often used as a model reaction to assess the ability of a potential catalyst. 4-AP, on the other hand, is a crucial intermediate compound used in pharmaceutical industries as it is largely used in the synthesis of painkillers and antipyretic drugs (Panigrahi *et al.*, 2007).

1.2. Problem statement

Metallic NPs are traditionally synthesized *via* chemical and physical procedures which are costly, have high energy consumption demands and involve the use of toxic materials which engender potential threats to the environment and human health (Ai *et al.*, 2011). As a result, these conventionally synthesized NPs find limited use in clinical and biomedical applications (Kulkarni and Muddapur, 2014). There is therefore a growing need to develop new and innovative processes for NPs synthesis which would resolve most, if not all, of the drawbacks associated with conventional synthetic methods. In recent years, the use of biological materials has emerged as an interesting alternative and this concept is regarded as green nanotechnology (Kulkarni and Muddapur, 2014; Jain *et al.*, 2011; Ai *et al.*, 2011).

Green nanotechnology is relatively new and aims at achieving certain goals in applying the principles of green chemistry to create eco-friendly technologies which tackle real life problems (Matus *et al.*, 2011). One of the major policy mandates, strategies and objectives of the Centre for Green Nanotechnology launched in South Africa, is the synthesis and development of green, biocompatible NPs for medical diagnostic/therapeutic agents, biological sensors, chemical sensors, smart electronic materials, nanoscale robots and environmentally benign breathing devices (Nanowerk, 2014).

Green synthetic methods for NP production, necessitates the development of processes that are relatively simple, cost-effective and harmless to the environment and human beings as compared to the conventional chemical and physical synthetic methods. Several biomaterials have been developed to synthesize metallic NPs and these procedures hold numerous advantages over conventional chemical methods. As stated before, green synthesized NPs are biocompatible, the processes employed are readily scalable, the organisms utilized are easily available (as the resources are renewable), the materials used and produced are safe to handle and the overall production process is less expensive in terms of materials used and energy efficiency (since the NPs are produced at room temperature and pressure conditions) (Allafchian *et al.*, 2016).

Marine seaweeds are abundant, easily available in nature and are easy to cultivate, which makes them good candidates and valuable resources in producing NPs (Singaravelu *et al.*, 2007). Several metabolites found in the seaweeds such as proteins, polyphenols and polysaccharides assist in the reduction of the metal salt (Vijayan *et al.*, 2014). In addition, as mentioned previously, they are low maintenance organisms which eliminates the necessary, complicated cell culture maintenance set ups such as those employed in microorganism cultures. Thus, our focus could be shifted to the use of seaweeds as clean, sustainable reducing agents for the synthesis of metallic NPs. Our aim is therefore to produce NPs using materials which are completely 'green' and clean, meeting the Principles of Green Chemistry (listed in Figure 1.1) for the production of NPs intended for further applications.

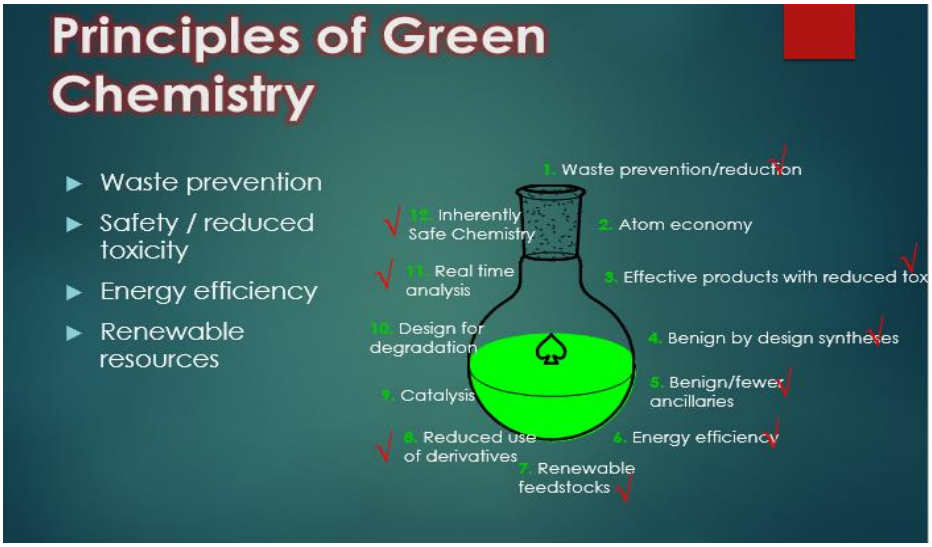

Figure 1.1: Twelve principles of green chemistry reproduced from Cioc et al., (2014).

1.3 Rationale and motivation

The research interests for this study have been encouraged by a need to be innovative in designing green synthetic methods for AuNPs through the use of a) various aqueous algal extracts as well as b) live green *Ulva lactuca* seaweeds. Several seaweeds extracts such as *Chlorophyta*, *Rhodophyta* and *Phaeophyta* (Ponnuchamy and Jacob, 2016) are reported to have been used in the synthesis of metal NPs such as AuNPs (Singaravelu *et al.*, 2007), AgNPs (Govindaraju *et al.*, 2009), superparamagnetic iron oxide NPs (SPIONS) (Mahdavi *et al.*, 2013), palladium nanoparticles (PdNPs) (Prasad and Padmesh, 2014) and platinum nanoparticles (PtNPs) (Shiny *et al.*, 2014). The resultant morphology and the stability of the NPs synthesized using seaweeds have been harnessed in a variety of applications such as biomedicine (Mahdavi *et al.*, 2013) and environmental applications. Thus, this study initially focuses on examining eleven different aqueous algae extracts from red, brown and green seaweeds in their ability to produce AuNPs at room temperature.

The AuNPs produced by the aqueous extracts or live organisms could then find application as a catalyst in the reduction of a common environmental pollutant, for example 4-NP, often present in

industrial wastewater, to produce 4-AP which is a crucial intermediate in the pharmaceutical industry. Seaweeds are rich in secondary metabolites such as polysaccharides, phenolic compounds (such as phlorotannins/polyphenols), proteins/enzymes and other chelating agents which may be responsible for the reduction of metal ions to form NPs. AuNPs thus produced will likely be capped by the polysaccharides present in the aqueous extracts or cell walls of the live seaweeds. These polysaccharides are loosely bound on the NP surface, an important requirement for potential catalysts, since the catalyst surface is intimately involved in the reaction.

Several analgesic and antipyretic drugs such as paracetamol, phenacetin *etc.* are manufactured using 4-aminophenol (4-AP) as a strong intermediate compound. 4-AP has found further purpose in applications such as in photographic development, corrosion inhibition, anticorrosion-lubrication and hair-dye (Rode *et al.,* 1999; Corbett, 1999). Since 4-AP is an important intermediate compound, there is always a greater need to develop newer and cheaper methods for the catalytic reduction of 4-NP (Saha *et al.,* 2009). Traditional procedures employed in the reduction of 4-NP, have typically involved the use of iron/ acid as a reducing agent (Crossley, 1922), but the usage of metallic reagents comes with certain limitations, since metal oxides are released in high quantities as sludge from these reactions - a serious drawback.

It is therefore also necessary to develop new and environmental friendly procedures for the reduction of 4-NP, and the reduction of 4-NP has been studied in the presence of several metallic catalysts such as Pd (Kantam *et al.,* 2008), nickel (Ni) (Rizhi, 2007), Pt (Vaidya *et al.,* 2003) and titanium dioxide (TiO_2)-supported Ni (Chen *et al.,* 2006). The reduction of 4-NP by sodium borohydride ($NaBH_4$) in the presence of an appropriate catalyst has also been researched previously (Saha *et al.,* 2009). The mechanism of 4-NP reduction involves the use of $NaBH_4$ as a hydrogen donor to the NO_2 group of 4-NP to produce 4-AP with NH_2. Coinage metals, as nanomaterials, have also been employed as catalysts including: nanoscale Ni (Chen *et al.,* 2006), Au and Ag (Haruta *et al.,* 1987; Esumi *et al.,* 2004; Panigrahi *et al.,* 2007; Pradhan *et al.,* 2007; Praharaj *et al.,* 2004), bimetallic Pt-Ni (Ghosh *et al.,* 2004) and resin bound Ag (Jana *et al.,* 2006).

Despite the success of application and acceptance of AuNPs as catalysts in the reduction of 4-NP (Figure 1.2), the aggregation and dissolution of naked AuNPs, leads to a loss of catalytic activity, and this remains a big challenge. As a result, several authors anchored AuNPs onto solid support systems such as polymers (Percebom *et al.*, 2016; Quan *et al.*, 2016; Zyuzin *et al.*, 2016), metal oxides (Korotcenkov *et al.*, 2016; *Zhao et al.*, 2015), silica (Laveille *et al.*, 2016), carbon materials (Lozano-Martı´n *et al.*, 2015; Simenyuk *et al.*, 2015) and biomaterials (Wei and Lu 2012) to enhance their stability as catalysts.

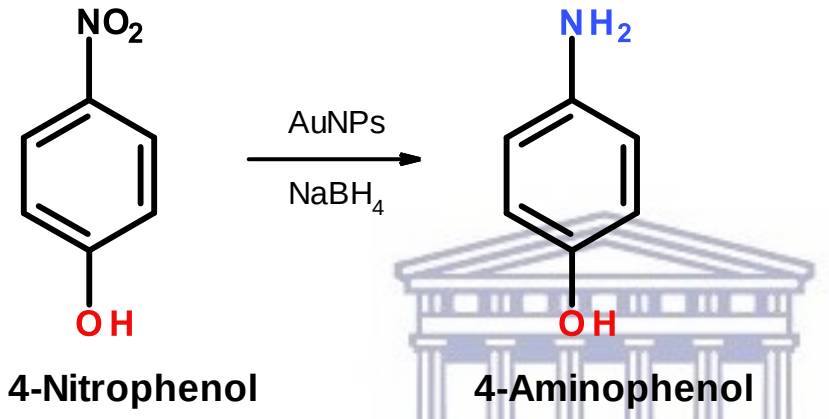

Figure 1.2: The reduction of 4-NP by NaBH4 to produce 4-AP using AuNPs as a catalyst.

There are limited reports on the use of biomaterials as a solid support, but Sharma *et al.* (2007) reported on the use of *Sesbania drumondi*, a perennial shrub commonly known as poison bean, as a solid support. *U. lactuca* is known to be capable of heavy metal uptake (Troell *et al.*, 2006), however, this seaweed has not been investigated for their ability to synthesize NPs. Therefore, this work examines the design and synthesis of AuNPs embedded on *U. lactuca* which will be assessed for their catalytic activity and stability. Herein, we report on the synthesis and catalytic function of AuNPs embedded on *U. lactuca* in the reduction of 4-nitrophenol in the presence of $NaBH_4$.

1.4 Aims and objectives

1.4.1 Main aims

The study was comprised of two main aims and they are as follows:

1. The first aim was to screen the aqueous extracts of a variety of green, brown and red seaweeds to assess their ability to synthesise AuNPs.
2. Following the information obtained from 1 above, the second aim of this project was to design and develop a green synthetic procedure for the synthesis and characterization of AuNPs using live *Ulva lactuca* marine organisms. The synthesized AuNPs were then investigated for their catalytic ability in reducing 4-nitrophenol.

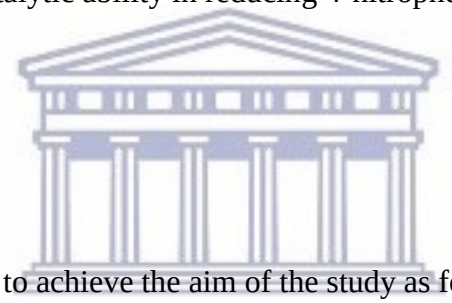

1.4.2 Specific objectives

Several objectives were set-out to achieve the aim of the study as follows:

1. Collection of seaweeds.
2. Aqueous extraction of eleven different seaweeds to produce the crude aqueous extracts used.
3. Synthesis of AuNPs using the crude aqueous extracts in screening the different seaweeds for their ability to produce AuNPs.
4. Biosynthesis and characterization of AuNPs using live *U. lactuca* organisms instead of the simple aqueous extracts.
5. Investigate the catalytic activity of the AuNPs bound to *U. lactuca* in the reduction of 4-NP by $NaBH_4$.

1.5 Research questions

- Can algal aqueous extracts be used as reducing agents in the synthesis of AuNPs?
- Can live *U. lactuca* organisms be used to biosynthesize simple, eco-friendly AuNPs?
- Can the *U. lactuca* bound AuNPs effectively catalyse the reduction of 4-nitrophenol (4-NP) by $NaBH_4$ to form 4-aminophenol (4-AP)?

1.6 Outline of the thesis

Chapter 1: The chapter gives some background to the study, including a brief discussion on the conventional methods used for metallic nanoparticle synthesis, issues encountered using conventional methods, applications of these nanoparticles, the importance of green synthetic methods in addition to a brief background on the green seaweed *Ulva lactuca.* The research problem and its importance, the study's aim and objectives, research questions as well as the outline of the thesis are also presented.

Chapter 2: This chapter presents the general literature on the principles of green chemistry, the biosynthesis of nanoparticles using marine organisms, the methods used in the synthesis of different nanoparticles, some background on *Ulva lactuca,* techniques used in the characterization of nanoparticles and applications of gold nanoparticles.

Chapter 3: This chapter discusses the results obtained in screening the aqueous extracts of different seaweeds for their ability to produce AuNPs.

Chapter 4: The chapter reports the synthesis of AuNPs using the live marine seaweed *U. lactuca* and the characterization of the resultant NPs produced using a multitude of techniques such as UV-vis spectroscopy, HRTEM, ICP-AES, XPS, XRD, SEM, TGA and FTIR spectroscopy.

Chapter 5: This chapter presents some background to the catalytic ability of the gold nanoparticles synthesized using *U. lactuca* in the reduction of 4-nitrophenol (4-NP) to 4-aminophenol (4-AP) as a model reaction for catalysis, followed by the assessment of these gold nanoparticles (AuNPs) bound to *Ulva lactuca* seaweed (as a solid support) synthesised in this study.

Chapter 6: This chapter presents overall conclusion of the study as well as the future recommendations that can be done after this work.

Chapter 2 Literature review

Summary

This chapter presents the general literature on the principles of green chemistry, the conventional methods used in the synthesis of different nanoparticles including the biosynthesis of nanoparticles using plants and marine organisms, the techniques used in the characterization of nanoparticles, applications of gold nanoparticles, and finally some background on *Ulva lactuca*.

2.1. The Principles of Green Chemistry

Growing concern for the environment has led to the emergence of Green Chemistry as an important aspect for all chemistry fields. Green Chemistry is the design of chemical products and processes that reduce or eliminate the use and generation of hazardous substances. Green Chemistry is based on twelve principles as explained below (Anastas and Warner, 1998) and this is further described in Figure 2.1.

The principles include:

1. Prevention

Waste prevention is better than treating or cleaning up after waste has been created.

2. Atom Economy

Synthetic methods should be designed to maximize the incorporation of all the materials used in the process into the final product.

3. Less Hazardous Chemical Syntheses

Wherever feasible, synthetic methods should be designed to use and generate substances that possess little or no toxicity to human health and the environment.

4. Designing Safer Chemicals

Chemical products should be designed to be fully effective, yet have little or no toxicity.

5. Safer Solvents and Auxiliaries

The use of auxiliary substances (e.g., solvents, separation agents, etc.) should be unnecessary wherever possible or innocuous when used.

6. Design for Energy Efficiency

The energy requirements of chemical processes should be recognized for their environmental and economic impacts and these should be minimized. If possible, synthetic methods should be conducted at ambient temperature and pressure.

7. Use of Renewable Feedstocks

A raw material or feedstock should be renewable, rather than depleting, whenever technically and economically achievable.

8. Reduce Derivatives

Unnecessary derivatives should be minimized as much as possible to avoid the addition of reagents that lead to waste generation.

9. Catalysis

Catalytic reagents (especially selective ones) are better than stoichiometric reagents.

10. Design for Degradation

Chemical products should be designed is such a way that the end-product can be degraded into harmless products that do not persist in the environment.

11. Real-time analysis for Pollution Prevention

The development of analytical methodologies for real-time monitoring, in process monitoring and control prior to the production of harmful materials.

12. Inherently Safer Chemistry for Accident Prevention

The materials used in chemical processes/reactions should be chosen in such a way that they reduce the possibility of chemical accidents such as explosions and fires.

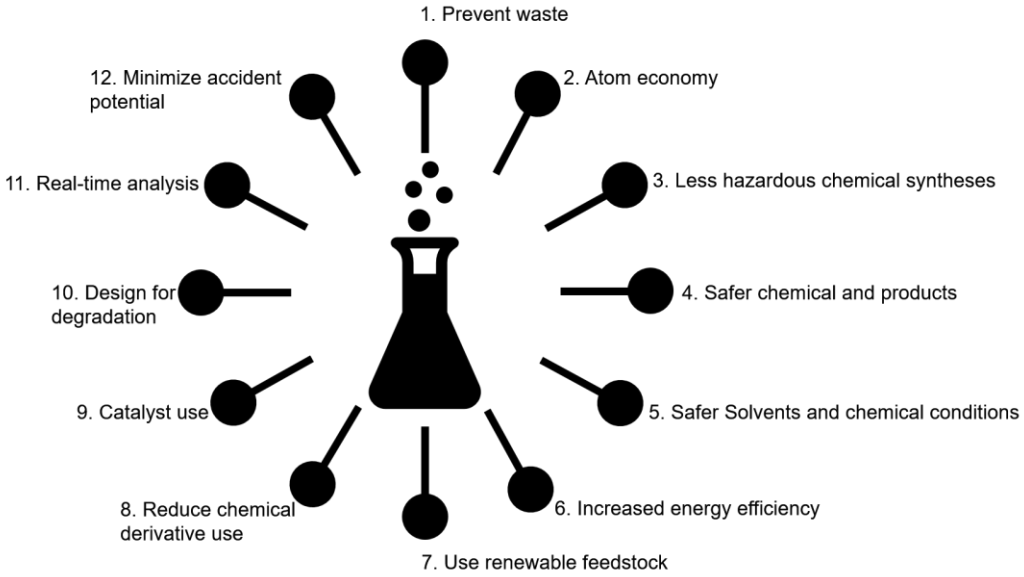

Figure 2.1: The Twelve Principles of Green Chemistry (Anastas and Warner, 1998).

2.2. Typical methods for synthesizing gold nanoparticles

NP synthetic methods generally involve one of two approaches (Figure 2.2), *i.e.* either the "top-down" approach or the "bottom-up" approach (Sepeur, 2008). Figure 2.2 shows the top-down approach where NPs are produced by reducing the size of an appropriate starting material (Meyers *et al.,* 2006) using a variety of physical and/or chemical treatments to achieve the size reduction. A major limitation in the use of a top-down synthetic approach is the introduction of imperfections to the surface structure of the product. This is due to the fact that the surface chemistry and other various physical characteristics of the NPs depend on the surface structure (Thakkar *et al.,* 2010). This would have major implications for catalysts for example.

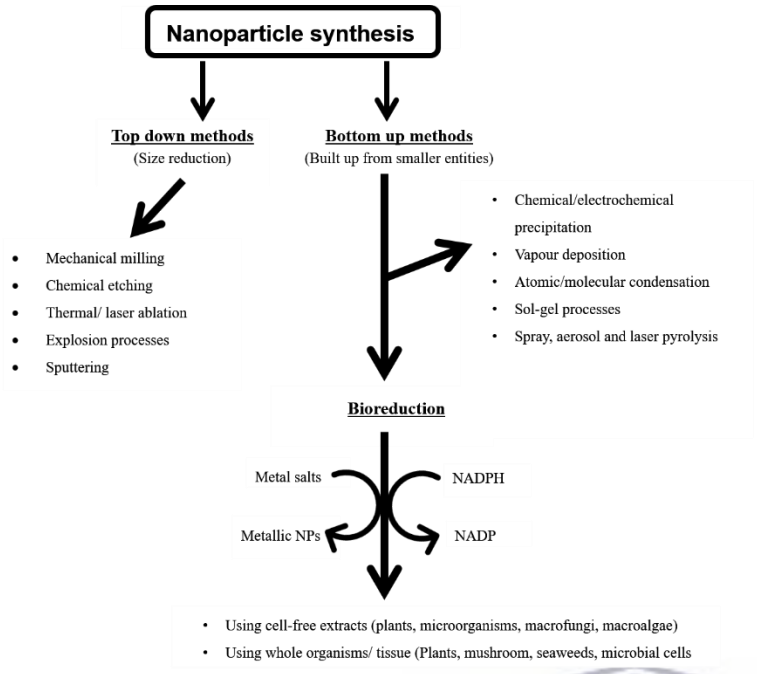

Figure 2.2: The different approaches for synthesizing NPs, including cofactor-dependent bioreduction (Mittal *et al.,* 2013).

In a bottom-up synthetic processes, NPs are produced from smaller units, for example by assembling atoms, molecules and smaller particles (Mukherjee *et al.,* 2002). Bottom up production firstly involves the formation of the nanostructured building blocks to be used in the NPs synthesis process (Figures 2.2 and 2.3). This is then followed by their assembly to produce the final NPs (Thakkar *et al.,* 2010). This bottom-up approach synthesis employs the chemical and biological methods of production as shown in Figure 2.3. Following reduction of the metal salt using a suitable reducing agent or bioagent, the NPs grow and are finally stabilized using a suitable capping agent.

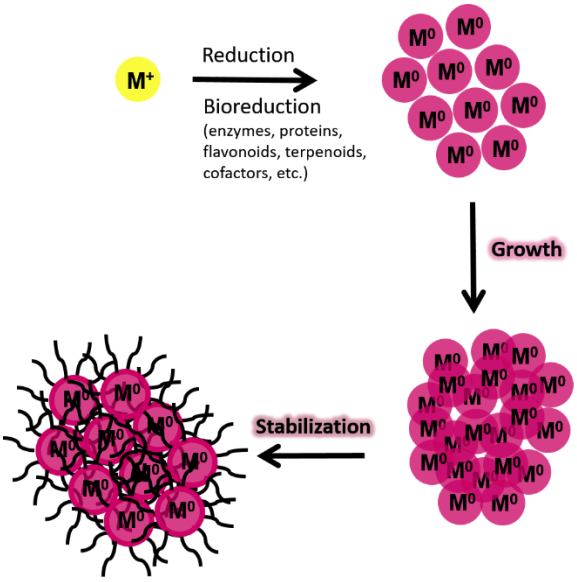

Figure 2.3: Production of NPs synthesis (M^+ is the metal ion) (Mittal *et al.*, 2013).

AuNPs, as well as other metal based NPs, have been previously synthesized using several methods (Ghosh *et al.*, 2004). Commonly used methods for the preparation of AuNPs include chemical, physical, and biological methods, all of which are discussed below.

2.2.1. Chemical methods

Chemical synthetic procedures used in the synthesis of AuNPs normally involve two main parts. The first part involves the use of reducing agents such as borohydrides, aminoboranes, formaldehyde, hydrazine, hydroxylamine, polyols, citric and oxalic acids, sugars, carbon monoxide, sulfites, hydrogen or acetylene (Herizchi *et al.*, 2014). Secondly, stabilizing agents are used to avoid aggregation (Zhao *et al.*, 2013) and typical reagents include trisodium citrate dihydrate, sulfur ligands (thiolates in particular), phosphorus ligands, oxygen-based ligands, nitrogen-based ligands (including heterocyclic compounds), dendrimers, polymers and surfactants (cetyltrimethylammonium bromide (CTAB)) (Herizchi *et al.*, 2014). Some of the most typically used chemical synthetic methods are described below.

2.2.1.1. The Turkevich method

The Turkevich method was initially developed in 1951 by Turkevich *et al.* (1951). Since then it has become one of the most well-known chemical synthetic procedures used, and it involves the reduction of the $HAuCl_4$ salt by citrate in water. The general procedure involves a boiling of a $HAuCl_4$ (0.30 mM) solution initially, followed by the rapid addition of trisodium citrate (0.255 mM) (in a sodium citrate to Au 1:0.85 ratio) to this solution with efficient stirring (Navarro *et al.*, 2013). The formation of the AuNPs is then indicated by the colour change in solution from light yellow to wine red. The resultant AuNPs produced are found to have a diameter of about 20 nm. The citrate ions play two roles in this procedure: they act as both a reducing and a stabilizing agent (Hu *et al.*, 2006; Turkevich *et al.*, 1951). Figure 2.4 shows the synthesis scheme for AuNPs using the Turkevich method.

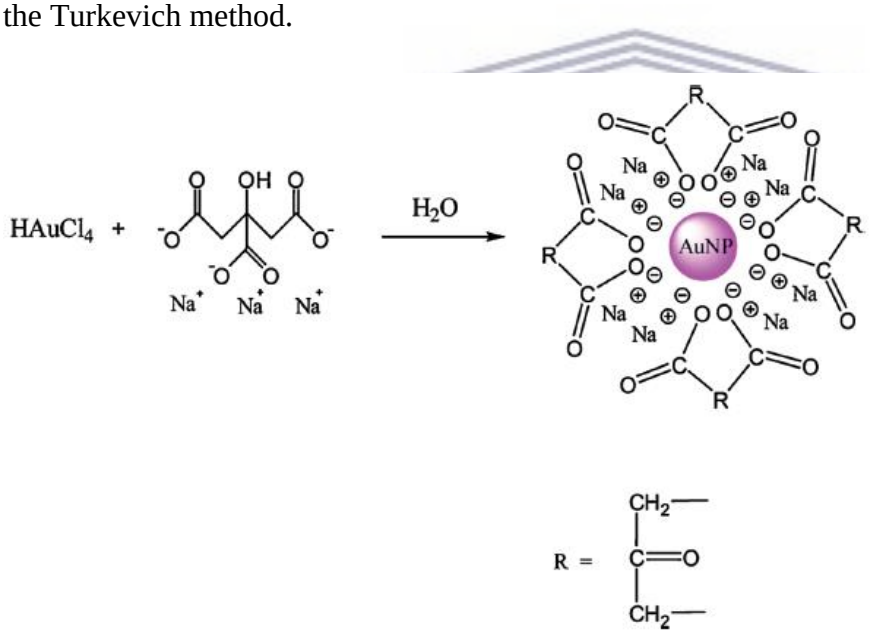

Figure 2.4: AuNPs synthesis using the Turkevich method (Zhao *et al.*, 2013).

Frens (1973) modified the Turkevich method to yield AuNPs with a diameter of 15 to 150 nm by adjusting the ratio of the reducing agent/stabilizing agent (trisodium citrate/gold). It was shown that a high citrate concentration rapidly stabilizes the AuNPs, whilst lower citrate concentrations lead to the aggregation of small particles into larger particles (Zhao *et al.*, 2013, KimLing *et al.*, 2006).

Theoretical models and experimental results have indicated the vital role sodium citrate plays in the pH of the solution as well as its role in controlling the size of the NPs (Li *et al.*, 2011, Kumar *et al.*, 2007). AuNPs with a small size and narrow size distribution range have been successfully synthesized by Ojea-Jiménez *et al.* (2011) by addition of the reagents in an inverse / reverse sequence (addition of $HAuCl_4$ into a boiling sodium citrate solution) as shown in Figure 2.5.

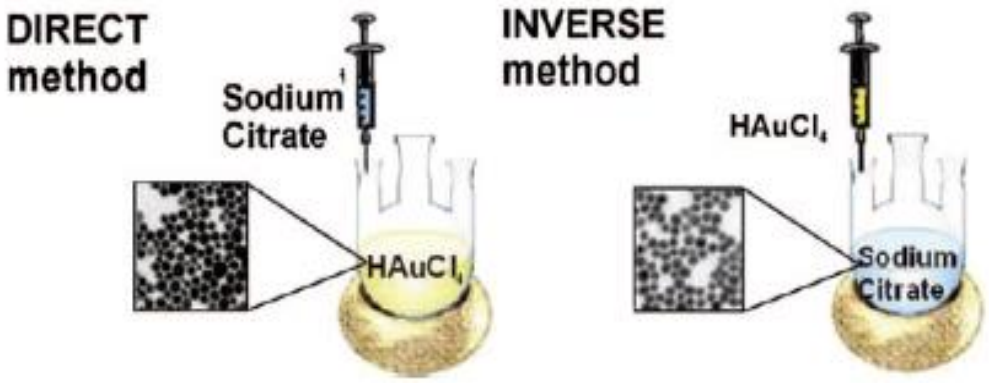

Figure 2.5: Direct and inverse sequence of reagents (sodium citrate and $HAuCl_4$ solution) addition for the synthesis of AuNPs by the Turkevich method (Ojea-Jiménez *et al.*, 2013).

A large amount of literature has focused on the effect of certain parameters such as temperature (Link and El-Sayed, 1999), pH (Patungwasa and Hadak, 2008), citrate (Volkert *et al.*, 2011) and $HAuCl_4$ concentrations (Zabetakis *et al.*, 2012), on the characteristic properties of AuNPs synthesized using citrate as a reducing agent. All of which should be taken into consideration.

2.2.1.2. The Brust-Schiffrin method

The Brust-Schiffrin method was first developed by Brust and Schiffrin in 1994. This simple procedure effectively produced thermally- and air-stable AuNPs with uniform size and dispersity. This method is useful when AuNPs need to be dispersed in organic solvents, rather than the water-soluble NPs produced by the Turkevich method. In this method (Figure 2.6), $AuCl_4^-$ ions are transferred to a toluene phase from an aqueous solution utilizing a surfactant such as

tetraoctylammonium bromide (TOAB) which serves as both the phase transfer catalyst and the stabilizing agent, while $NaBH_4$ functions as the reducing agent in the presence of e.g. dodecanethiol (which acts as the stabilizer). The addition of $NaBH_4$ results in a colour change of the organic phase from orange to deep brown, indicating the formation the AuNPs (Brust *et al.*, 1994).

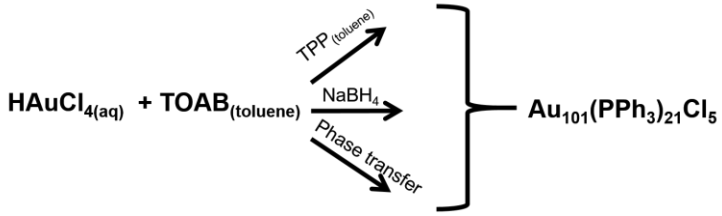

Figure 2.6: The one phase Brust–Schiffrin method employed in the synthesis of AuNPs and the first step of the reaction prior to the reduction step with $NaBH_4$ (Brust *et al.,* 1994). TPP: triphenyl-phosphine; TOAB: tetraoctylammonium bromide.

The method shown above in Figure 2.6 generally involves the reaction between chlorauric acid solution and tetraoctylammonium bromide (TOAB) solution with triphenylphosphine (TPP) in toluene and sodium borohydride ($NaBH_4$) as an anti-coagulant and a reducing agent, respectively (Manna *et al.*, 2003; Dahl et al., 2007).

2.2.2. Electrochemical methods

The electrochemical synthesis of NPs was initially developed by Reetz and co-workers in 1994 (Reetz and Helbig, 1994; Reetz *et al.,* 1995). They showed that metallic NPs could be synthesized electrochemically using tetraalkylammonium salts as stabilizers for the metal clusters in a non-aqueous medium. AuNPs have been successfully synthesized electrochemically on the surface of multi-walled carbon nanotubes using glassy carbon electrodes (Song *et al.,* 2013). In another study, AuNPs were synthesized utilizing a simple two-electrode cell; where oxidation took place at the anode, while reduction occurred at the cathode. The electrochemical apparatus used is showed in Figure 2.7 (Huang *et al.,* 2006).

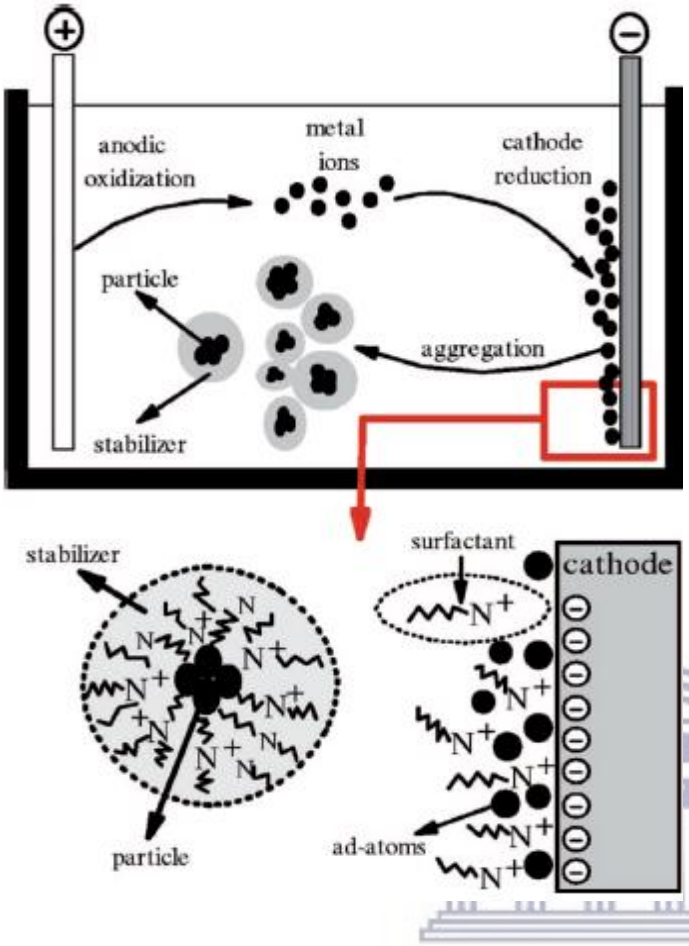

Figure 2.7: The electrochemical system setup used to synthesize AuNPs (Huang *et al.*, 2006).

In the past decade, electrochemical processes have been confirmed to be superior in the synthesis of NPs, due to the modest equipment used, decrease in costs associated with the production processes, lower processing temperatures, the high quality of the NPs produced and the ease of controlling the yields obtained (Freeman *et al.*, 1995; Chen and Yang 2002; Haruta and Daté, 2001; Kuge *et al.*, 2000; Kamat *et al.*, 1998).

2.2.3. Seed-mediated growth method

Seed-mediated growth methods are common methods employed in the synthesis of gold nanorods in a 2-step reaction. This procedure involves the reduction of the metallic gold salt using a strong

reducing agent at first - a phenomenon known as seeding, and then subsequent reduction with a weak reducing agent in the company of structure-directing agents such as CTAB (Murphy and Jana, 2002), benzyldimethylhexadecylammonium chloride (Nikoobakht and El-Sayed, 2003), tetraoctylphosphineoxide (Peng *et al.*, 2000; Peng and Peng 2002) and oleic acid (Puntes *et al.*, 2001) to form nanorods (Stanglmair *et al.*, 2014; Mlambo *et al.*, 2013).

In the first step (seeding), the gold salt is reduced in water (without any heating) with a strong reducing agent such as $NaBH_4$ to produce 3.5-4 nm spherical seeds (Murphy *et al.*, 2005). The formed seeds are normally faceted as nanospherically shaped, single crystalline NPs (Shenhar and Rotello, 2003) and are capped by the addition of citrate or any other surfactant. The seeds are allowed to grow (or ''Age''), while additional metal salts, capping agents and weak reducing agents are prepared in a separate flask. Ascorbic acid (Vitamin C) is a commonly used, weak, reducing agent and, although it is unable to reduce gold metal salts to a nanosize at room temperature, upon subsequent addition of the prepared seeds, the reaction occurs on the surface of these seeds to produce larger NPs. Afterwards the structure-directing agent plays an important role in obtaining nanorods. In a study a carried out by Murphy *et al.* (2005), CTAB was found to be an appropriate structure-directing additive for the production of gold nanorods that grow to 20 nm in width and 600 nm length, beginning with the ~3.5-4 nm spherical seeds as shown in Figure 2.8.

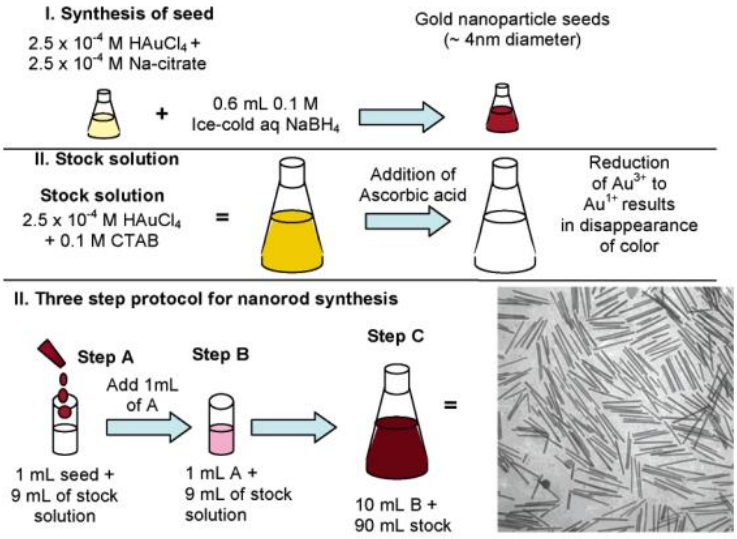

Figure 2.8: Seed-mediated growth method for the synthesis of gold nanorods of controlled aspect ratio.I. Shows the formation of 4 nm gold seeds II. Shows the formation of Au nanorods and transmission electron micrograph of gold nanorods with average length of 500 nm (Stanglmair *et al.*, 2014; Murphy *et al.*, 2005).

2.2.4. Biological methods

The chemical methods employed in synthesizing AuNPs are by far the most common, yet they involve the use of expensive, toxic reagents as reducing and stabilizing agents, limiting the applications of these NPs since they may exhibit detrimental effects in biomedical applications (Noruzi *et al.* 2011; Shankar *et al*. 2004). Therefore, there is an increasing need to develop environmentally friendly, less expensive procedures for the synthesis of NPs that do not involve the use of toxic chemicals. Lately, a great deal of research has focused on the development of green synthetic approaches to produce NPs using eco-friendly and bioinspired methods. Through the knowledge acquired in studying the capabilities of natural biomolecules to alter the shape and size of the nanocrystal, NPs of greater quality may easily be obtained. Biological methods that involve the synthesis of NPs using microorganisms, marine seaweeds, enzymes, and plants or plant extracts have been reported (Shankar *et al.*, 2004).

2.2.4.1. Biosynthesis of nanoparticles using terrestrial plants

As previously mentioned in Chapter 1, several whole (live) plants and plants extracts have been used in the synthesis of AuNPs due to their ease of availability, low cost, eco-friendliness and lack of toxicity. Plant extracts have also been used to synthesize AuNPs such as such as *Memecylon umbellatum* (Arunachalam *et al.,* 2013), *Macrotyloma unifl orum* (Aromal *et al.,* 2012), *Brevibacterium casei* (Kalishwaralal *et al.*, 2010; Mittal *et al.*, 2013), *Citrus limon, Citrus reticulata and Citrus sinensis* (Sujitha and Kannan, 2013), *Piper pedicellatum* (Tamuly *et al.,* 2013), *Terminalia chebula* (Kumar *et al.*, 2012), *Memecylon edule* (Elavazhagan and Arunachalam, 2011), *Nyctanthes arbortristis* (Das *et al.*, 2011), *Murraya koenigii* (Philip *et al.*, 2011), *Mangifera indica* (Philip, 2010), Banana peel (Bankar *et al.,* 2010), *Cinnamomum zeylanicum* (Smitha *et al.,* 2009), and *Cochlospermum gossypium* (Vinod *et al.,* 2011). AuNPs with size diameters of 5-15 nm have been synthesized by Kumar *et al.* (2011) using the extract of *Zingiber officinale* (Ginger) which showed a dual role as both a reducing and stabilizing agent. Onion (*Allium cepa*) extracts have been used as a reducing agent in the synthesis of AuNPs and the authors suggested that the reduction ability of the onion to produce AuNPs was due to vitamin C content present in the extract (Parida *et al.*, 2011).

Live, whole plants that have been used in the synthesis of NPs include: *Azadirachta indica* (Shankar *et al.,* 2004), *Medicago sativa* (Gardea-Torresdey *et al.,* 2002), *Aloe vera* (Chandran *et al*., 2006), *Cinnamomum camphora* (Huang *et al.,* 2007), *Pelargonium graveolens* (Shankar *et al*., 2004), *Coriandrum sativum* (Narayanan and Sakthivel, 2008), *Terminalia catappa* (Ankamwar, 2010) and lemongrass (Shankar *et al.,* 2004b).

2.2.4.2. Biosynthesis of nanoparticles using marine organisms

The synthesis of metallic NPs and metal oxides using different species of algae has stimulated researchers to further explore and develop additional nature-friendly methodologies (Manivasagan and Kim, 2016). However, there is little supporting literature on the synthesis of NPs using marine

algae aqueous extracts. Table 2.1 lists the various algae that have been used to synthesize different NPs together with a comparison of the sizes obtained together with a variety of applications that they have been used for.

Table 2.1 reveals that although all marine algae appear to be capable of producing NPs, it is the brown algae in particular that have found success. A variety of different shapes and sizes were obtained for both AuNPs and AgNPs, suggesting that these seaweeds are able to produce NPs that may be used in a variety of biocompatible applications. Marine algae are abundant and easily available in nature which makes them good candidates and valuable resources for the production of NPs (Singaravelu *et al.*, 2007). NP synthesis using algae is normally carried out in three important steps (i) algal extract preparation (in water or organic solvents with heating or boiling for a specific time), (ii) the preparation of metallic salt solutions, and (iii) incubation of the algal extracts with the metal salt solutions followed by continuous stirring or without stirring for a certain duration under controlled conditions (LewisOscar *et al.*, 2014; Rauwel *et al.*, 2015).

Table 2.1: Biosynthesis of nanoparticles using marine algae

Marine Algae	Nanoparticle	Morphology	Size (nm)	Use	Reference
Sargassum wightii (Brown)	Gold	Well dispersed	8 – 12	—	Singaravelu *et al.*, 2007
Sargassum wightii (Brown)	Silver	—	—	Antibacterial	Govindaraju *et al.*, 2009
Turbinaria conoides (Brown)	Silver	—	—	Fabric strengthening	Sheeba and Thambidurai, 2009
Gelidiella acerosa (Brown)	Silver	Spherical	22	Antifungal	Vivek *et al.*, 2011
Ulva fasciata (Green)	Silver	Spherical	28 – 41	Antibacterial	Rajesh *et al.*, 2012
Fucus vesiculosus (Brown)	Gold	—	—	Biosorption	Mata *et al.*, 2009
Cladosiphon okamuranus and *Kjellmaniella Crassifolia* (Green)	Gold	Spherical	8.54 – 1074	—	Soisuwan *et al.*, 2010
Rhizoclonium Fontinale (Red)	Gold	Spherical	—	—	Parial *et al.*, 2012
Turbinaria conoides (Brown)	Gold	—	0.75	Biosorption	Vijayaraghan *et al.*, 2011
Chlorella vulgaris (Green)	Silver, gold	Triangular	44, 26 – 48	—	Xie *et al.*, 2007
Sargassum Myriocystum (Brown)	Gold	Triangular and spherical	15	—	Dhas *et al.*, 2012
Stoechospermum Marginatum (Brown)	Gold	Spherical	18.7 – 93.7	Antibacterial	Rajathi *et al.*, 2012
Tetraselmis Kochinensis (Green)	Gold	Spherical	5 – 35	—	Senapati *et al.*, 2012
Chaetomorpha Linum (Green)	Silver	—	30	—	Kannan *et al.*, 2013

The type (brown, green or red algae) of algae used and the extract concentration are factors that affect the synthesis of NPs and NP morphology. Algae contain a variety of biomolecules such as polysaccharides, peptides and pigments, which may be responsible for the reduction of metal salts. Proteins have amino groups and cysteine residues, and the presence of sulfated polysaccharides are held responsible for the stabilization and capping of metallic NPs in aqueous solutions (Singaravelu *et al.*, 2007). Compared to other traditional methods, the reaction is complete in a much shorter time (Govindaraju *et al.,* 2009; Vijayaraghan *et al.,* 2011; Senapati *et al.,* 2012).

2.3. Techniques used to characterize nanoparticles

The characterization of NPs is generally based on their size, shape, surface area, morphology and dispersity. These properties and characteristics ultimately determine the suitability of a set of NPs for a particular application (Jiang *et al.,* 2012). The most commonly used techniques for the characterization of NPs include the following: UV–Visible spectrophotometry (UV-vis), scanning electron microscopy (SEM), transmission electron microscopy (TEM), fourier transform infrared (FTIR) spectroscopy, energy dispersive X-ray spectroscopy (EDX) and X-ray diffraction (XRD) (Feldheim and Colby, 2002; Sepeur, 2008; Shahverdi *et al*., 2011).

2.3.1. UV-vis spectroscopy

UV-vis spectroscopy is a commonly used technique which allows the estimation of a NP's size, concentration and aggregation level, particularly with AuNPs and AgNPs (Amendola and Meneghetti, 2009; Pal *et al*., 2007). Light wavelengths in the 200–800 nm range are generally used for characterizing various metal nanoparticles in the size range of 2–100 nm (Feldheim and Colby, 2002). Absorption measurements in the wavelength range of 400–450 nm are typically used to characterise AgNPs (Huang and Yang, 2004), while those between 500–550 nm are used for

AuNPs (Shankar *et al.*, 2004) due to the intense absorption attributed to the Surface Plasmon Resonance bands of the AgNPs and AuNPs in these regions.

2.3.2. Zeta (ζ) potential

Zeta (ζ) potential measurements are used to reveal the net charge on the surface of the NPs in solution (Hunter, 2001). The ζ potential therefore shows how the NPs will interact in the solution, giving information about the stability of the NPs in solution. The ζ potential is determined by applying a potential to a cell equipped with two electrodes which contains the NP solution (Figure 2.9).

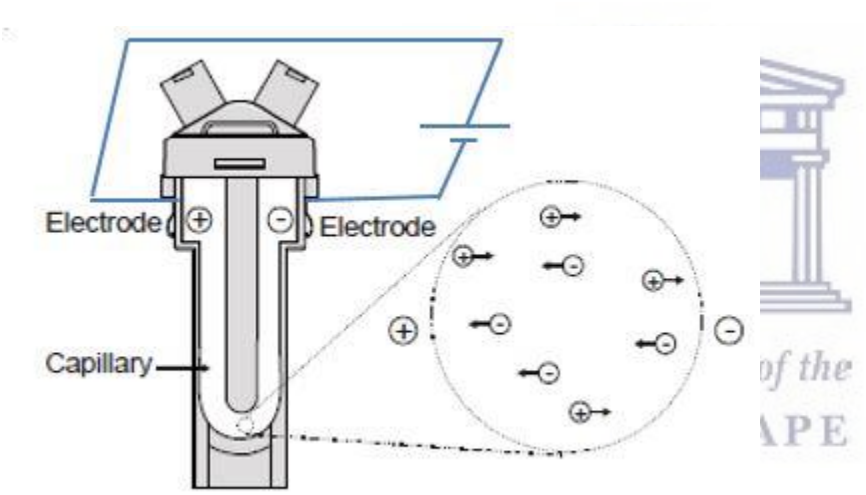

Figure 2.9*:* Zeta potential capillary cell set-up with electrodes. (http://www.materials-talks.com/blog/2015/09/24/zeta-deviation-larger-than-the-mean-how-can-that-be/)

The NPs migrate to the electrode with a charge opposite to their own when the electrophoretic mobility of NPs is measured (Pons *et al.*, 2006) and the Smoluchowski equation (equation 1) employs these values to calculate the ζ potential (Smoluchowski, 1917; French *et al.*, 2009)

$$\upsilon_E = 4\pi\varepsilon_0\varepsilon_r \frac{\zeta}{6\pi\mu}(1 + \kappa r) \quad (1)$$

where ε_0 and ε_r are the relative dielectric constant and the electrical permittivity of a vacuum respectively, μ is the solution viscosity, r is the particle radius and $\kappa = \left(\frac{2\eta_0 z^2 e^2}{\varepsilon_r \varepsilon_0 k_B T}\right)^{1/2}$ is the Debye–Hückel parameter, η_0 is the bulk ionic concentration, z is the valence of the ion, e is the charge of an electron, k_B is the Boltzmann constant, and T is the absolute temperature. ζ potential values of greater than positive or less than negative 30 mV indicates that the NPs are stable (Zhang and Wu, 2010), while factors that affect ζ potential include pH, temperature and the surface chemistry of the NPs (Sapsford *et al.,* 2011).

2.3.3. Dynamic light scattering (DLS)

The Dynamic Light Scattering (DLS) technique, sometimes called Quasi-elastic light scattering (QELS), is used to measure surface charge, size and size distribution of the NPs and other molecules in the submicron region (Patri *et al.,* 2006; Sapsford *et al.,* 2011). Generally, DLS is used for the characterization of particles which have been dispersed in a liquid. The Brownian motion of particles or molecules in suspension cause laser light to be scattered at different intensities. Analysis of these intensity fluctuations yields the velocity of the Brownian motion. The particle size is then determined from the translational diffusion coefficient by the use of the Stokes-Einstein equation (equation 2) (Brar and Verma, 2011; Pons *et al.,* 2006; Sapsford *et al.,* 2011).

$$d(\mathrm{H}) = kT / 3\pi\eta\mathrm{D} \qquad (2)$$

where: d(H) is hydrodynamic diameter, D is the translational diffusion coefficient, k is the Boltzmann's constant, T is the absolute temperature and η is the viscosity.

2.3.4. Electron microscopy

Particles smaller than 1 μm cannot be viewed under light/optical microscope due to the restrictions imposed by diffraction effects. The conventional optical microscope has a maximum useful magnification of about 1 000 x. Thus, to obtain higher resolutions and higher useful magnifications, a decrease in wavelength of the electromagnetic/imaging radiation is required necessitating the use of electron beams. Electron microscopy (EM) involves the acceleration of electrons to higher energies of 2-100 KeV (0.027-0.0009 nm) (Goldstein *et al.,* 1992).

EM's order of magnification is in the region of 1 million, which can reveal details at a resolution of less than 0.1 nm. The electron wavelength of these microscopes are 1 000 x shorter than those of visible light and thus electrons produce better images and have the best resolving power. In EMs, interactions between the electron beam and the sample results in a signal generation that can be transmitted, backscattered and diffracted to form an image with the information needed. The most commonly used electron microscopes are the transmission electron microscope (TEM) and scanning electron microscope (SEM) (Golding *et al.,* 2016; Galbraith and Galbraith 2011; Winey *et al.,* 2013).

2.3.4.1. Transmission electron microscopy (TEM)

The TEM was the first microscope to be developed in 1931 by a German physicist Ernest Ruska with help of Max Knolls (Ruska and Knoll, 1931). Since the development of the TEM (Figure 2.10), particles can be viewed at the atomic level in solids and surfaces in various fields which include life sciences, nanotechnology, medicine, biology, material sciences, forensic analysis as well as education. TEM allows the gathering of information about the particle size, size distribution, morphology, composition and crystallinity (Knoll and Ruska, 1932). High resolution transmission electron microscope (HRTEM) images make it easier for researchers to analyse the structure and texture of the samples due to their ability to view samples at the molecular level (Howe *et al.,* 2008).

As mentioned earlier, NP characterisation by TEM reveals information about particle size, shape, crystallinity and interparticle interaction (Wang, 1998). In TEM, an electron beam from the cathode in the electron gun is released and is focused into a small, thin, clear beam by two condenser lenses. This entire chamber is kept under ultra-high vacuum conditions. The condenser aperture restricts the electron beam from removing high angle electrons before it reaches the sample. It is crucial to ensure that the sample is thin enough to allow penetration by electrons. The contact between electron beam and sample produces elastic and inelastic electrons scattering in the forward direction after the sample has been detected and the electrons carries information about the sample. The image is magnified by a series of magnetic lenses up until it is recorded by a sensitive detector like a CCD (charge-coupled device) camera. The CCD camera detects the image which is then displayed on the computer in real-time (Rosenauer *et al.,* 2014; Guzzinati *et al.,* 2015; Wang, 2000).

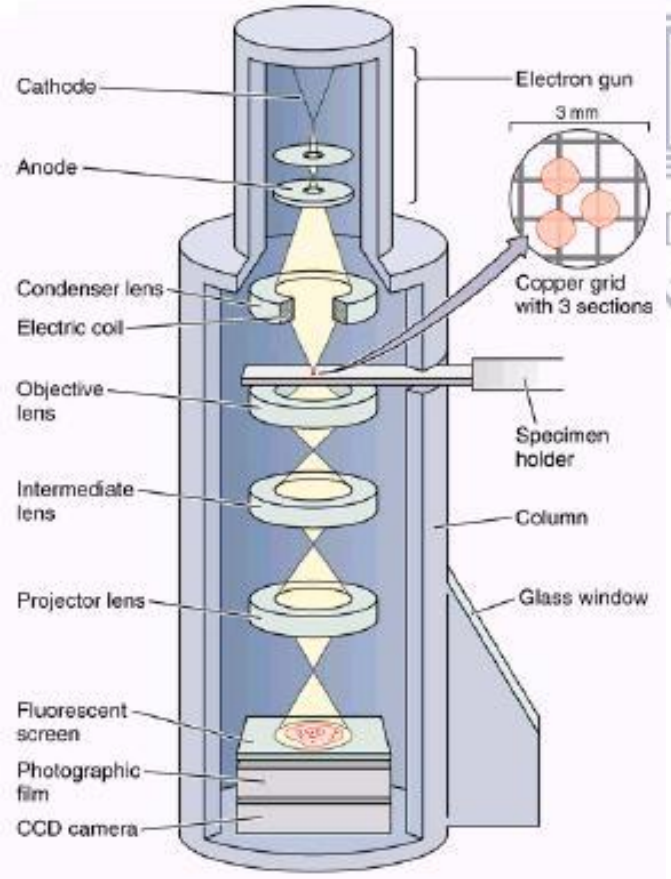

Figure 2.10: Diagram of transmission electron microscope (Mescher, 2009).

Since the electrons pass through the sample to the detector, the sample must therefore be prepared in such a way that it is ultrathin, so that upon interaction with the electrons, the electrons will be able to pass through to the detector and the data collected. The sample preparation process is laborious, especially when working with biological materials. Sample preparation involves three main steps, namely: chemical fixation, dehydration and finally embedding (Hayat, 2000). Biological samples comprise a high water content and thus, to be able to view it using TEM, the first step of preparation involves fixation, wherein the sample is fixed in such a way that the cell structure or tissue morphology is as close to the living material as possible. This is then followed by dehydration by washing using acetone or ethanol, then passed via a solvent such as propylene oxide and finally infiltrated and fixed in a liquid resin e.g. epoxy and LR White resin. The resin block is then thick sectioned in a process known an ultramicrotomy. In this process, thick sections of about 50-70 nm are collected on metal mesh 'grids' which are then stained with electron dense stains and therefore ready to view under EM (Sobol, 2010; Giddings, 2003; McDonald, 2009; Douglas and Tyla, 2010).

TEMs are equipped with several detectors which includes backscattered, bright-field and dark-field STEM detectors. These detectors are not only involved in imaging, but they also reveal chemical composition of the sample. The equipped detectors includes: EDX which is used for elemental identification of metal NPs and SAED which reveals the crystallography of the same sample (Strasser *et al.,* 2010). TEM is a very useful instrument with a number of advantages as well as disadvantages as listed in a Table 2.2

Table 2.2: Advantages and disadvantages of TEM

Advantages	Disadvantages
• TEMs have high magnification of over one million times or more	• TEMs are large and very expensive
• TEMs are used in wide-range of applications including a variety of different scientific, educational and industrial fields	• Sample preparation is laborious
• TEMs provide information on element and compound structure	• Potential artefacts from sample preparation
• Images produced are high-quality and detailed	• Operation and analysis requires special training
• TEM provides information of surface features, shape, size and structure	• Samples should be electron transparent, able to tolerate the vacuum chamber and small enough to fit in the chamber
• With thorough training, they are easy to operate	• TEMs require special infrastructure and maintenance
	• Images are black and white

2.3.4.2. Scanning electron microscopy (SEM)

Similarly to TEM, SEM also involves the interaction of an electron beam with the sample, resulting in the production of secondary electrons with smaller energies of less than 50 eV. The emission efficiency of the secondary electrons used depends on certain factors such as surface geometry, surface chemical characteristics and bulk chemical composition. SEM therefore reveals information about the surface topology, morphology and chemical composition of the NPs. This tool offers high resolution capabilities which are useful in studying the NPs features on the nanoscale range which are important to their properties and functionalities (Goldstein *et al.,* 1992). A usual setup for SEM (as shown Figure 2.11) also begins with an electron source.

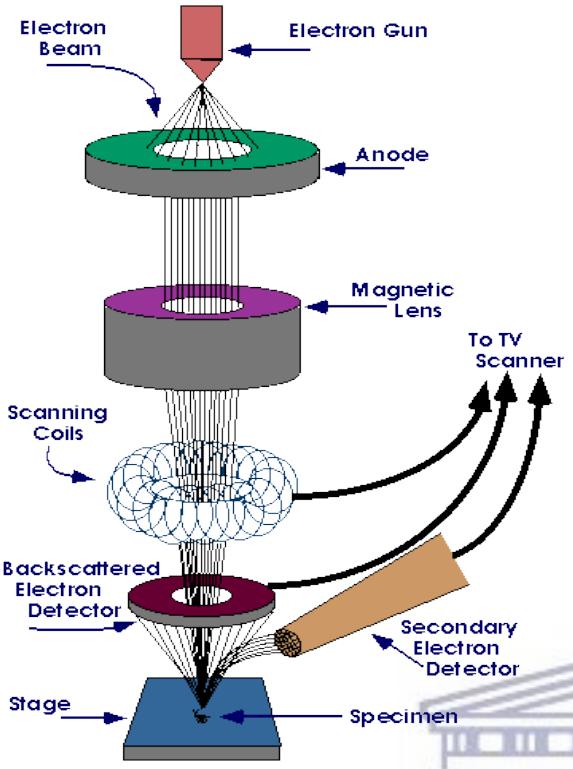

Figure 2.11: Diagram of scanning electron microscope (https://www.purdue.edu/ehps/ rem/ rs/sem.htm).

An electron beam is generated from the electron gun followed by condensation by the first condenser lens which forms the beam and reduces the amount of current (Figure 2.11). The condenser lens, in junction with the condenser aperture, eliminate the high-angle electrons from the beam. In the second condenser, the lighter electrons are focused into a thin, fitted, clear beam and the objective apertures play a further role in eliminating high-angle electrons from the beam. The beam of electrons is scanned with set of coils within the condenser. The objective lens then focuses the scanning beam to the selected sample one point at a time (Goldstein *et al.*, 1992; Hanada *et al.*, 2008).

Table 2.3: Advantages and disadvantages of SEM

Advantages	Disadvantages
• Much higher magnifications can be achieved (up to 1,000,000x), with an ultimate resolution of 1 nm.	• SEMs are expensive and bigger in size and therefore needs bigger infrastructure which is free of any electric, magnetic or vibration interference.
• Gives more information than just the surface topography e.g. crystal structure, chemical composition and electrical properties.	• Difficulty in maintenance such as keeping steady voltage to electromagnetic coils and circulation of cool water.
• The technological advances in modern SEMs allow the generation of data in digital form.	• The preparation of samples can result in artefacts.
• Very short specimen preparation time while the specimen is attached to a sample holder.	• SEMs are limited to solid, inorganic samples.
• SEM allows non-destructive evaluation of the specimen.	• SEMs carry a small risk of radiation exposure associated with the electrons that scatter from beneath the sample surface.
• Large specimens of about 200 mm diameter wafers, or even larger can be specially adapted in SEMs.	• Requires specialized training to operate and safety precautions must be observed.

Contact between electron beam and the sample produces back scattered electrons (BSE), X-ray, secondary electrons (SE), and Auger electrons in a thick or bulk sample. These different electrons are detected and the signal detected carries the information about the specimen being investigated which can be displayed on the monitor. BSE is much more sensitive to heavier elements than SE. The X-ray radiation is used to reveal EDX information which identifies the elemental composition of the sample (Hanada *et al.*, 2008; Liu *et al.*, 2008).

2.3.5. X-ray powder diffraction (XRD)

In X-ray powder Diffraction (XRD), light is scattered by a periodic array in a long-range order resulting in the formation of constructive interference angles and therefore diffractions. The atoms in a crystal are arranged in a periodical manner and thus they diffract the light. X-rays have wavelengths which are the same as that of the distance between atoms. XRD is used for phase identification and characterization of the crystal structure of the materials (Chauhan and Chauhan; 2014). X-rays pass through the NPs and the resulting diffraction pattern gives information about the atomic arrangement in a crystal. Amorphous materials such as glass lacks a periodic array with long-range orders and as such they do not form any significant peak in diffraction patterns (Sharma, 2000; Dann, 2002; Skoog *et al.,* 2007), resulting in broad reflections.

In XRD the broadness of the peak reveals crucial information about the analyte and the size of a crystalline material is determined by measuring the broadness of the reflections in a diffraction pattern. The broadening of the XRD is inversely proportional to the size of the crystalline particles, thus, the more narrow the peak, the larger the crystallite size. Several factors affect the broadening (narrowness or wideness) of the peak such as the periodicity of the individual crystallite domains, reinforcing the diffraction of the X-ray beam. Absence of defects and proper periodical arrangements of crystals allow the diffraction of X-ray beam at the same angle, even via multiple layers of the sample and thus narrow peaks are obtained (Bearden, 1967; Skakle, 2005; Liss *et al.*, 2003). A random arrangement of crystals has a low periodicity degree, therefore resulting in broader peaks. The size of the nanoparticles may be calculated from the powder XRD diffraction pattern using the Debye-Scherrer equation (Borchert *et al.,* 2005) (equation 3).

$$d = \frac{k\lambda}{\beta cos\theta} \qquad (3)$$

where:

d is the size; *k* is the Scherrer constant (0.9); λ is the X-ray wavelength; β is the width of XRD peak at half height determined from the pattern; and θ is the Bragg diffraction angle (Mahdavi *et al.* 2013).

2.3.6. Fourier transform infra-red (FTIR) spectroscopy

For a molecule to absorb light at the infrared (IR) region, it must contain a time-variant dipole moment and its vibration frequency must be the same as that of the incident IR light (Johal, 2011). IR radiation absorption causes energy transfer to the molecules which induces stretching, bending or twisting of the covalent bonds, which may be explained by a stationary state of molecular vibrational Hamiltonians in the case of normal modes (Cantor and Schimmel, 1980). Molecules which lack dipole moments (e.g. N_2 and O_2) do not absorb IR radiation (Johal, 2011). In a molecule, the oscillations generally involve many pairs of atoms or covalent bonds, all of which are considered as a combination of the normal modes; thus, the IR spectrum, showing transmission against incident IR frequency, reveal information about the fingerprint of the molecule being investigated (Cantor and Schimmel, 1980).

In nanotechnology, FTIR spectroscopy is commonly used to reveal information about the capping agent on the NPs. Organic functional groups (e.g. carbonyls, hydroxyls), biomolecule conjugation (e.g. proteins bound to NPs surfaces), and the conformational states of the bound proteins (Perevedentseva *et al.*, 2010; Shang *et al.*, 2007; Baudot *et al.*, 2010) are detected. In recent years, attenuated total reflection (ATR–FTIR) spectroscopy has been become popular. ATR–FTIR employs the property of total internal reflection in combination with IR spectroscopy to examine the structure of the sample at a solid/air or solid/liquid interface. It is advantageous over conventional IR since it avoids the drawbacks of sample preparation and the failure to reproduce spectral lines (Johal, 2011; Hind *et al.*, 2001). In an ATR-FTIR, there is total internal reflectance which occurs within the equipped internal reflection element (IRE) crystal. IREs comprise of high refractive angles at specific angles which results in temporary waves that prolong from the IRE crystal-specimen into the specimen with depth of 0.5–5 μm. The strength of these waves decays in an exponential rate starting from the interface (Johal, 2011).

ATR–FTIR provides IR spectra for the investigation of certain properties such as alterations in surface characteristics and identification of chemical properties (Johal, 2011; Kazarian and Chan,

2006; Liu and Webster, 2007). Even though ATR– FTIR spectroscopy is used to examine surface properties of NPs, it has certain drawbacks such as lower sensitivity as a surface analytical technique at the nanoscale, due to the fact that the ATR–FTIR penetration depth has the same order of magnitude as that of the incident IR wavelength (Liu and Webster, 2007).

2.3.7. X-ray photoelectron spectroscopy (XPS)

X-ray photoelectron spectroscopy (XPS) is a spectroscopic, surface analytical technique used to reveal the chemical composition of samples, the oxidation state of elements (Menard *et al.,* 2006, Shem *et al.,* 2009; Schaaff *et al.,* 1997) and it may also be used to quantify the amount of ligand present on the surface of NPs. The photoelectron energy positions of each peak for the elements indicate whether the ligands being evaluated are indeed attached to the NPs e.g. where a shift in peak position is expected for S-H (unbound ligand) as opposed to S-Au (bound to AuNPs) in high resolution spectra. In this way, high resolution XPS is therefore used to determine the oxidation state of Au atoms (Kariis *et al.,* 1998). This information is obtained by background subtraction and deconvolution of the high resolution spectra.

A survey spectrum is regarded as the starting point during XPS analysis due to the fact that is identifies all the elements which are present on the surface of the sample (usually the first 10 nm) and it paves the way for subsequent high-resolution spectra (which indicates the chemical state of the sample). XPS spectra reveal photoelectron intensity versus the binding energy (BE) of the photoelectrons detected. Elements possess characteristic signals at specific binding energy values which used to identify an element. The spectral peak shape reveals the electron configuration of the photoelectron ejected from the sample i.e. whether it is the 1s, 2s, 2p, or 3s photoelectron (Shirley, 1972; Seah *et al.,* 1998). For example, the Au 4f peak of Au has a well separated spin-orbit splitting of Δ=3.7eV with an asymmetric peak shape. The binding energies of metallic Au(0) is 84.0 eV while of Au(I) is 85.0 eV and of Au(III) is 86.0 eV and thus, the peak position gives crucial information in identifying the elemental state of the sample (Veith *et al.,* 2005; Kruse and Chenakin, 2011).

Figure 2.12 shows the components of an XPS instrument. The sample area is illuminated by X-rays which results in the release of photoelectrons with wide range of energies and directions. The magnetic lens units focus the photoelelectrons and collect the information from the emitted photoelectrons which are further transferred via a series of apertures to the analyser entrance slit. Within the hemispherical analyser (HSA), electrostatic fields are formed which allows the electrons to pass through to the detector slits to the detector revealing the sample data.

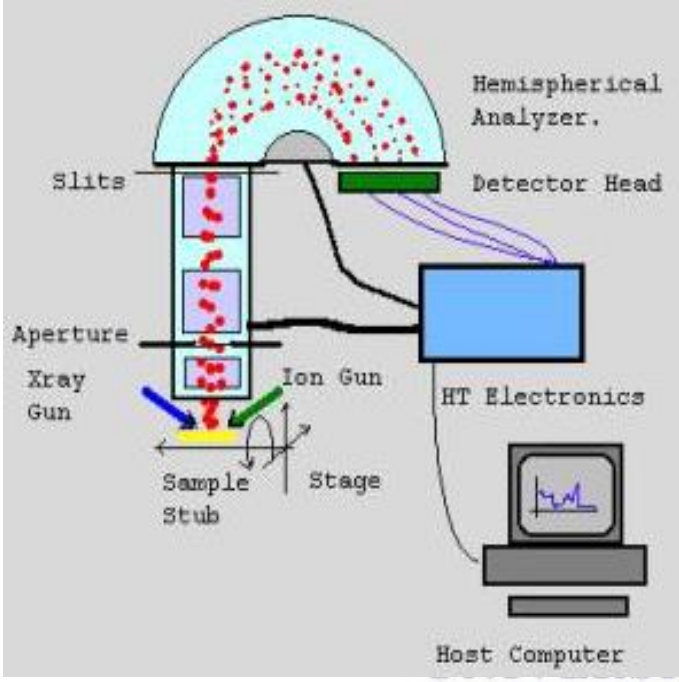

Figure 2.12: Schematic diagram of a small-spot XPS with raster imaging capability (Kelly, 2003).

2.3.8 Thermo-gravimetric analysis (TGA)

TGA is a thermal analysis technique which measures shifts in the physical or chemical properties of a sample as a function of time (with uniform temperature and/or constant weight loss), temperature (with constant heating rate) and atmosphere (Mohomed, 2016; Coats and Redfern, 1963). It is used to reveal information about the physical properties of the material such as vaporization, adsorption, sublimation, absorption, desorption and second order transitions. It also gives information about the chemical properties of a sample such as that in solid-gas reactions (e.g. oxidation or reduction), decomposition, chemisorptions and desolvation (especially dehydration) (Coats and Redfern, 1963).

TGA is usually used to determine properties of materials that display either weight loss or gain because of oxidation, decomposition and loss of volatiles (such as moisture). Some TGA applications include: characterisation of materials using decomposition patterns, reaction kinetics and degradation mechanism studies, sample organic content determination and sample inorganic content determination. This information can be used for confirming predicted sample structures (Coats and Redfern, 1963).

TGA relies heavily on a high degree of accuracy in three main measurements: change in mass, temperature and change in temperature. Thus, the basic components for TGA instrument are a weighing balance with pan loaded with the material, and a furnace which is programmable for certain temperatures and time. Furnace programming can be either for a uniform heating rate or that of heating to obtain constant weight loss over time (Tikhonov *et al.*, 2009; Coats and Redfern, 1963).

2.3.9 Inductively coupled plasma - atomic emission spectroscopy (ICP-AES)

ICP-AES also known as inductively coupled plasma optical emission spectrometry (ICP-OES) is a spectroscopic technique used to quantify the elemental composition of nanomaterials. ICP-AES involves the use of high energy plasma from an inert gas such as Argon (Ar) which forms excited atoms and ions which release the electromagnetic wavelength properties of a specific sample by rapidly burning the sample with flame temperature of about 6000 to 10000 K. The electromagnetic wavelength emission intensity of the sample of interest shows the concentration of the element present (Orbaek and Barron, 2014; McClenathan *et al.*, 2006; Huang and Hieftje, 1989). The schematic view of ICP-AES experimental setup is shown in Figure 2.13.

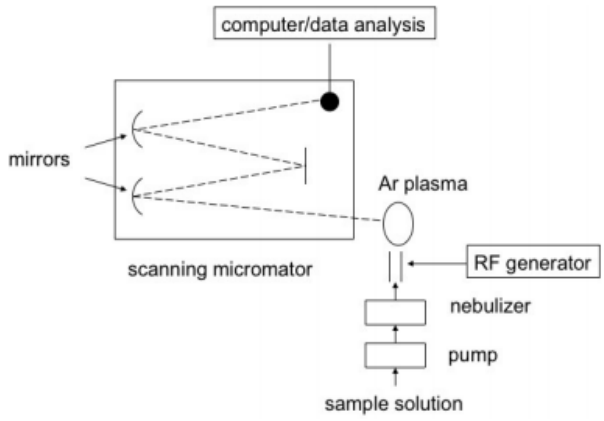

Figure 2.13: Schematic view of ICP-AES (Orbaek and Barron, 2014).

For ICP-AES, NPs must usually be digested in order to allow the atoms to be vaporized in the plasma consistently. Metal containing NPs are digested using a strong acid to bring atoms into the solution since failure to do this could hinder some metals being vaporized. This results in failure to quantify the sample accurately.

2.4. Applications of gold nanoparticles

Metallic NPs, or especially AuNPs, have many applications in biotechnology and biomedicine due to the large surface area-to-volume ratio of NPs as compared to larger particles. This results in larger surface energies for the NPs, giving them the ability to react with certain molecules, allowing them to find a wide range of applications in various fields. Nanotechnology is a relatively new interdisciplinary field which encompasses chemistry, engineering, biology, and medicine. It holds great promise in early detection, precise diagnosis and personalized treatment of several diseases, more especially cancer (Cai and Chen, 2007). NPs are smaller entities ranging between 1-100 nm in diameter compared to larger biomolecules such as enzymes, receptors and antibodies. NPs with their very small sizes, can interact with biological molecules either on the surface or inside the cells. This interaction may lead to a better diagnosis and treatment of diseases (Cai *et al.*, 2008). The most well-researched NPs include quantum dots (QDs) (Cai *et al.*, 2006; 2007b),

carbon nanotubes (CNTs) (Liu *et al.*, 2007), paramagnetic NPs (Thorek *et al.*, 2006), liposomes (Park *et al.*, 2004), AuNPs (Huang *et al.*, 2007b) including many others (Ferrari, 2005; Grodzinski *et al.*, 2006).

2.4.1. Therapeutic Agents

Cancer nanotechnology aims at fighting cancer and improving certain aspects of oncology such as molecular imaging, diagnosis, targeted drug delivery and bioinformatics. The advances made in cancer nanotechnology holds the potential for personalized cancer treatment in which cancer will be treated and diagnosed using the genetic and protein biomarkers of each individual. AuNPs have been studied in a number of different areas including *in vitro* assays, in *in vitro* and *in vivo* imaging, cancer therapy and drug delivery in cancer nanotechnology (Cai *et al.*, 2008).

Conventional cancer therapies include surgery, chemotherapy and radiation therapy. Taking advantage of the unique properties exhibited by AuNPs, they have been studied in combination with photothermal therapy in the treatment of cancer, thus holding potential to undergo clinical trials. It has been reported that when cancer cells are irradiated with laser pulses of an appropriate wavelength, targeted Au nanospheres, nanorods, nanoshells, and nanocages can have antibacterial (Zharov *et al.*, 2006) and anticancer activities (Loo *et al.*, 2005; Tong *et al.*, 2007). It was estimated that AuNPs' light absorption resulted in an increase in localized heating of the cancer cells to 70–80 °C (Huang *et al.*, 2006). Cancer cells are unable to tolerate higher temperatures. In addition, up to 150 antibodies could be functionalized on the gold nanoshell *via* a bifunctional polyethylene glycol (PEG) linker (Lowery *et. al.* 2006). Interestingly, the authors targeted either epidermal growth factor receptor (EGFR) or human epidermal growth factor receptor 2 (HER2) mainly, because the monoclonal antibodies that recognize these two proteins are readily available and these have been approved by the Food and Drug Administration (FDA) (Cai *et. al.*, 2008).

2.4.2. Drug delivery

AuNPs have been used as drug delivery vehicles. Tumour necrosis factor-alpha (TNF-α) is a cytokine with tremendous anticancer activity, however, it is systemically toxic which limits its therapeutic applications (van Horssen *et al.,* 2006; Mocellin and Nitti 2008). Using NPs, a multi-modal system made up of PEGylated-AuNPs loaded with TNF-α, cancer cell damage was maximized and a concomitant reduction in toxicity of TNF-α was realized (Visaria *et al.,* 2006). Combining localized heating with a NP-based delivery of TNF-α showed an improved therapeutic efficiency. This conjugate has therefore reached Phase I clinical trials and is called "CYT-6091". It is currently under evaluation for safety, pharmacokinetics profile and clinical efficacy (Visaria *et al.,* 2007).

Methotrexate (MTX) is a chemotherapeutic drug which inhibits the activity of dihydrofolate reductase (Huennekens, 1994). The *in vitro* and *in vivo* anticancer effects of MTX-AuNPs have been investigated using the mouse model of Lewis lung carcinoma. A MTX-AuNP conjugate showed suppression of the cancerous cells, whereas the same dose of MTX had no anticancer activity. These findings suggest that conjugating the NPs with chemotherapeutic agents can improve cancer activity as compared to the drugs alone (Chen *et al.,* 2007). It is thus apparent that, for AuNPs to be regarded as valuable drug delivery agents and for it to be indispensable to many other biomedical applications such as imaging and therapy, the NPs should be effective, specific, and reliable in targeting the specific site of infection with affecting healthy host cells (Chen *et al.,* 2007b).

2.4.3 Sensors

In the past decade, AuNPs have found new, previously unknown applications in different fields of science and technology, such as the coating of glass (Chaikin *et al.,* 2013) to alter their properties and for multicolour optical coding for bioimaging applications (Aaron *et al.,* 2008). AuNPs are also utilised in the enhancement of electroluminescence stability and quantum efficiency in blue-

light-emitting polymers (Park *et al.*, 2004b). The application of AuNPs in signal amplification for biosensing is another newly developed application (Cao *et al.*, 2011). The fabrication of materials at nanoscale level has enabled the development of sensors capable of detecting analytes such as chemical vapours at the very low concentrations of a few parts per millions (ppm) (Zhao *et al.*, 2015b).

2.4.4 Catalysis

AuNP-based technologies offer great potential to solve some of the great environmental issues such as greener synthesis methods, pollution control and water treatment. Gold is known to be a very stable metal and it is resistant to oxidation reactions. However, at the nanoscale, conditions are suitable for the AuNPs to behave as catalysts e.g. in the catalysis of 4-NP by $NaBH_4$ (Sharma *et al.*, 2007; Praharaj *et al.*, 2004), the catalysis of carbon monoxide (CO) oxidation (Haruta *et al.*, 1987), the catalysis of hydrogenation of unsaturated substrates (Mitsudome and Kaneda, 2013), electrochemical redox catalysis of CO (Guo and Wang, 2007) and alcohol dehydrogenation and oxygen reduction (Maye *et al.*, 2004), as well as catalysis by functional thiolate-stabilized AuNPs (Goettmann *et al.*, 2005).

4-Nitrophenol, alongside other phenols, has been listed by the U.S. Environmental Protection Agency (EPA) as an important pollutant with regards to water quality. Conventionally, these pollutants are removed using various methods such as catalytic liquid-phase oxidation which requires high temperature conditions (Levec and Pintar, 1995), making these methods expensive. The use of metallic NPs as catalysts for the reduction of 4-NP can be accomplished at room temperature, thus just the cost implications make the use of metallic NPs such as AuNPs an attractive, appropriate alternative for the removal of these phenols from industrial waste water. Several different types of metallic NPs have been used to catalyze the reduction of 4-NP by $NaBH_4$ including Pt, Pd, Ni, Ag, Au as well as alloy NPs (Mahmoud *et al.*, 2010; Ghosh *et al.*, 2004; Lu *et al.*, 2006).

AuNPs have been used to monitor and detect mercury (Hg) (James *et al.*, 2012), an important application since mercury is known as a dangerous material world-wide, causing diseases such as Alzheimer's and Autism (Mutter *et al.*, 2005). Mercury that exits the boilers in the utilities industry find their way into the atmosphere - amounting to over 100 tons of mercury in the atmosphere (Romero *et al.*, 2006). AuNP-based catalysts have the potential to provide a solution by catalyzing the oxidation of Hg (Zhao *et al.*, 2006). AuNPs have also been shown to be highly effective adsorbents in the removal of significant levels of Hg from drinking water (Pacheco *et al.*, 2006).

Another important application of AuNPs of relevance to the environment, is air quality (Yunus *et al.*, 2012). CO is a colourless, odourless gas which is acutely toxic. AuNPs have been shown to facilitate the oxidation of CO to produce the less toxic carbon dioxide which can be used by plants for photosynthesis (Mehrparvar *et al.*, 2013, Haruta *et al.*, 1987; Lopez *et al.*, 2003). In recent years, noble metal NPs have been extensively explored in water purification (Qian *et al.*, 2013) and pollutant detection (Wang and Yu, 2013).

2.4.5. Electronics

A more obvious application for gold nanoparticles would be the use of AuNPs as conductors for various devices ranging from printable inks to electronic chips. The electronics world is highly focused on making smaller and smaller devices, making the use of NPs ideal components for electronic chip design. Various components in electronic devices such as resistors, conductors and other elements are now connected by AuNPs (Huang *et al.*, 2003). AuNPs are also used occasionally in solar cells to occasionally provide clean energy (Lu *et al.*, 2016) and they also improve high capacity data storage (in flash memories and discs) (Global Market Insights, 2016).

2.5. Ulva lactuca

Discussion of the classification of *Ulva lactuca* is being presented for the work done on whole *Ulva* (Chapter 4).

2.5.1. Scientific classification

Classification of Ulva lactuca

Kingdom: Plantae
Phylum: Chlorophyta
Class: Ulvophyceae
Order: Ulvales
Family: Ulvaceae
Genus: Ulva
Species: *Ulva lactuca* (Linnaeus, 1753)
Common Name: Sea Lettuce

Marine seaweeds are multicellular eukaryotic organisms which belong to the kingdom Protista to any one of the three phyla, Phaeophyta (brown algae), Rhodophyta (red algae) and Chlorophyta (green algae) (Raven *et al.*, 2005). Even though all macroalgae from various phyla are referred to as seaweeds, they do not have same multicellular ancestor, thus they are classified as a paraphyletic group. *U. lactuca* is a green alga from the family of lactucaceae, genus *Ulva lactuca* and the genus was first identified by Linnaeus in 1753. Taxonomists and phycologists have subsequently focused of identifying other *Ulva* species, a difficult process because of their morphological plasticity (Wald, 2010).

The *Ulva* morphology consists of a simple structure that looks like bright green sheets, which may be due to certain factors such as environmental conditions, age of the thallus and life style, making

the delineation of the species difficult by morphological features alone. Thallus (leaf) of *Ulva* is only 2 cell layers thick as shown in Figure 2.14 (macroscopic image of *Ulva* thalli). It is transparent and can be easily viewed and examined under a light microscope. The cells of the *Ulva* contain chloroplasts which are responsible for converting solar light into energy (Wald, 2010). The chloroplast moves around the cell; during the day it is located on the border of the thallus to facilitate photosynthesis, whereas at night it is situated on the edge of the cell (Robertson-Andersson *et al.,* 2009).

Ulva have been used in bioremediation due to its tolerance and high affinity for ammonium, nitrogen and other mineral uptakes from shrimp pond effluent (Copertino *et al.,* 2009; Bolton *et al.,* 2009). *Ulva lactuca* play an important role in removing the high level of nitrates present in brackish wastewater, which arises as a result of agricultural runoff or from fish farms, such as the wastewater produced by salmon fish farms. This is a mutually beneficial relationship for *Ulva* as it now grows faster - enabling harvest of the *Ulva*, while the water is purified (Tsagkamilis *et al.,* 2010; Ale *et al.,* 2011). *Ulva* is further regarded as the perfect candidate for biofiltering due to its high rates of nutrient removal, high photosynthetic rates and high specific growth rates (Copertino *et al.,* 2009; Tsagkamilis *et al.,* 2010).

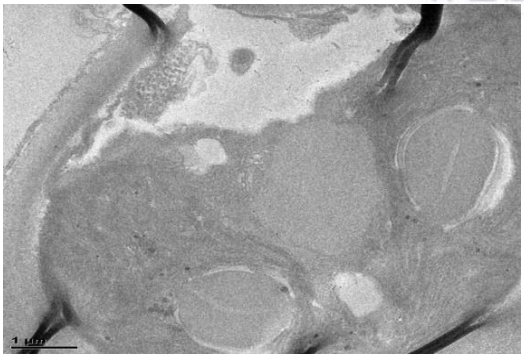

Figure 2.14: TEM image of the *Ulva* thallus

2.5.2. Distribution

Ulva is a green marine seaweed which is distributed all over the world. It is found attached to the rocks in coastal regions, in pools and shallow waters near the low waterline. *Ulva* is known to survive in salty waters, mainly in waters with organic enrichment such as ocean waters, and it is commonly found along the South African coastline (Figure 2.15) in mainly sheltered or moderately exposed shores (Bolton and Stegenga, 2002).

Figure 2.15: South African map showing the coastline which covers the Indian and Atlantic Ocean and more important Sea Point in Cape Town, South Africa where the *U. lactuca* was collected (Adapted from http://exploringafrica.matrix.msu.edu/module-twenty-nine-activity-one/).

2.5.3. Description

Ulva is a member of a huge genus of marine and brackish green seaweed. It is a thin, flat green seaweed which grows to only 2 cell layers thick. When *Ulva* grow, it lacks stipe (roots) however;

it grows attached to rocks (Figure 2.16) and other various substrates (Pedersen and Borum, 1996). The leaves of *Ulva* look like those of a lettuce and therefore it is often called Sea Lettuce. At its early stage of development, it is pale green, and it becomes bright green as it mature and it turns dark green when it is old. This seaweed can grow as long as 45 cm and 30 cm across (Provasoli and Pintner, 1980; Nakanishi *et al.*, 1996).

Figure 2.16: *U. lactuca* in nature growing attached to rocks (Nikolaisen *et al.*, 2011).

2.5.4. Uses of *U. lactuca*

Ulva has a wide range of usage in households where it is used as a source of food, in biotechnology industries, including bioremediation, integrated aquaculture systems and potential biofuel production (Neori *et al.*, 1996). It is simple to tear apart *Ulva* from the rock layer and it can easily accumulate in large drifting masses. Reports indicate that these *Ulva* masses make it possible for it to have many other uses such as making paper and fertilizers for crops by farmers (Sridhar and Rengasamy, 2012).

2.5.5. Cultivation of *U. lactuca*

Ulva species is filamentous which makes it robust and gives it a high growth rate, which makes it relatively simple to cultivate across a wide range of environments. Temperate species of filamentous *Ulva* is cultivated for commercial purposes on nets which are artificially seeded under monitored conditions, permitting a high level of control over the seeding density and consequently biomass production (Troell *et al.,* 2006). In South Africa, large-scale cultivation of the local abalone, *Haliotis midae,* has grown rapidly from its beginnings in the mid-1990s, and it has kept on growing ever since then due to the aquaculture of *Ulva* (Bolton *et al.,* 2009). At the moment, South Africa produces the largest quantities of cultured abalone outside Asia (Troell *et al.,* 2006; Robertson-Andersson *et al.,* 2008; FAO, 2004), yielding 1 100 tons in 2007 (Robertson-Andersson, 2007).

Abalones are herbivores and they were previously fed using *Ecklonia maxima* (Bolton *et al.,* 2009; Troell *et al.,* 1999; Robert-Anderson *et al.,* 2007). Abalone production in South Africa has become is very important due to its high economic value and the intention to protect this species due to illegal harvesting (Troell *et al.,* 2003). In 2004, abalone production reached a peak of 6 000 tons harvested (Robertson-Andersson *et al.,* 2008). South African abalone farms are located to the west of Cape Agulhas, the southernmost point of Africa (Figure 2.17) (Troell *et al.,* 2006; Bolton *et al.,* 2009). Two more farms are located further in the east namely the Marine Growers near Port Elizabeth and the Wild Coast Abalone at Haga Haga near East London.

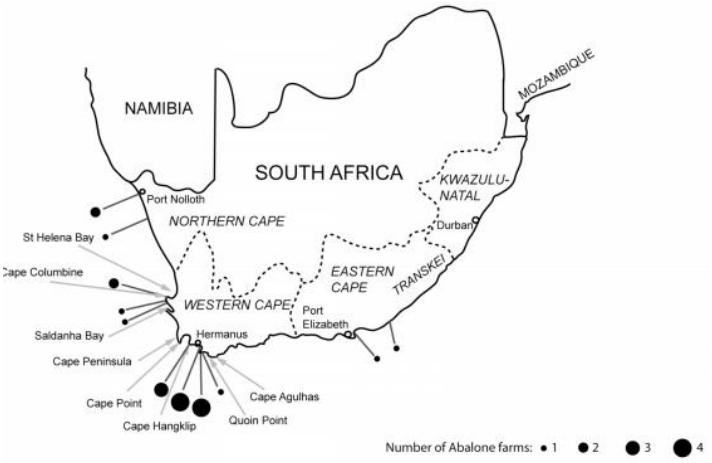

Figure 2.17: Abalone production farms in the west coast of South Africa (Maneveldt *et al.*, 2008).

Experimental studies in the cultivation of Wild Coast Abalone started at first with *Gracilaria* (red algae) (Fourie, 1994; Smit, 1997), and then later *U. lactuca* (Steyn, 2000) for abalone feed addition. Following this success, Wild Coast Abalone started producing large quantities of *Ulva*, becoming one of the largest producers in the world (Bolton *et al.*, 2009) with a series of 32 farms built in 1992 for growing *U. lactuca* and *Gracilaria*. This incorporated abalone/*Ulva* system yields *ca.* 2.5 tons of *Ulva* per working day for the entire year (Robertson-Andersson *et al.*, 2008).

2.5.6. Chemistry of *U. lactuca*

A study was carried out by Yaich *et al.* (2011) to determine the chemical composition and functional properties of the dried *U. lactuca* seaweed collected from the shoreline between the Taboulba and Sayada area in Tunisia. The soluble, insoluble and total dietary fibre content, mineral amount, amino acid and fatty acid profiles, swelling capacity (SWC), water holding capacity (WHC) and oil holding capacity (OHC) of the dried *U. lactuca* algae was investigated. It was found that the *U. lactuca* powder contained a high fibre content (54.0%), minerals (19.6%), proteins (8.5%) and lipids (7.9%) (Yaich *et al.*, 2011). The neutral fibres comprised of hemicellulose (20.6%), cellulose (9.0%) and lignin (1.7%), while the protein content analysis

showed that it contains essential amino acids, which represent 42.0% of the total amino acids. During the fatty acids profile analysis, it was found that the most constituent fatty acids are palmitic acid (60%), followed by oleic acid (16.0%). It was further revealed that the functional properties proved that SWC, WHC and OHC of *U. lactuca* differs with temperature and are comparable to those of some commercial fibre rich products (Yaich *et al*., 2011). Saritha *et al.* (2013) reported that *U. lactuca* has high protein content of 20.8% followed by carbohydrates with 13.2% then 4.4% lipid content. The fibre and protein content therefore implies that it could act as a rich dietary source for animals.

Ulvan is the main water-soluble polysaccharide found in the cell wall of green seaweed of the order Ulvales (*Ulva* and *Enteromorpha sp.).* About 8–29% of the algae dry weight is represented by ulvan (Robic *et. al.*, 2009), comprising sulfate, rhamnose, xylose, iduronic and glucuronic acids as major components (Lahaye and Ray, 1996; Percival and McDowell; 1967). Ulvan has been shown to have a structure with greater complexity and variability with the polysaccharides containing repeating units (Lahaye and Robic, 2007). The two major repeating disaccharide sequences of ulvan are ulvanobiouronic acid 3-sulfate composed of either glucuronic or iduronic acid (Figure 2.18). Furthermore, there are minor repeating units made up of sulfated xylose substituting the uronic acid or glucuronic acid as a branch on O_2 of the rhamnose-3-sulfate (Lahaye and Ray, 1996; Percival and McDowell, 1967; Lahaye *et al.*, 1997).

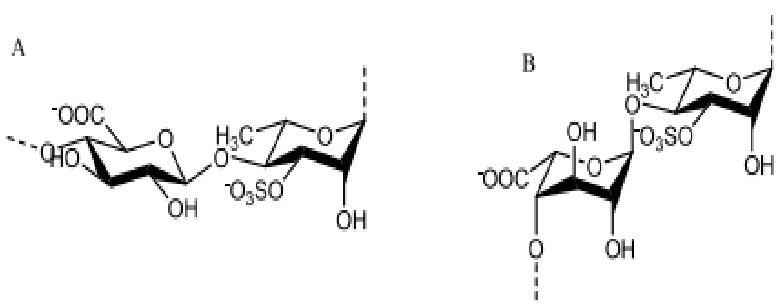

Figure 2.18: The main repeating disaccharide units of ulvan. A. [→4)-β-D-Glcp-(1→4)-α-LRhap3S-(1→]n; B. [→4)-α-L-Idop-(1→4)-α-L-Rhap3S-(1→]n. (Jiao et al., 2011).

2.5.7. Bioactivity of compounds isolated from *U. lactuca*

In recent years, bioactive compounds have been isolated from seaweeds all over the world and they are used as antibiotics, laxative, anticoagulants, antiulcer products and suspending agents in radiological preparation (Rajasulochana *et al.,* 2009). Algae contains a high content of amino acids, terpenoids, phlorotannins, steroids, phenolic compounds, halogenated ketones and alkanes, cyclic polysulphides, fatty acids, acrylic acid (Mtolera and Semesi, 1996; Taskin *et al*., 2007), proteins, polysaccharides, vitamins, minerals and fibres (Lahaye, 1991; Darcy-Vrillon, 1993). Marine green algae have been reported several times to have the antibacterial (Lavanya and Veerapan, 2011), antiviral (Trono, 1999), antifungal (Oumaskour *et al.,* 2012), anticoagulant (Yasantha *et al.*, 2007), antitumor and anti-inflammatory (Scheuer, 1990) activities. Alginate, carrageenan and agar isolated from seaweeds have been used for medicinal and pharmaceutical purposes (Siddhanta *et al.,* 1997).

The pharmaceutical potential of seaweeds is indicated by the presence of several secondary metabolites. In a study carried out by Manchu *et al.* (2014) in investigating the phytochemicals of three *Ulva* species, glycosides, carbohydrates, steroids, terpenoids and phytosterols were detected in all three seaweeds. Additionally, the *Ulva lactuca* and *U. intestinalis* samples showed the presence of flavonoids, quinones and proteins. *U. intestinalis* was found to be a better resource for bioactive compounds than *U. lactuca* and *U. fasciata* (Manchu *et al.,* 2014). Thus it is apparent that the in-depth chemistry of *U. lactuca* is not well known.

Ulvan is a soluble sulfated polysaccharide found in the cell wall of *Ulva* as previously explained section 2.26. Ulvan plays an important role in *Ulva* survival by its ability to produce allelopathic substances that prevent the growth of epiphytes thus it is able to compete for nutrients and light against phytoplankton and pathogens. Ulvan has other biological activities such as antioxidant, antimicrobial and antiviral properties (Ortiz *et al.,* 2006; Abd El-Baky *et al.,* 2008; Ale *et al.,* 2011).

Chapter 3 Screening of aqueous extracts for the synthesis of gold nanoparticles

Summary

To facilitate the selection of a suitable seaweed for AuNP production, several seaweeds were randomly selected and their aqueous extracts prepared. This chapter therefore discusses the screening of the aqueous extracts prepared from different seaweeds to determine their capacity to produce AuNPs. The aqueous extracts which were deemed promising were characterized using FTIR and UV-vis spectroscopies. The antioxidant, reducing power and radical scavenging capabilities of these extracts were also determined and related to their ability to produce NPs.

3.1. Introduction

One of the main goals of nanotechnology is to synthesize metallic NPs which are eco-friendly and biocompatible in a reproducible manner. As previously discussed in Chapter 1, metallic NPs are conventionally synthesized using numerous chemical and physical methods. Most of these methods are known to be expensive, inefficient in material usage and they have a high energy consumption. Thus, the future of nanotechnology is highly focused on green synthetic methodologies for NPs; in using methods which are not harmful to the environment and do not possess health risks to humans. Therefore, the demand for developing cleaner, harmless and environmentally benign production methods is ever increasing (Shankar *et al.*, 2004; Parial *et al.*, 2012).

In recent years, different algal extracts from the families Chlorophyta (green seaweeds), Rhodophyta (red seaweeds), and Phaeophyta (brown seaweeds) have been proposed for use in the synthesis of metallic NPs such as AgNPs and AuNPs (Sharma *et al.*, 2016). This was mainly due

ability of seaweeds to carry out the reduction of metal salts, which may be due to the presence of phytoconsitutents such as polysaccharides, phenolic compounds, proteins/enzymes and other chelating agents (Manivasagan and Kim, 2015). The NPs synthesized using seaweeds extracts possess the morphology, size and stability which make them applicable for biomedical and environmental applications (Singaravelu *et al.*, 2007).

NPs exhibit unique optical, chemical, photoelectrochemical and electronic (Krolikowska *et al.*, 2003; Kumar *et al.*, 2003; Chandrasekharan and Kamat, 2000; Peto *et al.*, 2002) properties which makes them incredibly important. These unique properties strongly depend on their size and shape (Alivisatos, 1996), while the unique optoelectrical properties of AuNPs makes them valuable in diverse fields such as electronics, colourings, coatings, catalysis as well as in the biomedical areas (Huang *et al.*, 2003, Xu *et al.*, 2004).

The applications for AuNPs in various fields is intimately tied to their size to shape ratio. The optical properties of the Surface Plasmon Resonance (SPR) band for AuNPs is directly dependent on the size of the AuNPs produced; i.e. AuNPs which are 20 nm in size display an orange-red colour which steadily shifts to blue as the particle size increases to 100 nm (Link and El-Sayed, 1999; Kreibig and Vollmer, 1995). Thus, the SPR band changes as the size and shape changes. Recently, efforts have been made towards understanding how organisms accumulate gold and how they convert the gold to non-toxic AuNPs (Mehta and Gaur, 2005).

Brown algal aqueous extracts have been employed in the synthesis of AuNPs in several studies. Singaravelu *et al.* (2007) reported the synthesis of AuNPs using brown algae *Sargassum wightii* extracts, while Vijayan *et al.* (2014) showed that Au(III) ions can be reduced to Au(0) by *Turbinaria conoides* aqueous extract. A *Fucus vesiculosus* extract was also found to produce AuNPs (Mata *et al.*, 2008). Interestingly, AuNPs syntheses using the green algae *Pithophora oedogonia*, have also been reported (Li and Zhang, 2016). Other classes of brown, green and red algae that have been used in the synthesis of AuNPs have already been discussed in Chapter 2.

Despite the large number of reports available in the use of algal extracts in the synthesis of metallic NPs, there are many others that have not been described. The aim of this study was to screen a number of aqueous extracts of red, green and brown algae as model biological systems for the production of AuNPs and to characterize these NPs for potential future applications in nanotechnology. Screening was carried out on the basis of (1) the capability of the seaweed extract to produce gold nanoparticles and (2) the time required for bioconversion.

3.2. Methodology

3.2.1 Seaweeds collection, preparation and chemicals

All marine seaweeds were obtained from Sea Point Coastal area in Cape Town, South Africa. The collected algae were washed with distilled water and stored at -20 °C until further use. Folin-Ciocalteu (F-C), sodium carbonate (Na_2CO_3), gallic acid, potassium ferricyanide, phosphate buffer, trichloroacetic acid (TCA), ferric chloride ($FeCl_3.6H_2O$), ascorbic acid, 2,2-diphenyl-1-picrylhydrazy (DPPH), butylated hydroxytoluene (BHT), gold(III) chloride trihydrate ($HAuCl_4 \cdot 3H_2O$) were all purchased from Sigma Aldrich. All aqueous solutions were prepared using MilliQ water (18 mΩ, Millipore).

3.2.2. Preparation of extracts

The aqueous extracts of eleven different algae (listed in Table 3.1) were prepared and these were screened for their ability to produce AuNPs. The pure algal aqueous extracts to be screened for NP syntheses were prepared by adding 1 g of the freeze-dried, powdered algae into 100 mL of distilled water, followed by boiling at 100 ^{o}C for 20 min in a 250 mL Erlenmeyer flask. These extracts were allowed to cool and then filtered through Whatman No. 1 Filter paper and the supernatant stored at -20 °C until further use.

Table 3.1: List of algae, the sample codes, seaweed class, scientific name and time taken for the characteristic pink colour attributed to AuNPs to develop, with the brown aqueous extracts being the only ones that showed the ability to produce the AuNPs

Sample codes	**Seaweed**	**Scientific name**	**Time produce AuNPs (min)**
1. NDK100328-3	Brown	*Sargassum incisifolium*	50
2. NDK130821-1	Brown	*Sargassum incisifolium*	70
3. PA100331-6	Green		
4. UWC150619	Red	*Laurencia glomerata*	
5. UWC150619-2	Red		
6. SB20140302-6	Red		
7. SB20140303-3	Red	*Portieria hornemanii*	
8. SB20140302-3	Brown	*Dictyota naevosa*	200
9. DO20140301-2	Red		
10. SB20140302-5	Green		
11.**Ulva*	Green	*Ulva lactuca*	

*no code given

3.2.3. Characterization of aqueous extracts

3.2.3.1. UV-vis spectroscopy

UV-vis spectra of the aqueous extracts of those extracts which produced AuNPs i.e. SB2014, NDK100 and NDK130 were measured using an Agilent Cary 60 UV-vis Spectrophotometer (Agilent Technologies, USA) in the wavelength range of 200 nm to 800 nm. Briefly, 100 µL of the extract was added to 2.9 mL of distilled water in a cuvette with 1 cm pathlength for UV-vis analysis.

3.2.3.2. FTIR spectroscopy

The freeze dried aqueous extracts were analyzed on a Perkin-Elmer Spectrum 400 spectrophotometer (using the Spectrum software) using an ATR accessory.

3.2.3.3 NMR spectroscopy

NMR spectra (^{1}H and HSQC) were acquired on a Bruker 400 MHz Avance IIIHD Nanobay spectrometer equipped with a 5 mm BBO probe at 333K using standard 1D and 2D NMR pulse sequences. All spectra were referenced to residual undeuterated solvent peaks at 60 $^{\circ}$C.

3.2.3.4. Antioxidant, reducing power, radical scavenging properties of the aqueous extracts

3.2.3.4.1 Determination of total phenolic content

Total phenolic content of the three extracts (SB2014, NDK100, and NDK130) was determined following the protocol used by Tobwala *et al.* (2014), which depends on the development of a bluish-grey complex between the Folin-Ciocalteu reagent (F-C reagent) and the phenols. An amount of 125 µl of the plant extract was added to 625 µl of the F-C reagent that was diluted 10-fold. The mixture was incubated at room temperature for 5 minutes followed by the addition of 500 µl of 75 mg/mL Na_2CO_3 solution. The mixture was briefly vortexed and further incubated at room temperature for 90 min. The samples were added to a 96 well microtiter plate in triplicate and the absorbance measured at 760 nm against a blank/control using gallic acid as a standard. The concentration of the extracts was measured as µg of gallic acid equivalents (GAE)/mg.

3.2.3.4.2 Determination of total reducing power

The total reducing power of the algal extracts were determined using the procedure previously described by Tobwala *et al.* (2014). Briefly, 2.5 mL of 0.2 M phosphate buffer (pH 6.6) and 2.5 mL of a 1% potassium ferricyanide solution were added to 1 mL of the algal extract and gently mixed. The mixture was incubated at 50 ^{0}C in a water bath for 20 min followed by the addition of a 10% trichloroacetic acid (TCA) solution followed by centrifugation at 6 000 rpm for 10 min. 2.5 mL of the supernatant was drawn and transferred into a 15 mL centrifuge tube containing 2.5 mL of distilled water and 0.5 mL of 0.1% ferric chloride ($FeCl_3.6H_2O$). The mixture was mixed well and incubated for 5 min followed by measurement of the absorbance as described above but with ascorbic acid as the standard. The concentrations were calculated as milligrams of ascorbic acid equivalent (AAE)/mg of dried plant material.

3.2.3.4.3. Determination of radical scavenging power

The radical scavenging power of the same three extracts were evaluated using the Tobwala *et al.* (2014) protocol. Briefly, 2.9 mL of DPPH (1×10^{-4} M) was mixed with 100 µL of the corresponding algae extract. The solutions were kept in the dark at room temperature for 30 min followed by measurement of the absorbance at 520 nm against blanks. The radical scavenging power was measured as [1 - A1÷A2] × 100%, wherein A1 and A2 are the absorbance with and without plant extract, respectively. Butylated hydroxytoluene (BHT) was used as the standard.

3.2.4. Biosynthesis of gold nanoparticles

In a typical synthetic process for the AuNPs, 5 mL of an aqueous algal extract was added to 45 mL of a 1 mM gold chloride solution in a 250 mL conical flask. The reaction mixture was kept at room temperature with mechanical stirring. The time taken for a change in colour from yellow

(gold salt solution) to pink (AuNPs solution) was noted and the sample allowed to stir for a further 1 h. The formation of the AuNPs was also monitored using a Cary 60 UV-vis spectrophotometer (Agilent Technologies).

3.2.5. Characterization of the synthesized AuNPs

UV-vis spectroscopic measurements were performed using the wavelength range of 200 nm to 800 nm by adding 300 µL of the algal extract that produced the AuNPs and 2.7 mL of water into a quartz cuvette. The reaction was allowed to proceed for 6 hours with the absorbance measured every 10 min. This data was collected and used to determine the rate at which the AuNPs were formed. The stability of the AuNPs was determined by using the Malvern Zetasizer (Malvern, USA).

Microscopic analysis was carried out to reveal nanoparticle sizes and shapes using an HRTEM Tecnai F20 with a field-emission gun (FEG) operating in bright field mode at 200 kV coupled with EDX revealing the elemental composition of the AuNPs. A drop of AuNPs was placed on the carbon-coated copper grid, making a thin film of sample on the grid which was allowed to dry. ImageJ was used to measure NPs size in TEM images. FTIR spectroscopy was used to identify the characteristic peaks associated with the metabolites present in the algae aqueous extracts that managed to produce the AuNPs.

3.3: Results and discussion

3.3.1. Preparation and characterization of the algal aqueous extracts

3.3.1.1. UV-vis spectroscopy

Preparation of the seaweed aqueous extracts resulted in the formation of brown coloured extracts as shown in Figure 3.1 where the differences in the colour intensity for each of the extracts can be

seen. NDK130 is the most intense followed by NDK100 and SB2014, respectively. It is assumed that the brown colour of these extracts is likely due to the presence of the water soluble polyphenolic compounds and polysaccharides (although these are optically transparent), since all these algae are brown algae (Mmola *et al.*, 2016).

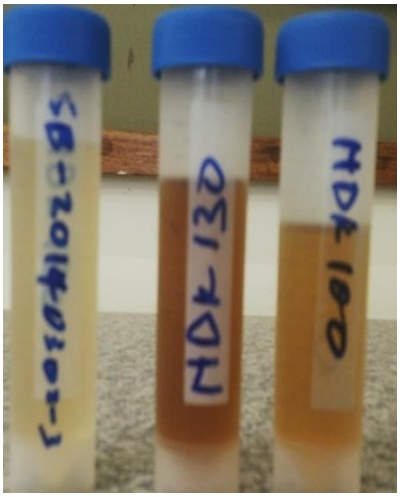

Figure 3.1: Images illustrating difference in colour intensity of the aqueous extracts using the algae SB2014, NDK130 and NDK 100 respectively.

The UV-vis absorption spectra of the prepared extracts are shown in Figure 3.2. It is clear that the extract with the most intense colour (NDK130) revealed the strongest absorption followed by NDK100 and then SB2014 as expected. All three samples revealed a λ_{max} absorption at ~273 nm. The data suggests that the darker the extract, the greater the amount of polyphenolic content, which was later confirmed by the determination of the polyphenolic content for these extracts (as given in Section 3.3.1.3.1). However, the colour of the extracts show minimal interference with the SPR band of the synthesized AuNPs since this band is usually between 520 and 550 nm (Gherbawy *et al*., 2013; Huang & El-Sayed, 2010; Jones *et al*., 2011).

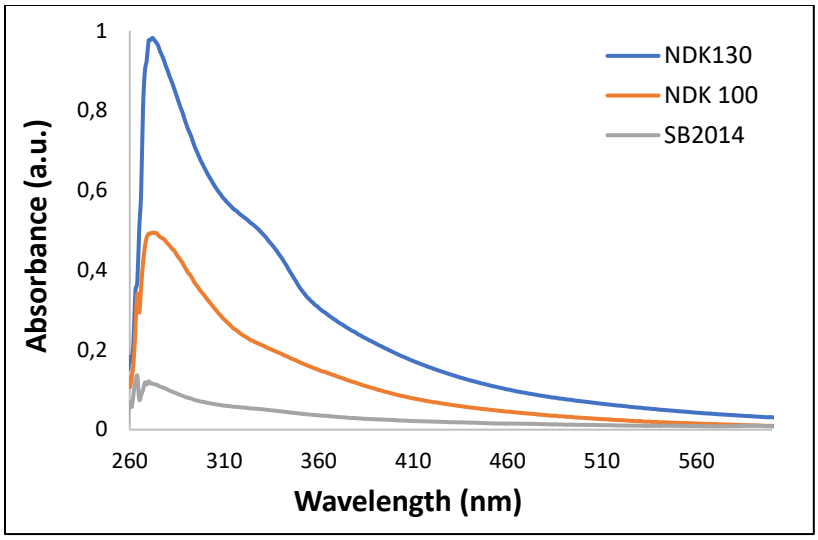

Figure 3.2: UV-vis absorption spectra for NDK130, ND100 and SB2014 respectively starting from the one with maximum absorbance.

3.3.1.2. FTIR spectroscopy

FTIR spectroscopy was used to compare the three aqueous extracts. The extracts appear to have the same chemical make up as can be seen in Figure 3.3. The only noticeable difference is mainly the relative transmittance of all the extracts which could be due to the concentration of biomolecules in them but not the molecular composition (Mmola *et al.*, 2016). It could be explained due to the fact that the extracts evaluated were all brown seaweeds.

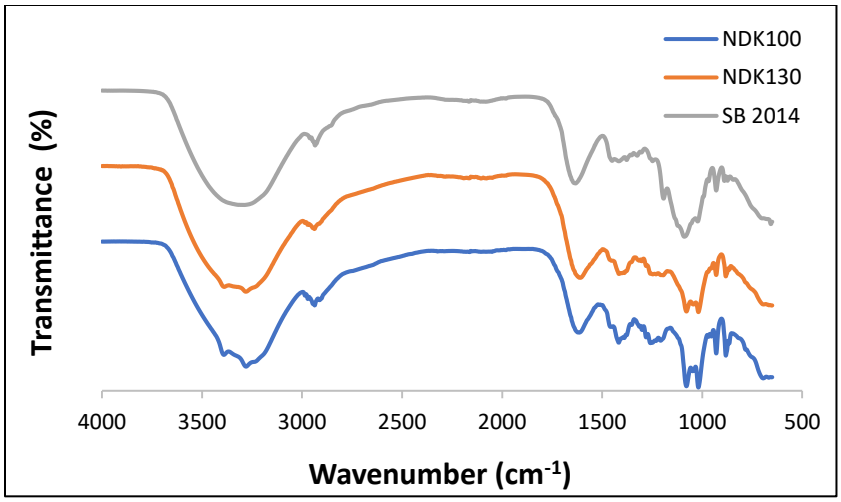

Figure 3.3: FTIR spectra of AuNPs synthesized using SB2014, NDK130 and NDK100 algae extracts.

3.3.1.3. NMR spectroscopy

Further comparison of these reducing agents was accomplished by NMR and the edited HSQC spectra are shown in Figures 3.4 and 3.5 for NDK130 and SB2014, respectively. The HSQC NMR spectra provide information about direct ^{1}H-^{13}C correlations. The purpose of this analysis was not to assign the structures of the polyphenols or polysaccharides present in the aqueous extract, but rather to provide a basis to allow one to identify the different structural features of the different extracts. In addition, using the edited HSQC, one can easily distinguish between methyl, methylene and methine signals. The large number of overlapping proton signals makes the analysis of the ^{1}H NMR spectrum (x-axis) very difficult.

However, the carbon signals (y-dimension) provide a significant amount of information. Firstly, methyl signals at ~ δ 18 is clearly apparent in Figure 3.4 for the NDK130 sample as are the sugar oxymethine carbons between δ 60 and 80. Finally, the anomeric carbons of sugars are visible around δ 100. Additionally, upon comparison of the two HSQC, significant differences in the HSQC spectra of NDK130 and SB2014 are immediately apparent in that the former contains many

signals in the aromatic region (δ_C 110-130 and δ_H 6-8), which are absent in the SB2014 sample. It is clear that the signals present suggest that the polysaccharides (δ_C 60-80 and δ_H ~3.5) are the major constituents in these extracts, whereas the polyphenols/phlorotannins are the minor constituents.

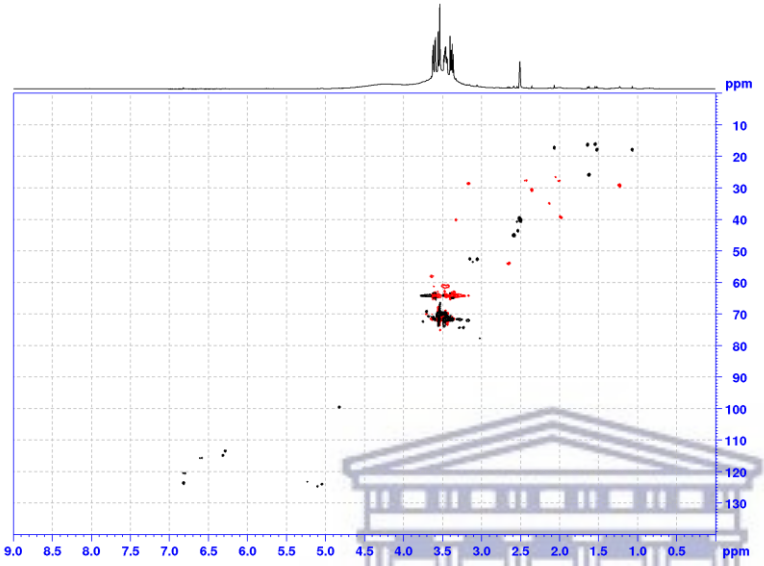

Figure 3.4: HSQC NMR spectra obtained for NDK130 obtained in D_2O at 60 ^oC.

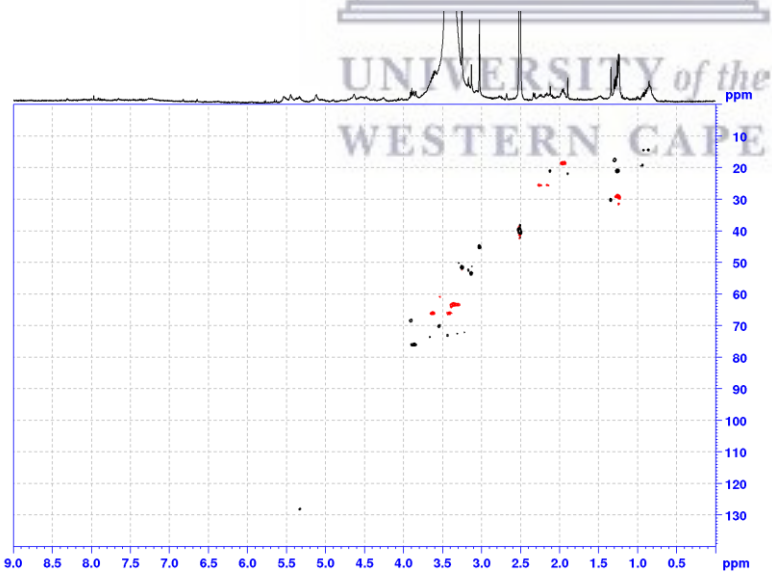

Figure 3.5: HSQC NMR spectra obtained for SB2014 obtained in D_2O at 60 ^oC.

3.3.1.4. Antioxidant, reducing power, radical scavenging properties of the aqueous extracts

3.3.1.4.1. Total phenolic content

The total phenolic content was used to determine using aqueous extract from three algae (SB2014, NDK100 and NDK130) prepared in using distilled water as a solvent. The total phenolic extracts of each algae are expressed as µg gallic acid equivalent/mg for each of the extracts is shown in Table 3.2. NDK130 appeared to be to the algae with the highest polyphenolic content (0.76 µg GAE/mg) followed by NDK100 and finally SB2014 with 0.14 □g GAE/mg). These data agree with the intensity of the absorption curves obtained in the UV-vis spectra and the colour observed for the various algal extracts.

Table 3.2: Total polyphenolic content and total reducing power for the aqueous extracts of SB2014, ND100 and NDK130.

Extract	Total Polyphenolic Content (GAE, in µg/mg of dried leaves)	Total Reducing Power (AAE, in µg/mg of dried leaves)
SB2014	0,143	0,379
NDK100	0,691	0,312
NDK130	0,761	0,734

3.3.1.4.2. Total reducing power

The reducing power is related to the antioxidant activity and can be used to assess the antioxidant potential of a sample (Tobwala *et al.,* 2014). The total reducing power of the extracts obtained for the algae are also shown in Table 3.2 with the largest reducing power obtained in the following order: NDK130 > NDK100 > SB2014. Total reducing power of NDK130 was 0,734 µg ascorbic

acid equivalent/mg, which was twice that of NDK100 and SB2014. It is therefore expected that this extract will have greater capacity to reduce the metal salt producing AuNPs (most likely through the concentration of reductants in the extract, hence stronger UV absorbance commented on above). .

3.3.1.4.3. Radical scavenging power

Free radical scavenging power plays a crucial role during the evaluation of the protective effects due to the toxicity of free radical biological systems. DPPH is often used to evaluate the radical scavenging power of various compounds (Bradford, 1976). Its follows the principle of the ability of antioxidants to reduce the DPPH radicals which results in the formation of a more stable DPPHH form (Tobwala *et al.,* 2014). When the radical scavengers are present, it results in the reduction of DPPH and therefore the corresponding absorbance is decreased. The DPPH scavenging activities of aqueous extracts of three different algae (SB2014, NDK100 and NDK130) are shown in Figure 3.6. Since all the extracts were prepared in same solvent (distilled water) it implies that the difference in scavenging activities was affected by the type of alga used as follows: NDK130 > NDK100 > SB2014. As before, the NDK130 extract showed a highest activity with the highest radical scavenging ability (29%) among the three brown algal extracts used.

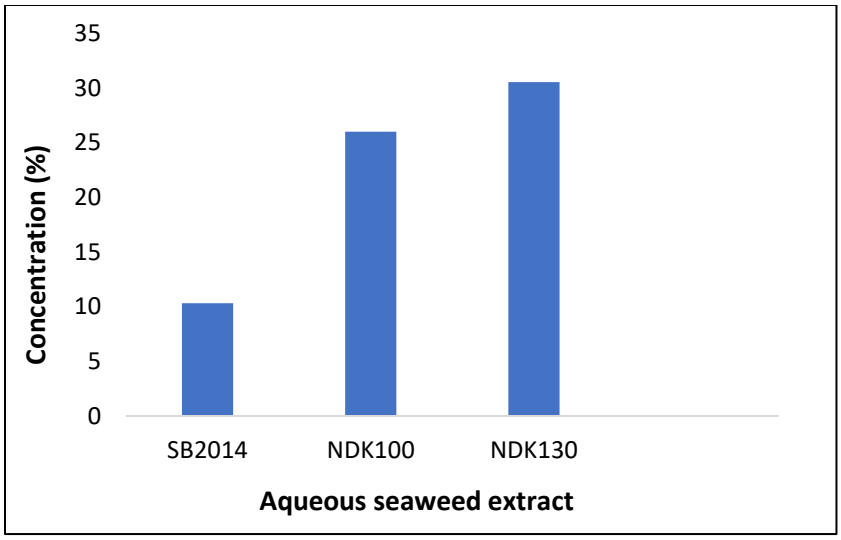

Figure 3.6: The DPPH radical-scavenging activity of aqueous extracts of SB2014, NDK100 and NDK130. The absorbance values were converted and expressed as a percentage and the data plotted as the mean of the triplicate scavenging effect (%).

3.3.2. Synthesis and characterization of AuNPs

3.3.2.1. Visual observation

Of the eleven aqueous extracts used, it was found that only three brown algal extracts were able to produce AuNPs and interestingly, only the aqueous extracts of brown algae were able to produce AuNPs, which may have been caused by the presence of certain water soluble reductant species in the brown algae which are not found in green and red algae in the study. The colour of the aqueous extracts before addition of the gold chloride solution is shown in Figure 3.7 (A) in the following order from left to right: *Dictyota naevosa* (SB2014), *Sargassum incisifolium* (NDK100) and *Sargassum incisifolium* (NDK130). The difference between the two Sargassum samples is that they were collected at different times of the year (i.e. different seasons)

The main components comprising the extracts were discussed earlier in Section 3.3.1.3. Figure 3.7 (B) shows the ruby red colour attributed to the successful formation of the AuNPs, where the NDK extract shows the deepest colour (Figure 3.7 (B)). This may be attributed to the fact that this extract also possessed the greatest polyphenolic content, reducing power and radical scavenging ability, since it was expected that this extract would produce the AuNPs with relative ease compared to the other two extracts. Formation of the NPs were confirmed using UV-vis spectroscopic analyses which revealed the presence of the surface plasmon resonance (SPR) band of the AuNPs at ~530 nm.

The characteristic pink colour of the AuNP solution and the presence of the SPR band is a result of collective oscillations of free electrons caused by an interacting electromagnetic field in metallic NPs (Mulvaney, 1996). The change in colour of the solution was observed within 20-30 min and the reaction was allowed to proceed for 2 hrs – all at room temperature and pressure conditions. In the past few years, marine seaweeds have been recognized as a possible source for synthesizing NPs, with numerous reports available for the synthesis of AuNPs using algae extracts. Singaravelu *et al.* (2007) synthesized AuNPs using a *Sargassum wightii* aqueous extract using a 15 h of incubation time. Furthermore, Mmola *et al.* (2016) also synthesized AuNPs using *Sargassum incisifolium* aqueous extracts within 50 min. The above mentioned algal extracts were found to produce AuNPs much more rapidly i.e. within 50-120 min.

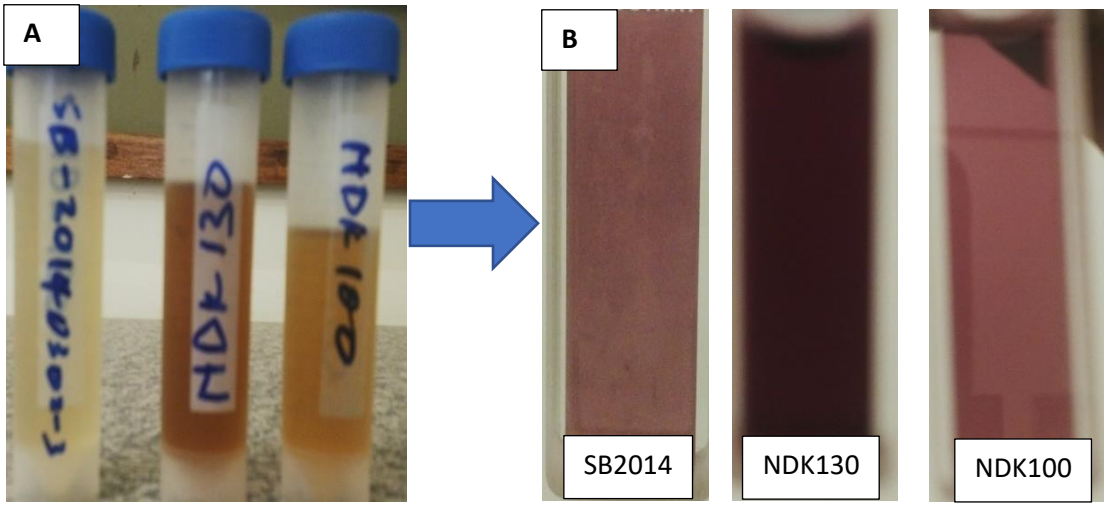

Figure 3.7: Visual observation of the formation of AuNPs where the colour change was observed after 1 h. The aqueous extracts of the three extracts observed to produce NPs (A) before addition of the gold salt solution and (B) the change in colour of the solutions 1 hr after addition of the gold salt solution.

3.3.2.2. UV-vis spectroscopy

To provide a better understanding of the AuNPs formation process, the time dependent increase of the SPR absorption band at ~540 nm was monitored. These UV-vis spectra are shown in Figure 3.8 (A-C). During the synthesis of the AuNPs, an increase in the reaction time generally showed an increase in the SPR absorbance from t = 0 to t = 6 h. The maximum absorbance peaks for the synthesized AuNPs after 6 hrs were recorded at 544 nm, 537 nm and 553 nm for SB2014, NDK100 and NDK130, respectively. The SPR band for the NDK130 extract was the most red shifted, while that of the SB2014 extract was the most blue shifted. The SPR band is highly sensitive to the nature, size, and shape of the formed NPs as well as the interparticle distance and surrounding media (Shetty *et al.*, 2006; *Liebig et al.*, 2016). Upon comparison of the UV-vis spectra for each of the extracts, unexpectedly, it became apparent that the SPR band for the NDK100 extract was well resolved and sharp, while that of the SB2014 and NDK130 (Figure 3.8 A and B respectively) extracts the SPR bands remained quite broad, with the absorption spectrum dipping below 0 at approximately 500 nm. This is likely due to scattering as AuNPs may be crashing out of solution.

Based on the shape and position of the SPR bands for NDK130 and SB2014 in particular, it was expected that the AuNPs produced would have a variety of shapes and sizes. This was later confirmed by TEM. The observed maximum absorption peak at ~540 nm was further used to construct the absorption vs. time graphs for the rate of formation of the AuNPs (Figure 3.9).

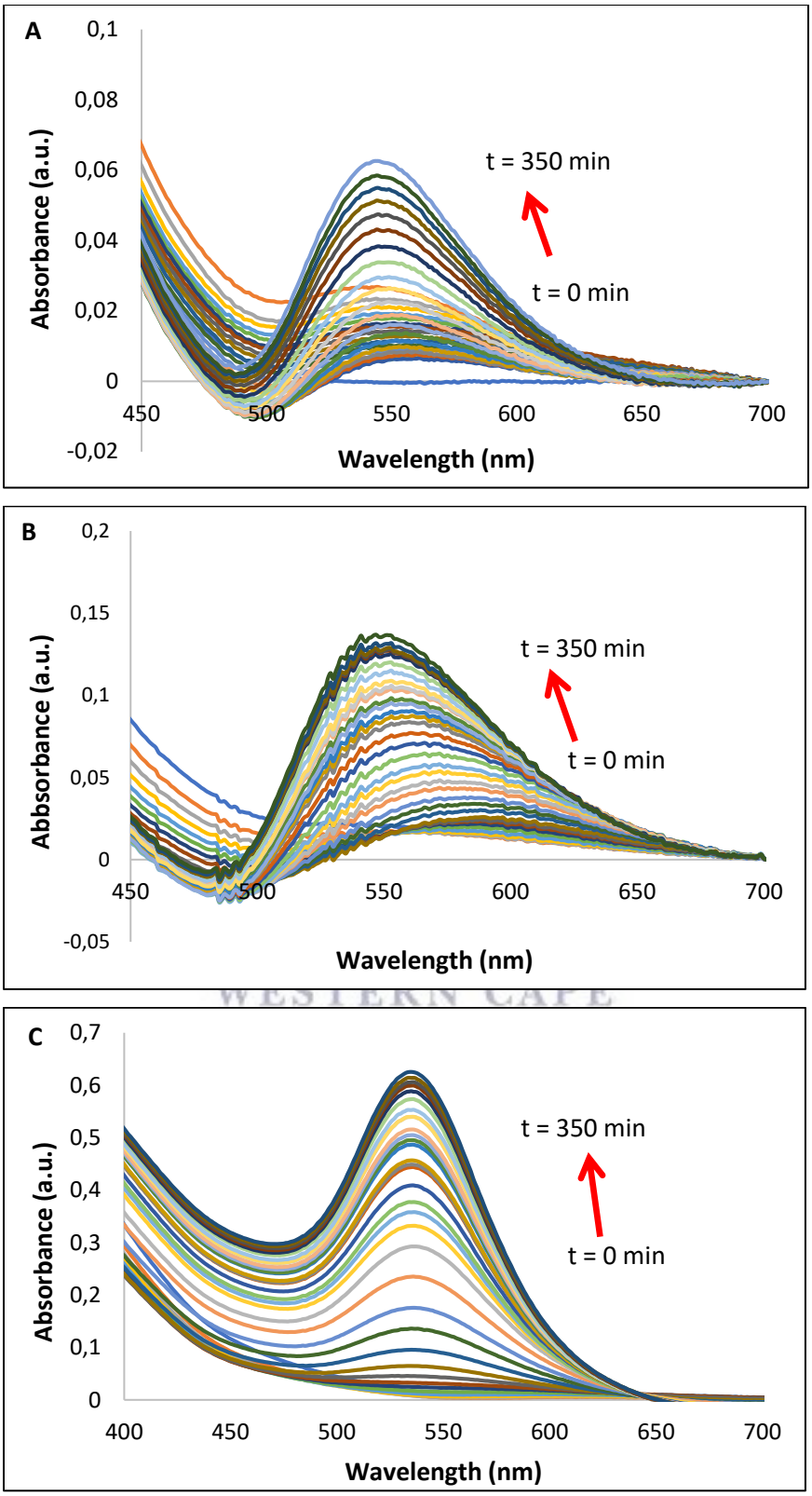

Figure 3.8: Time-dependent absorption measurements during gold nanoparticle syntheses using the aqueous extracts of (A) SB2014 (B) NDK130 and (C) NDK100 over a period of 6 hours.

3.3.2.3. Rate of formation of the AuNPs for each of the aqueous extracts

To analyze the speed of formation of the AuNPs after addition of the three aqueous extracts into the gold chloride solution UV-vis spectroscopy was used to monitor the reaction. 2.7 mL of a 1 mM gold salt solution was mixed with 300 µL of each of the algal aqueous extracts and the UV-vis spectra recorded every 10 min for 6 h. The maximum absorption for the SPR bands of each extract at each time interval was then plotted against time and these curves are shown in Figure 3.9.

Figure 3.9 shows the rate of formation curve for SB2014 extract which was obtained at 544 nm. It shows that the AuNPs only started to form after an induction period at about 2 hours, where they then started to form at an exponential rate. At 360 min it appears the NP formation is starting to level off, but the reaction was stopped due to time constraints before this was confirmed. However, a different trend was observed using NDK130 and NDK100 as shown in Figure 3.9, where it was observed that it took approximately 100 min and 50 min for the extracts respectively, for the AuNPs to start forming. The AuNP formation with NDK100, with the greatest change in absorbance, was particularly clear. Although it was expected that the NDK130 extract would produce the most NPs with greater efficiency (from the total polyphenolic and reducing power contents), this may be due to the NPs crashing out of solution (as observed by the dip at 500 nm in the UV-vis spectra of NDK130 Figure 3.8B). The same is true for the SB2014 extract, although this sample consistently possessed the least total polyphenolic and reducing power content. The data in Figure 3.8 therefore does not correspond to the colour change observed for the samples or with the total reducing and polyphenolic contents determined previously.

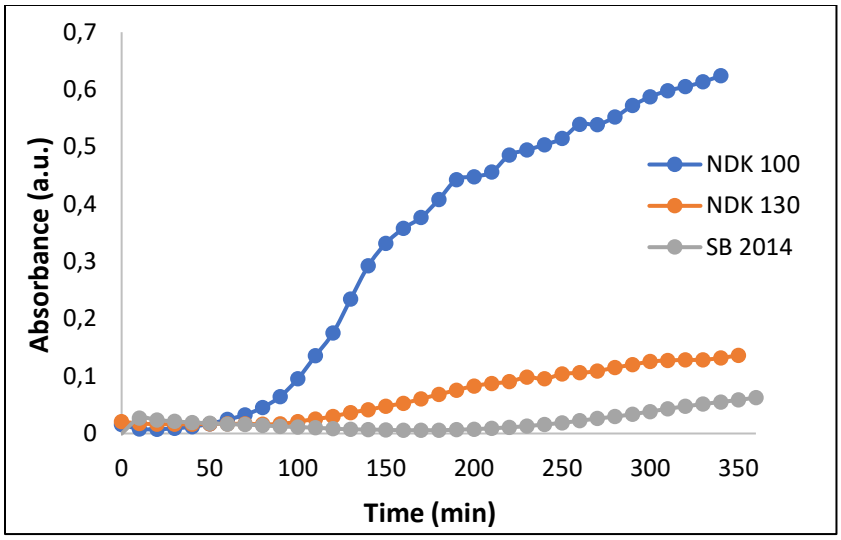

Figure 3.9: Rate of formation of NPs using the □$_{max}$ values for the SPR bands vs. time for each of the three algal extracts SB2014, NDK 130 and NDK100 at λ_{max} = 544, 553 and 537 nm, respectively.

3.3.2.4. Zeta-potential measurements

The zeta potential measurements for the synthesized AuNPs was determined using a Malvern Zetasizer after three days of synthesis and the values are found in Table 3.3 for all three algal extracts used. It can be observed that the zeta-potential values for the AuNPs listed below exhibit a negative potential charge on their surface. Although, it has been reported that for the NPs to be regarded as stable, their zeta potential values should be greater than +30 mV or lower than -30 mV (Koteswari *et. al.*, 2011). However, the NPs produced using our three extracts are not within the cut-off range which implies they are not stable, hence the chances of the NPs agglomerating and limiting their applications is high.

The zeta potential values exhibited by the SB2014 AuNPs is very close to zero (-1.36 mV) which shows that they are very unstable and this was also observed by quick colour change to blue within approximately four days of synthesis. However, the NDK100 and NDK130 AuNP samples have a zeta potential of -27.8 and -23.2 mV, respectively, which shows that they relatively stable. There

are few reports wherein unstable NPs have been stabilized by the use of a capping agent which then reduces their agglomeration, although it is assumed in this study that the polysaccharides present in the aqueous extracts are capping the NP. However, all the nanoparticles synthesized had a zeta potential within the cut-off range.

Table 3.3: Zeta potential measurements obtained for the AuNPs

Nanoparticle type	Zeta potential (mV)
SB2014	-1.36 ± 7.99
NDK100	-27.8 ± 9.09
NDK130	-23.2 ± 1.3

3.3.2.5. HRTEM analyses

HRTEM analyses provided some insight into the morphology and sizes of the AuNPs synthesized using the aqueous extracts of the algae SB2014, NDK100 and NDK130. The AuNPs formed possessed different shapes showing spherical, hexagonal and triangular NPs of different sizes when using the three different algae extracts as shown in Figure 3.10. The synthesized AuNPs were small in size, particularly for the spherical NPs, while the triangular and hexagonal shaped NPs were larger in size with diameters ranging from 30 to 50 nm for all three extracts. In comparison to other studies done by Raghunandan *et al.* (2009), Rajeshkumar (2013), Mmola *et al.* (2016), Noruzi *et al.* (2011), the brown algal aqueous extracts used to form AuNPs also revealed different shapes such as spherical, triangular and pseudo-spherical shapes with size ranging between 15 and 50 nm, similar to what was found in the current study. In the same way, Ghodake and Lee (2011) produced the AuNPs with same shapes with size diameter ranging between 15 and 20 nm with an SPR band at 530 nm. This suggests that brown algae are more likely to produce AuNPs of different shapes with smaller particles sizes.

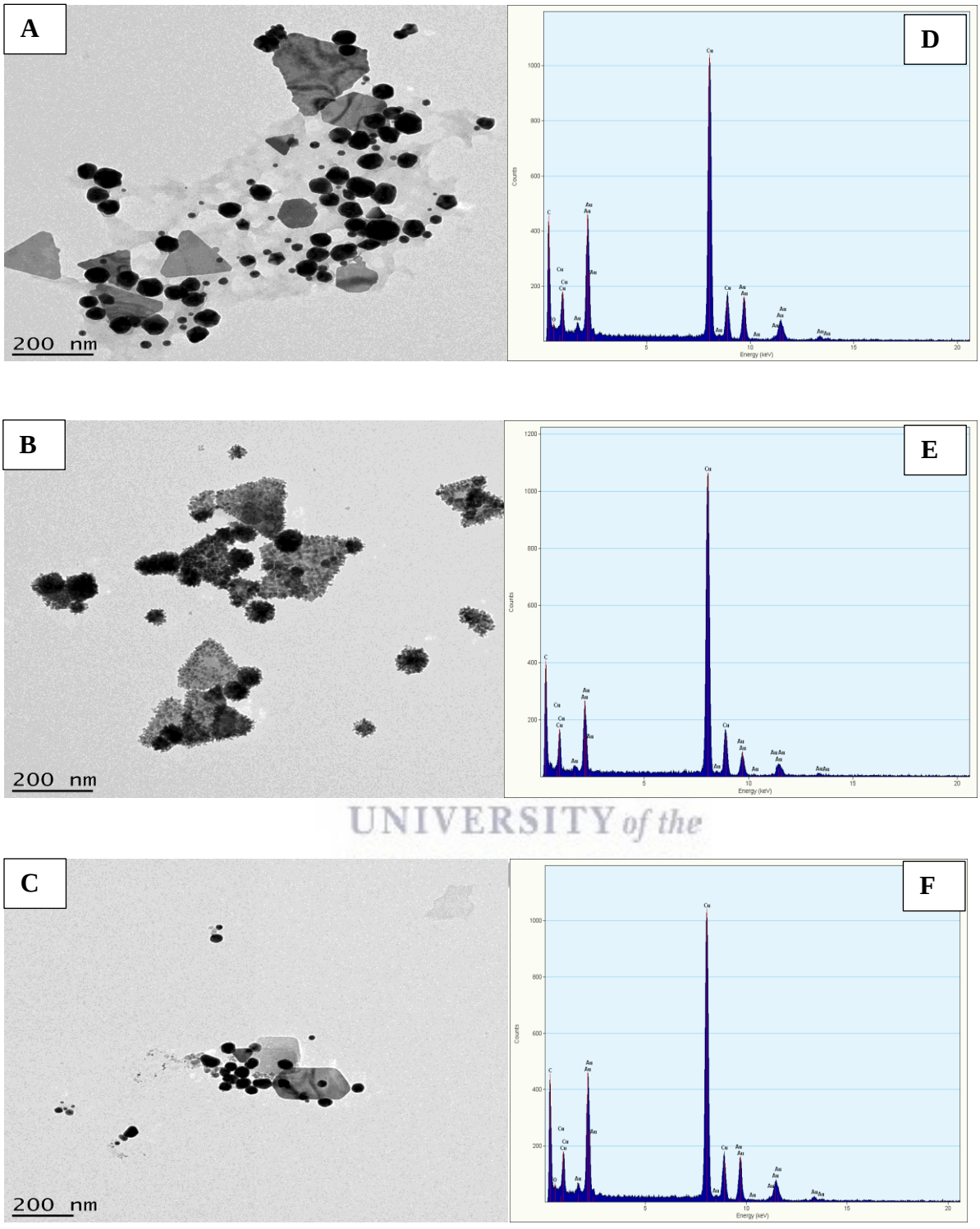

Figure 3.10: TEM images together with the EDX spectra obtained for the AuNPs synthesized using the various aqueous extracts: A) SB2014 B) NDK130 and C) NDK100. Scale bar: 200 nm.

The TEM images obtained for NDK130 as shown in Figure 3.10 (B) are particularly interesting. The "etching" observed for these AuNPs have been previously reported where the surfaces of gold nanospheres were modified using poly-L-histidine (Tian *et al.*, 2015). These features were explained by the researchers to be due to the presence of poly-L-histidine that resulted in control over the AuNPs growth which confirmed the role of poly-L-histidine in constant nucleation and growth of the NPs (Tian *et al.*, 2015). The NPs thus produced were found to have an interesting application in bioimaging. It is therefore likely that the NPs produced and shown in Figure 3.10 (B) may have been etched with proteins present in the aqueous extract of NDK130.

The EDX spectra obtained (Figure 3.10 D-F) confirmed that the elemental composition of the synthesized AuNPs was primarily Au followed by copper which is attributed to the copper grids used for TEM analyses. Trace amounts of chlorine, oxygen and potassium were also found and these could be attributed to sea salt (chlorine and potassium) or unused gold salt (chlorine). Trace oxygen could be attributed to adsorbed oxygen present on the sample surface.

3.4. Conclusion

A totally green, eco-friendly, one-step synthesis of AuNPs using algal aqueous extracts as reducing agents as was developed. The method is environmentally friendly and eliminates the use of toxic chemicals which are typically involved during conventional physical and chemical methods of NP synthesis. These AuNPs may find use in various biomedical applications, since the NPs produced are biocompatible and they may be further loaded with an active pharmaceutical ingredient such as an anticancer agent. Therefore, this rapid, environmental friendly and inexpensive route can be employed in the synthesis AuNPs with wide biotechnological and chemical applications.

Chapter 4 Synthesis and characterization of gold nanoparticles using live *Ulva lactuca*

Summary

The chapter reports the synthesis of AuNPs using the live marine seaweed *U. lactuca* and the characterization of the resultant NPs produced using various techniques such as UV-vis, HRTEM, ICP-AES, XPS, XRD, SEM, TGA and FTIR.

4.1. Introduction

As previously mentioned, the traditional methods usually employed in the synthesis of NPs contain many hazardous effects to the environment and human health, resulting in research driven into developing innovative ways for synthesizing NPs using non-toxic chemicals. Numerous novel green methods for the production of NPs have been realized using a variety of natural resources such as plants, algae, bacteria and fungi. In recent years, the synthesis of NPs using biological materials have been shown to be a viable alternative due to the various advantages they hold such as: biocompatibility, broad size distributions, readily scalable processes and the use of organisms are easily available and renewable (Hulkoti and Taranath, 2014; Allafchian *et al.*, 2016). Biomaterials that have been used to synthesize NPs include marine algae (Asmathunisha and Kathiresan, 2013; Singaravelu *et al.*, 2007), whole plants (Makarov *et al.*, 2014) and many others that have already been discussed in Chapters 1 and 2.

However, there are no reports in the literature in the use of live marine algae in the synthesis of NPs. Although several live terrestrial plants have been reported to be able to accumulate heavy metals and to successfully produce several metallic NPs. Some examples of terrestrial plants capable of bioaccumulating heavy metals and synthesizing NPs include *Sesbania drummondii* (Sharma *et al.*, 2007) and *Arabidopsis* (Parker *et al.*, 2014), which were used to produce AuNPs and PdNPs, respectively. *U. lactuca* has also been reported to have excellent heavy metal uptake

capabilities and the metals include mercury (Costa *et al.,* 2011; Kumar *et al.,* 2009) and cadmium (Muse *et al.,* 2005). Thus, it was deemed necessary to investigate the live *Ulva's* ability to produce AuNPs, especially since reports of its crude extract was successfully used to synthesize AgNPs (Sangeetha and Saravanan, 2014). However, as reported in Chapter 3 earlier, our *Ulva* aqueous extracts were not able to synthesize AuNPs. This Chapter thus reports on the successful synthesis of AuNPs using a live green seaweed *U. lactuca*.

To appreciate the potential applications of NPs, a thorough knowledge of the NPs' properties via characterization needs to be determined. These properties include the nanoparticle size, composition, morphology, crystalline nature and many others. The characterization techniques therefore included: UV-vis spectroscopy, TEM and SEM was used to reveal average nanoparticle size, morphology, crystallinity, where EDX was used mainly for elemental composition, ICP-AES for quantification of the synthesized NPs, zeta-potential measurements were carried out to determine the charge of the NP capping agent, XPS for identifying the elements present as well as the oxidation state of the gold, XRD was used to give an insight into the crystalline nature and size of the NPs, while FTIR was used for identifying functional groups of the capping agent involved in the synthesis process. The above techniques were all discussed in Chapter 2.

4.2. Methodology

4.2.1. Chemicals and seaweed preparation

Hydrogen tetrachloroaurate trihydrate ($HAuCl_4 \cdot 3H_2O$), glutaraldehyde, phosphate-buffered saline (PBS), piperazine-N,N-bis (2-ethanesulfonic acid), ethanol and osmium tetroxide were purchased from Sigma Aldrich. NIST (National Institute of Standards and Technology, Gaithersburg MD, USA) traceable standards for ICP-AES were purchased from Inorganic Ventures (300 Technology Drive, Christiansburg, VA 24073). The marine green seaweed *U. lactuca* and sea water were collected from the Marine Research Aquarium at Sea Point in Cape Town, South Africa. Collected *U. lactuca* samples were washed with distilled water and suspended in a fish tank filled with seawater and equipped with a fish tank pump to keep the organisms alive.

4.2.2. Biosynthesis of gold nanoparticles

AuNPs were synthesized by the addition of live *Ulva* (10 g wet weight) into a 100 mL solution of $HAuCl_4 \cdot 3H_2O$ at varying concentrations (i.e. 0.1, 0. 5, 1.0 and 5.0 mM) in a 250 mL conical flask. The samples were kept for seven days in normal laboratory lighting and temperature conditions. The AuNPs produced in solution as well as the *Ulva* leaves were collected at different time intervals for subsequent characterization. The AuNPs obtained from the solution were collected at t = 0 min, 1 min, 10 min, 20 min, 30 min, 50 min, 70 min, 90 min, 120 min, 4 hrs, 6 hrs and day 7; whereas the AuNP coated *Ulva* leaves were collected at t = 0 min, 4 h, day 1 and day 7. Where dry samples were required (e.g. for FTIR, TGA and XPS analysis), the *Ulva* leaves were allowed to dry in the fumehood at room temperature. For XRD, FT-IR and TGA analyses, the leaf sample was cryoground in liquid nitrogen after drying to obtain a fine powder.

4.2.3. Characterization of gold nanoparticles

4.2.3.1. UV-vis spectroscopy

The reaction using the live *Ulva* organism steeped in a gold chloride solution was measured optically by adding 3 mL of the obtained AuNPs solution into a 1 cm pathlength UV quartz cuvette and it was subsequently monitored using an Agilent Cary 60 UV-vis Spectrophotometer (Agilent Technologies, USA) in the wavelength range of 200 nm to 800 nm.

4.2.3.2. Inductively coupled plasma - atomic emission spectroscopy (ICP-AES)

Aliquots of the AuNPs from the solution in which the *Ulva* was steeped, were collected at various time intervals and centrifuged at 6000 rpm for 30 minutes. The supernatant was collected and the pellet discarded. The samples were prepared for ICP-AES by diluting the supernatant aliquots in

a 1:10 ratio with distilled water. The determination of the Au concentration remaining in the solution (where it was assumed the rest was taken up by the *Ulva*) was then accomplished through the use of a Thermo ICap 6200 ICP-AES. The instrument was calibrated and validated using NIST (National Institute of Standards and Technology, Gaithersburg MD, USA) traceable standards in order to quantify the gold in solution.

4.2.3.3. Transmission electron microscopy (HRTEM)

The size, shape, crystallinity and elemental composition of the AuNPs produced in the solution in which the *Ulva* were steeped were determined using HRTEM coupled with EDX and SAED detectors. The HRTEM images, EDX data and SAED patterns were obtained using an HRTEM Tecnai F20 with a field-emission gun (FEG) operating in bright field mode at 200 kV. The AuNPs samples were prepared by drying a single drop of undiluted solution on a lacy carbon mesh on top of a copper grid and dried under electric bulb. ImageJ was used to measure NP sizes in the TEM images.

The biological samples analyzed by TEM refer to the AuNPs embedded in the live *Ulva* organism and these were prepared as follows: the AuNPs supported on and in the *U. lactuca* thalli were collected after day 1 together with a control sample of *U. lactuca* (i.e. without exposure to the gold solution) were prepared for TEM by thorough rinsing with seawater. The samples were then cut 1 x 2 mm pieces and fixed in a 2% glutaraldehyde in 50 mM piperazine-*N*,*N*-bis (2-ethanesulfonic acid) solution adjusted to a pH of 6.8. These thalli pieces were subjected to a vacuum briefly to aid infiltration of the fixative into the sample tissues and the samples were thereafter incubated in the fixative for 2 h at room temperature. The samples were then washed with the 50 mM piperazine-*N*,*N*-bis (2-ethanesulfonic acid) buffer solution and fixed in a 2% osmium tetroxide solution in water for 2 h at room temperature. After rinsing the samples with water, the samples were dehydrated through an ethanol series and embedded in Spurr's resin. Thin sections of this resin were then prepared and collected onto Cu-support grids. An FEI Tecnai20 TEM equipped with a LaB_6 emitter operating at 200 kV was used. The TEM was fitted with a Gatan Tridiem GIF

with 2kx2k CCD camera using a Digital Micrograph suite of program to reveal the location of the synthesized NPs on the *U. lactuca* thallus (leaf).

4.3.2.4. Field emission scanning electron microscopy (FESEM)

Leaf (thalli) samples were collected at different time intervals and placed in 10 mL seawater. Thereafter the samples were fixed in a 2% glutaraldehyde solution. The *Ulva* samples were then air dried and mounted onto aluminium stubs using carbon glue. The samples were then coated with carbon. The samples were viewed in a FEI Nova NanoSEM 230 using a backscatter detector. The settings used were 20 KeV landing energy with 4.2, 5.6, 5.8, 6.1, 6.2, and 6.7 mm working distance.

4.3.2.5. X-ray photoelectron spectroscopy (XPS)

The XPS analyses were carried out with a PHI 5400 XPS spectrometer using a non-monochromatic AlKα X-ray source (1487 eV, 15 kV and 300 W) and hemispherical sector analyzer. The instrument work function was calibrated to give a binding energy (BE) of 83.96 eV for the Au $4f_{7/2}$ line for metallic gold and the spectrometer dispersion was adjusted to give a BE of 932.67 eV for the Cu $2p_{3/2}$ line of metallic copper. The photoelectron take-off angle for all measurements was 45°. Survey scan analyses were carried out with pass energy of 178.95 eV and scan rate of 2.5 eV/s, while high resolution analyses were carried out with pass energy of 44.75 eV and scan rate of 0.625 eV/s. Charge correction was done by referencing to the adventitious carbon peak at 284.8 eV.

Spectra were analyzed using XPSPEAK 4.1 software (Kwok, available on the web), while a Shirley background was used for all peaks. For the Au 4f fits, the spin orbit split option in the software was activated and a 3.67 eV energy difference between the splits was used according to Moulder *et al.* (1992). The powder specimens as well as the leaf specimens were mounted on adhesive vacuum carbon tape. The XPS survey spectra were corrected for X-ray satellite peaks

(present because a non-monochromatic X-ray source was used) and smoothed. The analyses area was 3 x 10 mm^2. The base pressure in the working chamber was < 5 x 10^{-9} Torr measured by a nude ionization gauge. The initial analysis was done on the as is samples, thus without prior cleaning or neither otherwise, nor in situ ion sputtering. An additional set of measurements were collected for the powder samples after 10 minutes sputtering by Ar ions at 3 keV and 9 x 9 mm^2 raster.

4.3.2.6. X-ray powder diffraction (XRD)

The XRD patterns for the lyophilized samples of the powdered AuNPs supported on the *Ulva* leaf were acquired on a Bruker AXS (Germany) D8 Advance diffractometer (voltage 40 KV; current 40 mA). The XRD spectra were recorded in the range 30-90º using a CuKα (λ=0.154 nm) monochromatic radiation X-ray source. The size of the NPs was calculated using the Debye-Scherrer as previously described in Chapter 2 (equation 3).

4.3.2.7. FTIR spectroscopy

IR spectra of the freeze-dried, powdered samples were recorded on a Perkin Elmer Spectrum 400 FTIR/FT-NIR spectrophotometer equipped with an ATR accessory.

4.3.2.8. Thermal analysis

Thermogravimetric analyses of the freeze-dried, powdered AuNPs supported on *U. lactuca* were carried out using a TGA Analyzer 4000 (Perkin Elmer) under a nitrogen atmosphere with a purge rate of 20 mL/minute in the temperature range of 50–900 ºC at a rate of 10 ºC/min.

4.3. Results and discussion

Samples of the solution in which the *Ulva* were submerged, as well as the AuNPs embedded on or in the *Ulva* thalli itself, were collected at different time intervals. The results and discussion will therefore be divided into these the two sections, i.e. solution and solid (for the *Ulva* thallus) sample analyses.

4.3.1. Solution sample analyses

4.3.1.1. Visual observation

The reduction of the metal salt from Au(III) to Au(0) was monitored by observing the colour change after addition of the live *Ulva* into the gold solution as shown in Figure 4.1 (A-E). The colour changes from the characteristic yellow of the Au salt solution and green of *Ulva* thalli to dark pink for the solution and the *Ulva* thalli. The NPs formed in the solution and in/on the leaf sample was then subjected to further characterization as discussed later in this chapter. This deep pink colour was observed upon immediate exposure of the seaweed into the Au salt solution at a 1 mM concentration, which implies the immediate formation of the AuNPs in the solution and on/in the seaweed itself. It was noted that the pink colour started to form on the seaweed thalli after about 10 min; while the solution itself remained colourless at first and then eventually turned pink as well after about 30 min. The pink colour of the *Ulva* leaf as well as the solution was most intense between 90 min and 2 h, indicating formation and increased concentration of the AuNPs on the *Ulva* as well as in the solution.

Interestingly, after 2 days the solution itself started to turn colourless once again with a completely clear solution obtained on day 7, but the *Ulva* remained a deep pink colour throughout. This suggested that the NPs initially formed in solution were now incorporated into the seaweed itself. On the other hand, the other Au salt concentrations used, with the 0.05 mM solution shown in Figure 4.1, and 5.0 mM (not shown), the gold chloride solution showed no change in colour which

suggests that these concentrations may be too dilute (at 0.05 mM) or too concentrated (at 5.0 mM) to synthesize the NPs. It is possible that with the 5.0 mM solution, the *Ulva* may be carrying out some bioremediation processes whereby the Au salt is taken up by the living organism, but since the levels are too high, they may not be able to reduce the metal salt sufficiently. The 1 mM concentration was therefore regarded as the optimum concentration for the synthesis of AuNPs using *Ulva.* All results discussed hereafter are therefore for those NPs synthesized using the 1 mM solution.

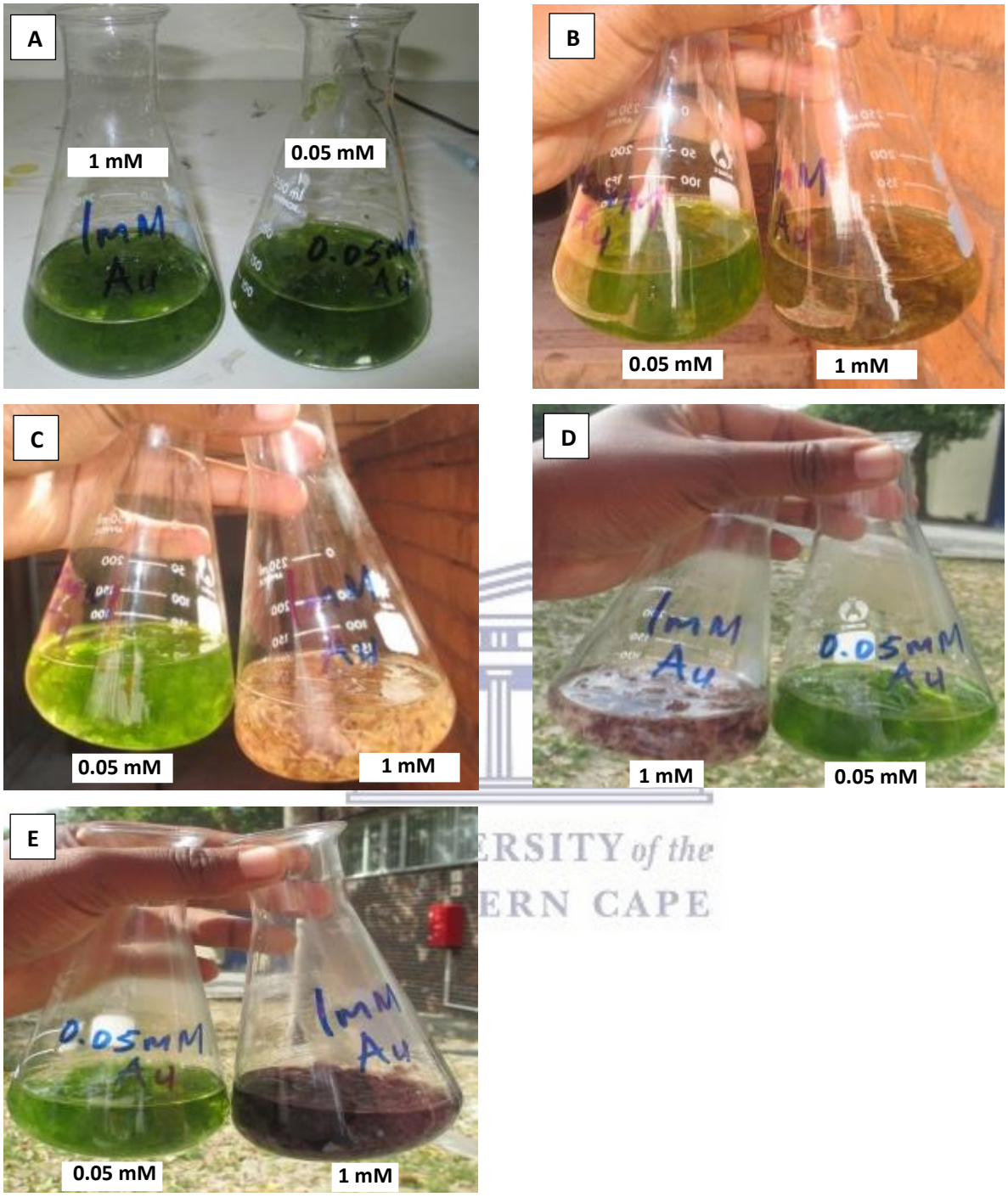

Figure 4.1: Green synthesis of AuNPs using live *Ulva* organisms at gold chloride solution concentrations of 0.05 mM and 1 mM. Colour change at t = (A) 0 min, (B) 10 min, (C) 30 min, (D) 4 h and (E) 6 h. The *Ulva* sample at 0.05 mM remains green throughout.

4.3.1.2. UV-visible spectroscopy

UV-vis spectroscopy is widely considered to be a useful technique to determine the formation of AuNPs (Pimprikar *et al.,* 2009). Figure 4.2 (A-B) shows the UV–Vis spectra of the AuNPs that were formed, recorded as the function of time. The colour change from light yellow to purple or pinkish red in the solution is due to the excitation of the SPR in the AuNPs caused by the light passing through and this observation was by using UV-vis spectral analysis (Ramakrishna *et al.,* 2015; Inbakandan *et al.,* 2010). Changes in SPR of the synthesized AuNPs with respect to time of collection is shown in Figure 4.2 (A-B).

Initially, the broad surface plasmon resonance (SPR) band for the AuNPs occurred at 550 nm initially, then together with a shoulder at 660 nm, with the maximum absorbance increasing from the start at t = 0 to 90 min as shown in Figure 4.2 (A). The initial SPR band at 550 nm at 30 min indicates formation of spherical NPs, but the appearance of the shoulder at 660 nm at 50 min is likely due to the presence of variously shaped AuNPs. This was confirmed using TEM and is discussed later. The optical absorbance (Figure 4.2 (A)) of the AuNPs increased as the reaction time increases up to t = 90 min, which may indicate an increase in the concentration of NPs being synthesized, since the Beer Lambert law indicates that a substance's concentration and is directly proportional to its absorbance (Swinehart, 1962). However, after 90 min to 6 h, the maximum absorbance starts to decrease at both 550 and 660 nm as shown in Figure 4.2 (B), which suggests a decrease in the NPs concentration in the solution. At first, it was thought that the observed decrease in absorbance was due to the AuNPs aggregating and crashing out of solution. However, based on the visual observations (discussed in section 4.3.1.1), this decrease is more likely due to the AuNPs being taken up by the live seaweed. This was further confirmed after 2 days starting the reaction by the disappearance of the dark pink colour of the solution becoming completely colourless.

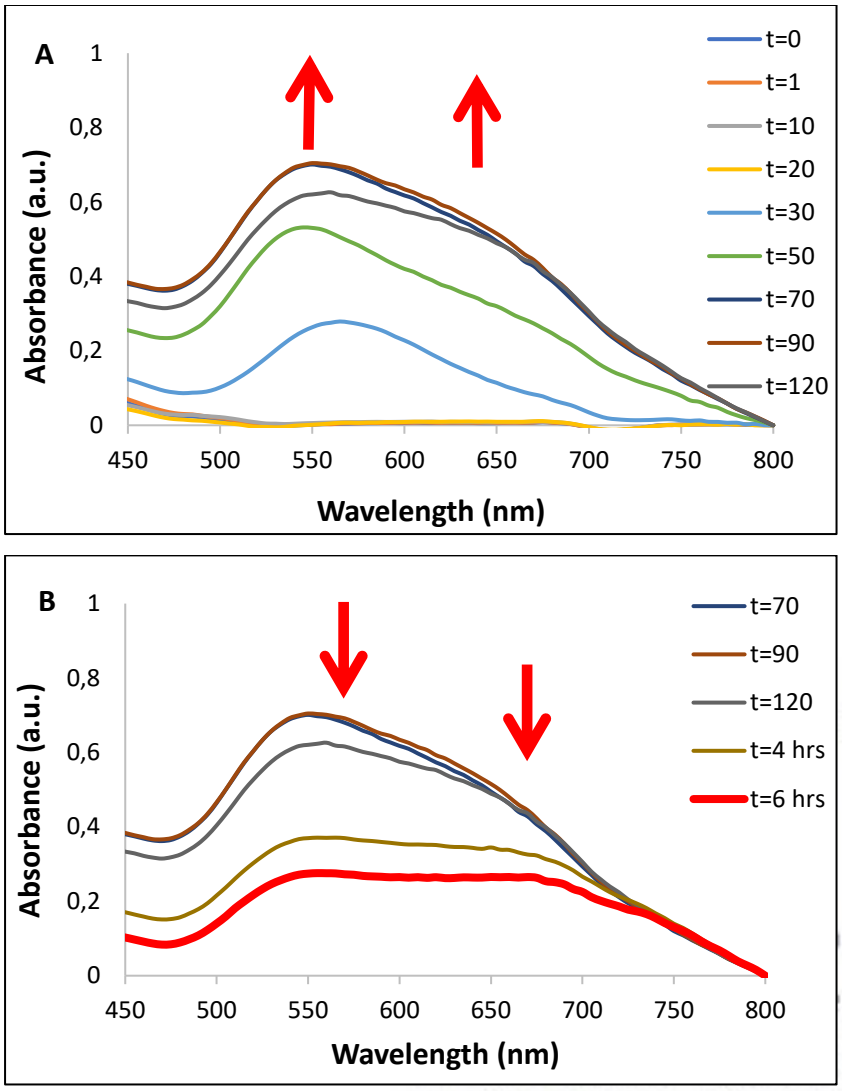

Figure 4.2: UV-vis absorption spectra (in water) of the AuNPs in solution synthesized using the live marine algae *U. lactuca* showing: (A) an increasing absorbance at both 550 nm and 660 nm from t = 0 to t = 90 min, followed by: (B) a decreasing absorbance at both 550 and 660 from t = 120 min and 4 h. The concentration of the gold salt solution used here is 1 mM.

4.3.1.3. Rate of AuNPs formation

A graph for the speed of AuNP formation is shown in Figure 4.3, which was constructed using the absorbance data collected from the UV-vis spectra at 550 nm and 660 nm and this is given as a function of time. This graph clearly indicates the increase in the formation AuNPs after an initial

induction period of 30 min following the addition of the live *U. lactuca*, up until 100 min where a maximum in absorbance was reached. From 100 min onwards, a decrease in absorbance was then observed, indicating that the NPs are either settling out of solution (and therefore aggregating) or there is a decrease in the AuNP concentration which could only be due to the AuNPs being taken up by the *Ulva*. The latter is in agreement with the visual observations and the UV-vis spectra (Figure 4.2) discussed earlier, which indicated that the NPs are being taken up by the seaweed.

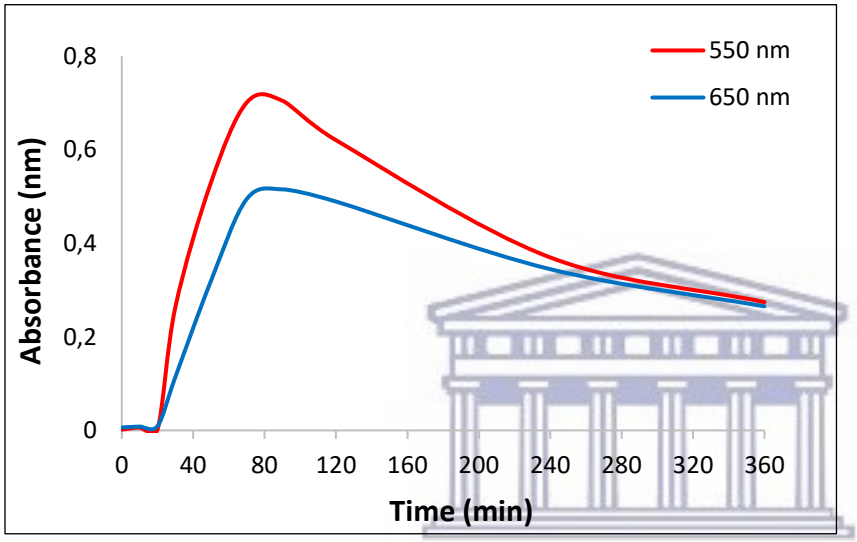

Figure 4.3: Speed of AuNP formation constructed using UV-vis absorbance data collected at 550 nm and 650 nm vs. time.

4.3.1.4. Inductively coupled plasma - atomic emission spectroscopy (ICP-AES)

The percentage of Au salt that remained in the solution was quantified using ICP-AES and it is shown in Figure 4.4 in a plot of the percentage of Au salt versus time following the addition of *Ulva* to the Au salt solution. The samples for ICP-AES were prepared in such a manner that only the Au salt (not the AuNPs) would be detected. The samples were were centrifuged at 6000 rpm for 30 min to precipitate out any AuNPs present (which should collect as a pellet) leaving the Au salt in the supernatant. The supernatant was collected, diluted in a 1:10 ratio and then the amount of Au remaining in the solution as the reaction progresses was quantified by ICP-AES. This should

give an indication of the amount of gold salt (and AuNPs formed or taken up) by the *Ulva* at various time intervals.

The amount of Au salt present in the solution (Figure 4.4.) decreased significantly to less than 40% of the initial concentration within the first 10 min, indicating rapid uptake of the metal salt by the *Ulva* (at this stage, no AuNPs were observed in the reaction solution, but the *Ulva* thalli had started to turn pink). It is also clear from Figure 4.4, that the Au salt remaining in solution is reduced to zero after only 90 min, which suggests that the Au(III) was completely reduced to form AuNPs with a Au(0) state or that it was taken up by the seaweed (as either AuNPs or the metal salt). These data suggest that *Ulva* is indeed very good at heavy metal removal from its surrounding environment and this is in agreement with that was observed by Ibrahim *et al.* (2016) where they showed the efficient capability of *Ulva* in taking up heavy metals from wastewater.

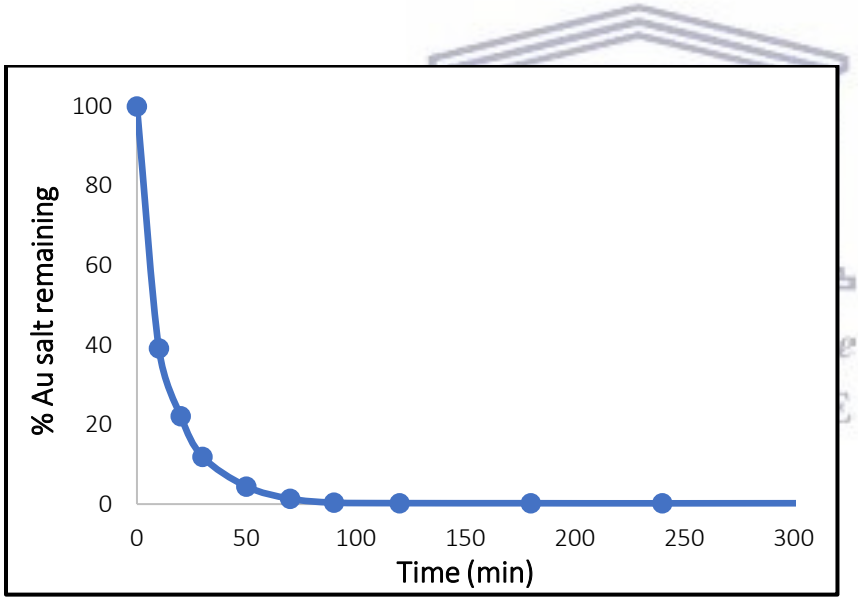

Figure 4.4: Plot of the percentage Au salt present in the supernatant of the reaction solution collected at various time intervals from t = 0 min to day 7 as obtained by using ICP-AES analyses.

4.3.1.5. High resolution transmission electron microscopy (HRTEM)

HRTEM provided further insight into the morphology, shape variation and size ranges obtained for the AuNPs produced at various time intervals, as illustrated in Figure 4.5 (A-E). The NPs were well dispersed and no real agglomeration was noticed at the start (t = 30 min and t = 90 min). Interestingly, apart from the presence of spherical AuNPs, very large (more than ~200 nm) triangular shaped AuNPs were also formed at t = 30 min. The occurrence of variously shaped NPs was hinted at previously by the presence of a small shoulder in the UV-vis spectra obtained at t = 50 min (Figure 4.2 A). It was, however, found that the majority of AuNPs synthesized were spherical, with some triangular and rod shaped NPs also present (Figure 4.5 (A-E)). Figure 4.5 also clearly shows that the NPs become aggregated from 90 min onwards. This is in agreement with the UV-vis spectra (Figure 4.2 A) obtained which showed a decrease in absorbance intensity from at this stage.

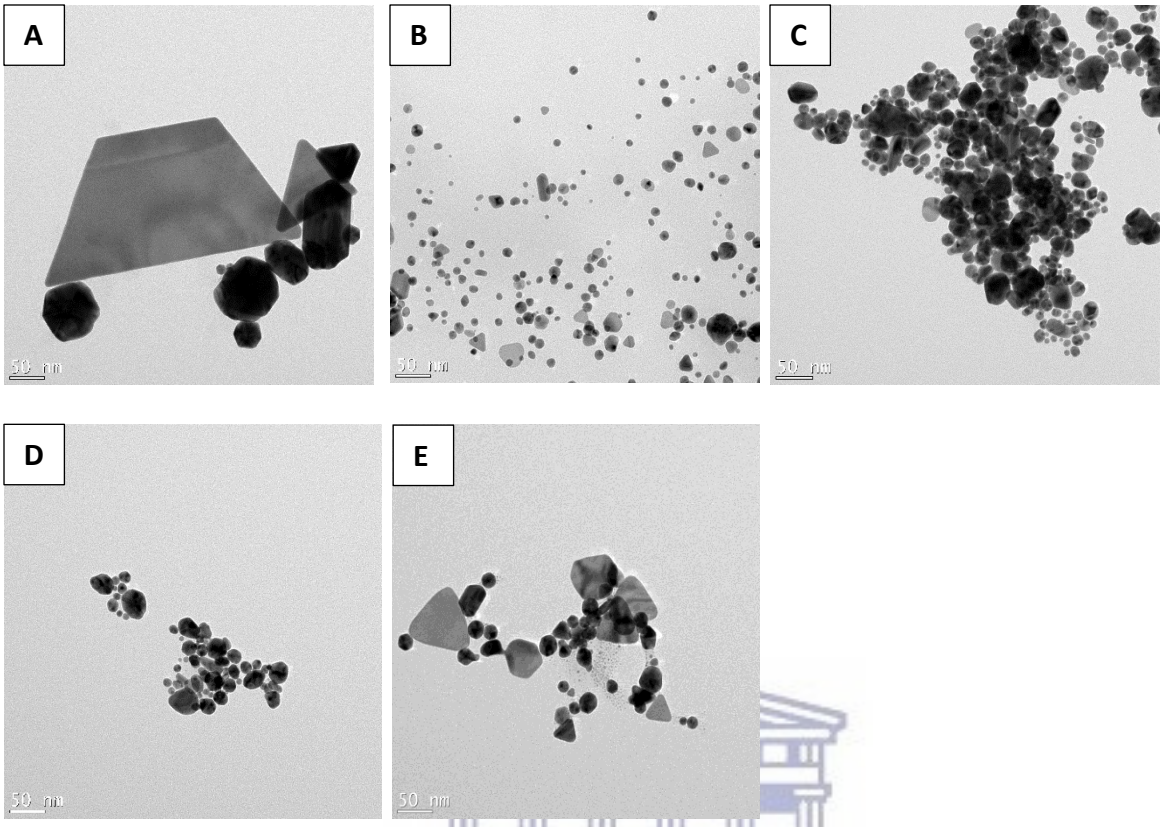

Figure 4.5: TEM micrographs of AuNPs synthesized using *Ulva* at time intervals show spherical, triangular and rod-shaped NPs. (A) t = 30 min (B) t = 90 min (C) t = 120 min (D) t = 4 h (E) t = 6 h. Scale bar: at 50 nm.

The ImageJ software was used to calculate the AuNP size ranges at the different time intervals and the sizes were found to be as follows: (A) 69.155 ± 30.717 nm at (t = 30 min), (B) 14.751 ± 6.258 nm (at t = 90 min), (C) 22.645 ± 9.149 nm (at t = 120 min), (D) 18.134 ± 7.832 nm (at t = 2 hours) and (E) 26.646 ± 5.852 nm (at t = 6 hours) for the spheres. From these data, it is clear that there is no real correlation between size range and time intervals which may be due to imaging of a particular selection of the grid which only contained these NPs, from sample preparation error or that a range of NPs shapes and sizes are inconsistently produced at various times.

4.3.1.6. Energy Dispersive X-ray spectroscopy (EDX) and selected area diffraction (SAED) analyses

According to the EDX data acquired simultaneously during HRTEM analyses, the presence of Au in the sample was positively confirmed and it was present in the greatest quantity (Figure 4.6 A).

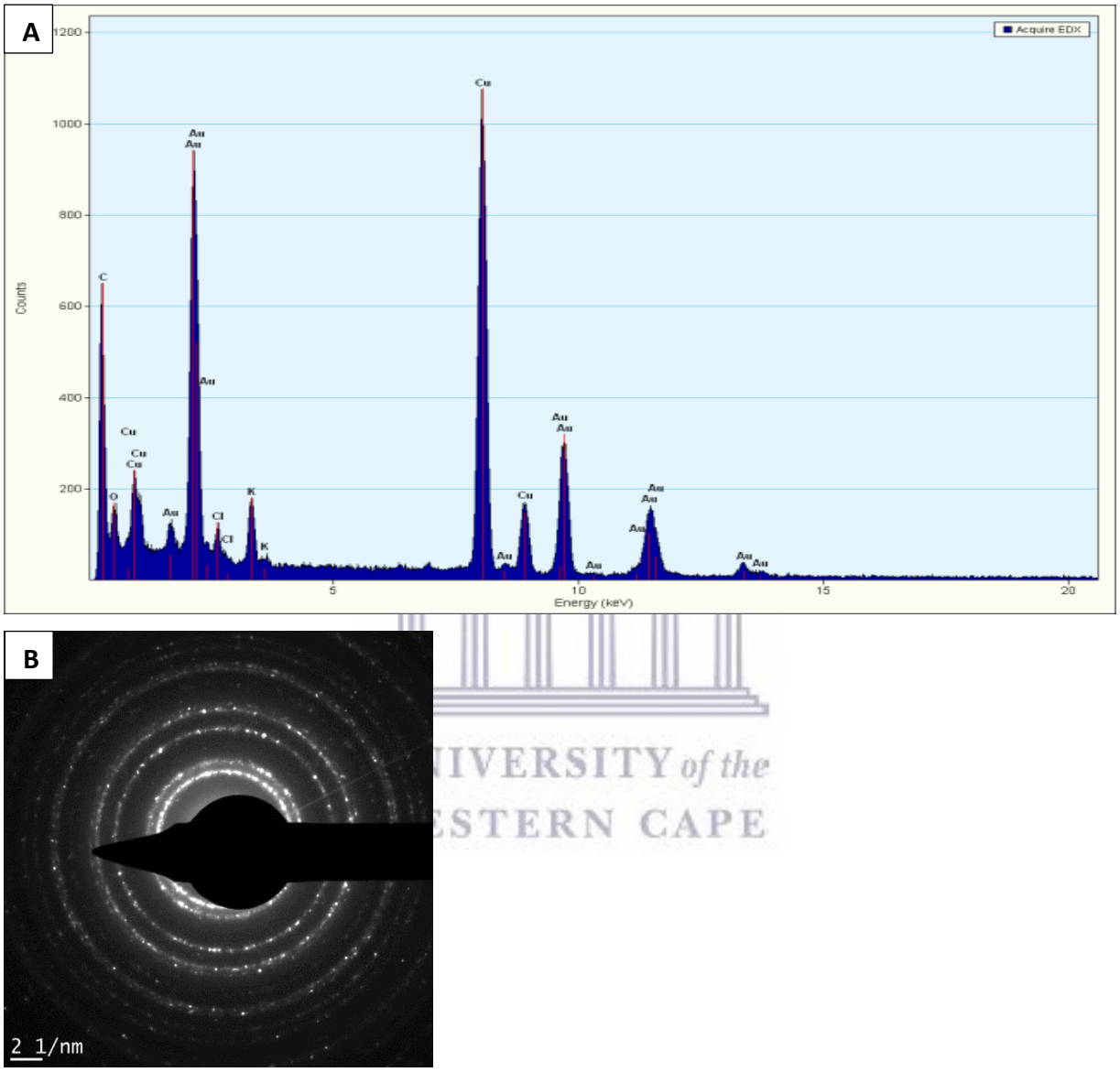

Figure 4.6: Energy dispersive X-ray spectrum (A) of the sample obtained for the AuNPs produced in the reaction solution at t = 4 h and (B) the SAED pattern obtained for these AuNPs.

The occurrence of sodium and chloride in the sample was also revealed, which may be due to the presence of sea salt which is associated with the seaweed (or unreacted metal salt in the latter case). It further shows the presence of Cu and oxygen which are probably due to the copper grid and oxygen which may have been adsorbed onto the sample from the air. The SAED pattern shown in

Figure 4.6 (B), obtained for the sample collected at 4 h, suggested that the AuNPs synthesized were polycrystalline in nature. The SAED pattern results correspond with the results obtained from the XRD analyses. The appearance of the rings is attributed to the set of diffraction planes (1 1 1), (2 0 0), (2 2 0), (3 1 1) and (2 2 2) for face-centered cubic gold (Bearden, 1967; Skakle, 2005; Liss *et al.*, 2003).

4.3.2. Solid sample analyses

The following section describes the results and discussion obtained for the characterization of the *Ulva* thallus (as opposed to the solution in which the *Ulva* were steeped) samples obtained using HRTEM, SEM, XRD, XPS, FTIR and TGA.

4.3.2.1. High resolution transmission electron microscopy

HRTEM was carried out to evaluate whether AuNPs were indeed formed and the location of formation of the AuNPs on/in the *Ulva* thalli itself, since visual observation implied that the AuNPs are also formed within or on the seaweed itself due to the colour change (Figure 4.1). Figure 4.7 (A) shows the TEM images obtained for the *Ulva* sample that has not been immersed in the gold chloride solution. This image clearly shows the *Ulva* cell structure (without any NPs). Figure 4.7 (B-C) were obtained for the *Ulva* samples following subjection of the Ulva to the gold chloride solution and it shows the presence of small dark spots which imply formation of the AuNPs on and in the *Ulva* thallus.

Figure 4.7 (B) shows the presence of the AuNPs on the leaf surface of the *Ulva,* whereas figure 4.7 (C) shows the formation of AuNPs in the chloroplasts suggesting the consitutents within the chloroplasts (i.e. chlorophyll) are responsible for formation of the AuNPs. Figure 4.7 (D) shows that the NPs are consistently located with a uniform pattern of distribution along the cell walls (CW), in the chloroplasts (Cp) and on the leaf surface. The shape of the NPs in the cells were

found to be mostly spherical, while the size of these NPs was found to be approximately 9.6 nm (this was later confirmed by XRD analyses). The presence of the AuNPs on the surface of the *Ulva* thallus was further confirmed using XPS and FESEM.

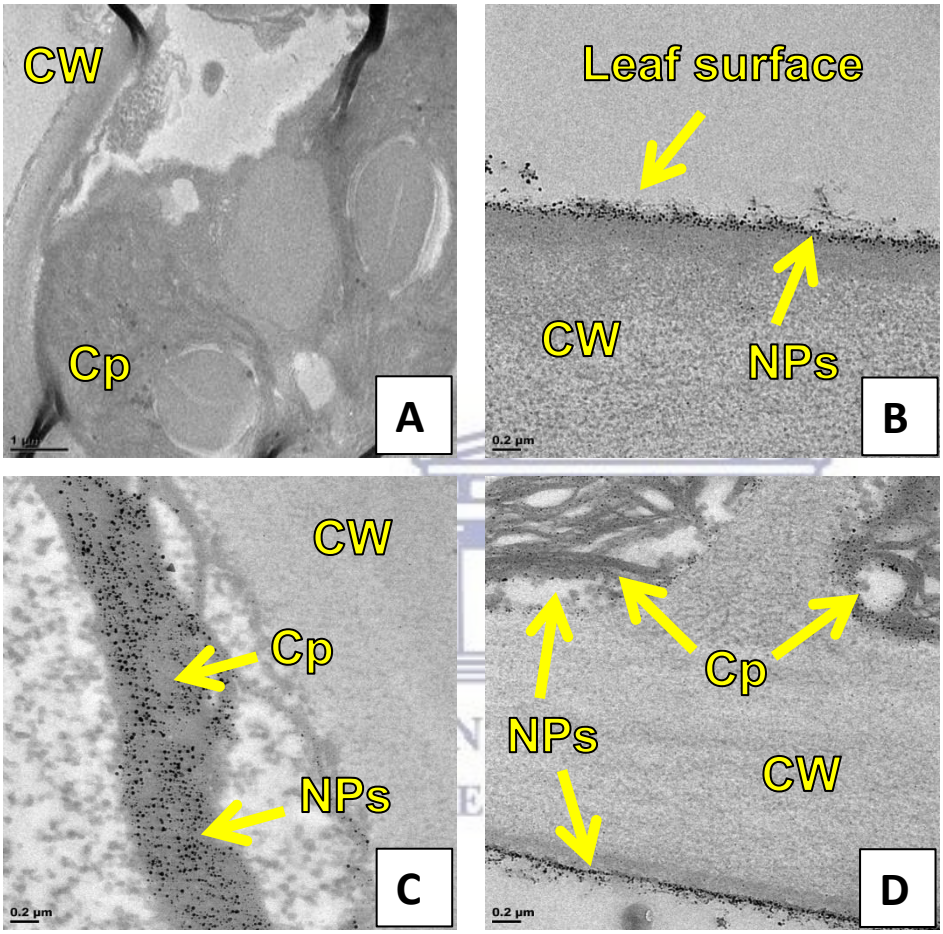

Figure 4.7: TEM images of the *U. lactuca* cells: (A) not immersed into the gold solution (control), and (B-D) AuNPs embedded on/in the *Ulva* cells. The AuNPs are found on the located on the leaf surface, lining the cell walls (CW) and in the chloroplasts (Cp). (Scale bar = 0.2 µm).

The active uptake of heavy metals has been reported in marine seaweeds such as *Cladophora fasicularis, Ulva lactuca, Chaetoporpha sp, Caulerpa sertularioides* and *Valoniopsis pachynema* (Kumar *et al.*, 2009). In *U. lactuca*, it has also been reported that this seaweed is capable of accumulating mercury from wastewaters (Costa *et al.*, 2011; Kumar *et al.*, 2009). The presence of

AuNPs in the cell wall as well as the chloroplasts of *U. lactuca* as shown by the TEM images in Figure 4.7 (B-D) indicates the ability of *Ulva* to accumulate gold after reducing it to its nanoscale. The terrestrial plant *Sesbania drummondii* is also capable of accumulating heavy metals and has been shown to have the ability to accumulate AuNPs in their roots in the cytoplasm and other organelles (Sharma *et al.*, 2007). There are few reports to conclude that all biomaterials capable of accumulating heavy metals are also capable of reducing these heavy metals into their nanoscale and accumulate them within or on their surfaces. It is thought that live organisms are likely to convert/reduce metal salts which are toxic to their nanoparticles since the latter is considered non-toxic, while the former is poisonous.

4.3.2.2. Field emission scanning electron microscopy

FESEM analysis was carried out on *Ulva* leaf samples coated with AuNPs which were collected after immediate addition of the *Ulva* into gold chloride solution, as well as after 4 h and 7 days (Figure 4.8 (B-D)). A control *Ulva* thallus sample was also analyzed and this shown in Figure 4.8 (A). FESEM revealed the absence of gold in the control sample, while the presence of elemental gold was confirmed on the *Ulva* surface even after a few seconds of exposure (t = 0 min, Figure 4.8 B) as indicated by the white spots as shown in Figure 4.8 (B-D), although the data does not indicate whether the Au is in the metallic state. The information obtained using FESEM is therefore in agreement with the XPS and biological TEM data which indicated the presence of AuNPs on *Ulva* cell surface.

Elemental composition as revealed by the EDX data further indicated the presence of a high amount of gold (Figure 4.8 E) for the area selected in Figure 4.8 (D). The EDX analysis of the *Ulva* leaf sample further confirms the presence of Ca and Mg which may be due to mineral salts from the ocean which were present in the seaweed. Traces of other elements such as Cu, C and O are also present, which are due to the copper grid used for the analyses, while the C and O are expected for an organic sample as well as adsorbed oxygen.

Synthesis of the AuNPs supported on biomaterials has shown to be advantageous in catalytic reactions such as in reduction of 4-nitrophenol (Sharma *et al.*, 2007). Furthermore, such NPs on

the biological material surface can be purified and obtained in larger quantities as compared to those trapped on the inside of polymers for example and they can be further employed for various applications (Vijayaraghavan *et al.*, 2011; Mata *et al.*, 2009).

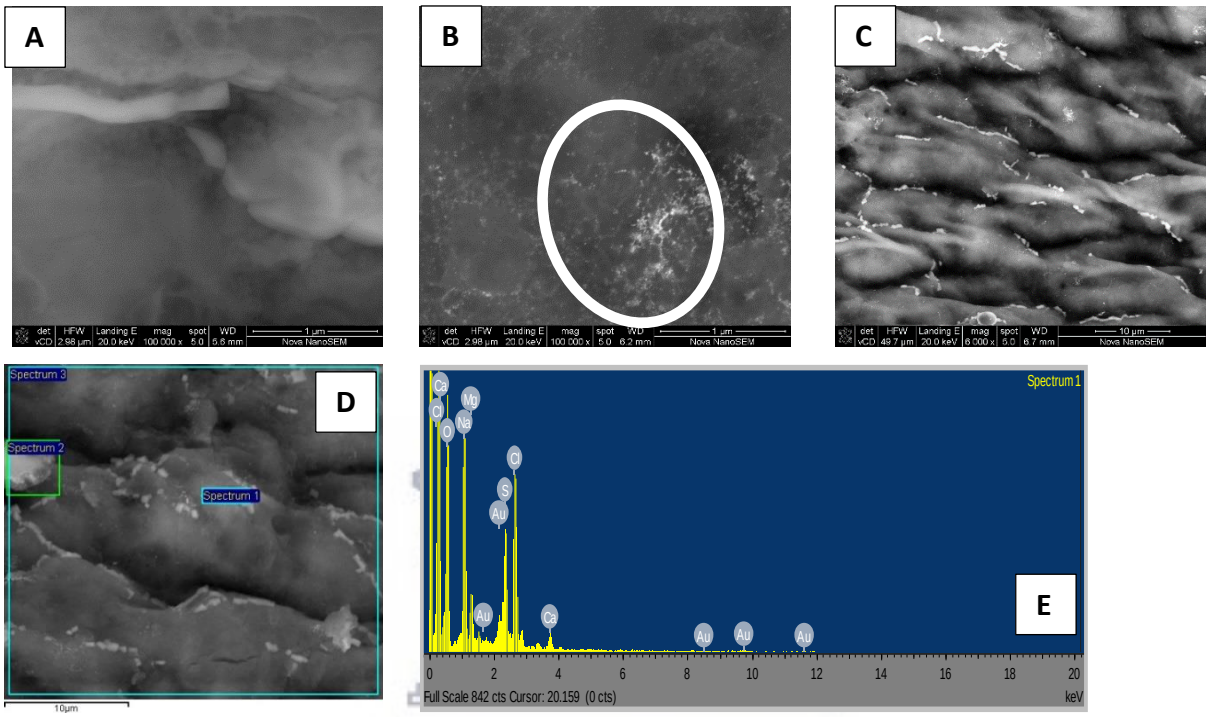

Figure 4.8: FESEM images of the surface of Ulva thalli where (A) is the control *Ulva* thallus, (B) t = 0 min, (C) t = 4 h and (D) t = 7 days; (E) is the EDX spectrum of a selected area of the Ulva thallus as shown in (D).

4.3.2.3. X-ray powder diffraction

The "green" synthesized AuNPs, incorporated into the *Ulva* leaf samples which was subsequently freeze-dried, were clearly observed in the XRD powder patterns. Their crystalline state was confirmed by the well resolved reflections, substantiating the SAED data obtained previously. Figure 4.9 shows the XRD patterns obtained for the AuNPs prepared using the live *Ulva* seaweed. The XRD patterns showed five clear peaks which correspond to the crystalline face centered cubic (fcc) phase (Singh *et al.*, 2013). The diffraction peaks were observed at 2θ = 38.36° (111), 44.13°

(200), 64.78° (220), and 77.98° (311) and 83.5° (222) which are identical to those reported for standard Au metal (Au(0)) based on the JCPDS 04-0784 file (Saxena *et al.*, 2010). The line broadening shown by the reflections in the XRD diffractograms are typical for NPs, where the smaller the NPs size, the broader the reflections obtained (Bearden, 1967; Skakle, 2005; Liss *et al.*, 2003). Similar XRD results were obtained for AuNPs synthesized using the brown algal aqueous extract from *Sargassum marginatum* (Rajathi *et al.*, 2012). Using the Debye-Scherer equation (equation 3). The crystallite size of the synthesized AuNPs was found to be 9.585 nm.

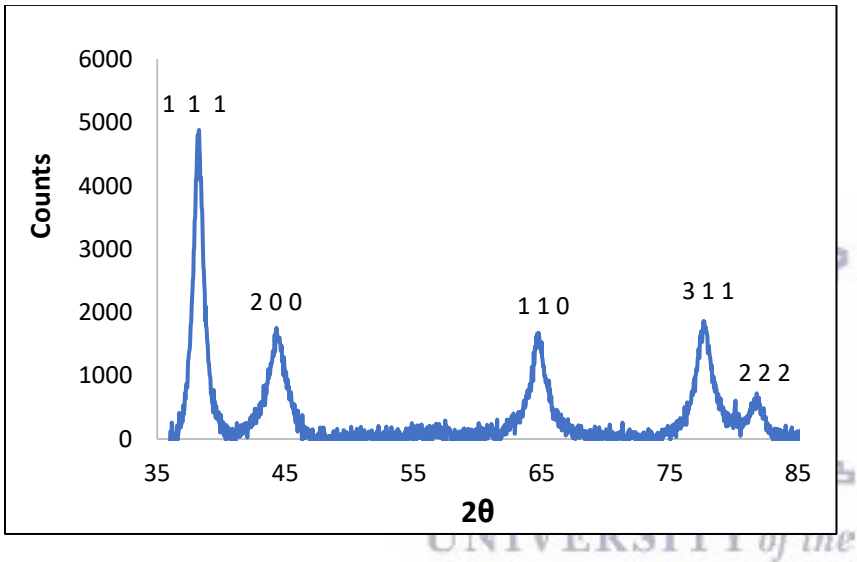

Figure 4.9: Powder XRD pattern obtained for the powdered *Ulva lactuca* leaf-AuNPs sample.

4.3.2.4. X-ray photoelectron spectroscopy (XPS)

XPS was used to evaluate the composition and chemical environment of the elements present on the *Ulva* leaf material coated with AuNPs. An XPS survey scan as shown in Figure 4.10 (A) revealed the presence of carbon (C 1s), oxygen (O 1s), nitrogen (N 1s) and silicon (Si 2s) photoelectrons at 300, 650, 420 and 160 eV, respectively, in addition to the expected Au photoelectrons at 84 eV for Au 4f and ~350 eV for Au 4d. The Si 2s signal may be due to the glassware used in preparing the AuNPs, while the carbon, oxygen and nitrogen detected are expected from an organic sample.

Figure 4.10 (B) shows the high-resolution XPS spectrum of the Au 4f core level photoelectrons of the *Ulva* leaf sample prepared with the gold salt solution concentration of 1 mM. Two distinct peaks separated by 3.67 eV binding energy were visible, namely the Au $4f_{5/2}$ and Au $4f_{7/2}$ peaks at ~ 84 eV. The two peaks are due to the spin orbit splitting of the Au 4f level. The well separated spin orbit pair at 84.0 eV indicates that the gold present on the leaf surface is in the metallic state (Au(0)). The binding energy together with the deconvolution or fit (given in green) obtained shows Au to be only in its metallic state i.e. Au(0) and not as bulk gold (Au(III)) where higher binding energies are expected (Bozˇanic *et al.*, 2013). Most importantly, the spectrum revealed the presence of AuNPs on the surface of the *Ulva* leaf, since XPS is a surface analytical technique where photoelectrons are typically ejected from the first 3Å of the sample surface (Drummond and Bryson, 1996).

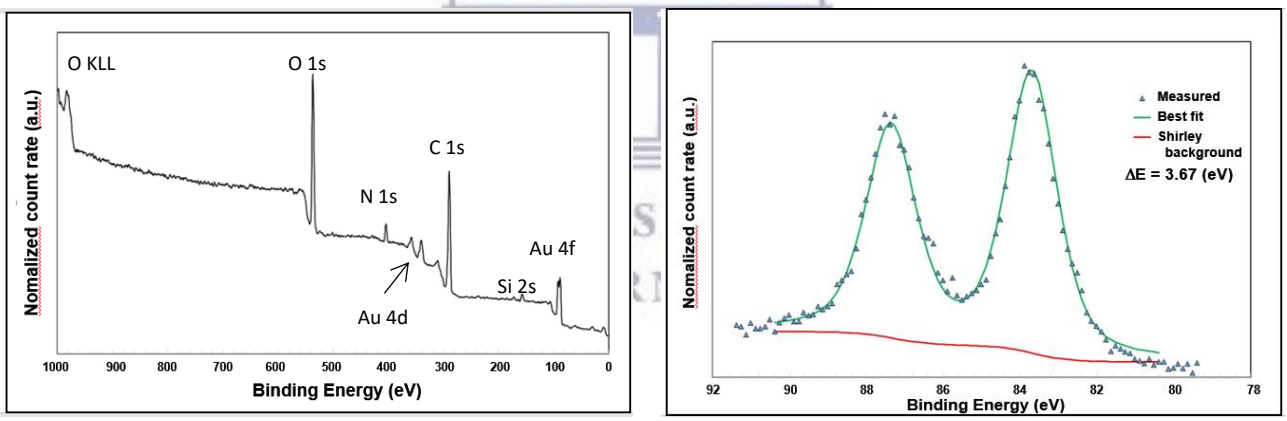

Figure 4.10: Survey scan (A) of the *Ulva* thalli, and (B) high resolution XPS spectrum of the Au 4f spin-orbit pair showing the presence of Au(0) only (at BE 84.0 eV).

4.3.2.5. FTIR spectroscopy

FTIR was used for characterization of the capping agent's functional groups. The capping agent plays a crucial role in the stabilization of the AuNPs. The FTIR spectra of the *Ulva* alone and that of the biosynthesized AuNPs supported on *Ulva* are shown in Figure 4.11. This may provide some

information any change in the functional groups involved in the bioreduction processes (Perevedentseva *et al.*, 2010;). The FTIR spectrum of the biosynthesized AuNPs supported on *Ulva* and *Ulva* alone show three similar characteristic bands at 3359.88, 1627.26 and 1051.51 cm^{-1}. The strong broad absorbance at 3359.88 cm^{-1} corresponds to the N–H stretching vibrations of the free NH group. The intense medium absorbance at 1627.26 cm^{-1} is more likely to be a characteristic band of C=O stretch (frequency and intensity) or possibly one of the higher frequency C-H inplane bends associated with benzene C=C. The band at 1051.51 cm^{-1} can be assigned to the CH bending vibrations of a CH_3 group. The results suggested that the capping ligand of the AuNPs may be an aromatic compound or amines (Sangeetha and Saravanan, 2014). For the AuNPs *Ulva* sample, spectrum reveals either new bands or enhanced signals at 3023, 1500 and 1200 cm^{-1}.

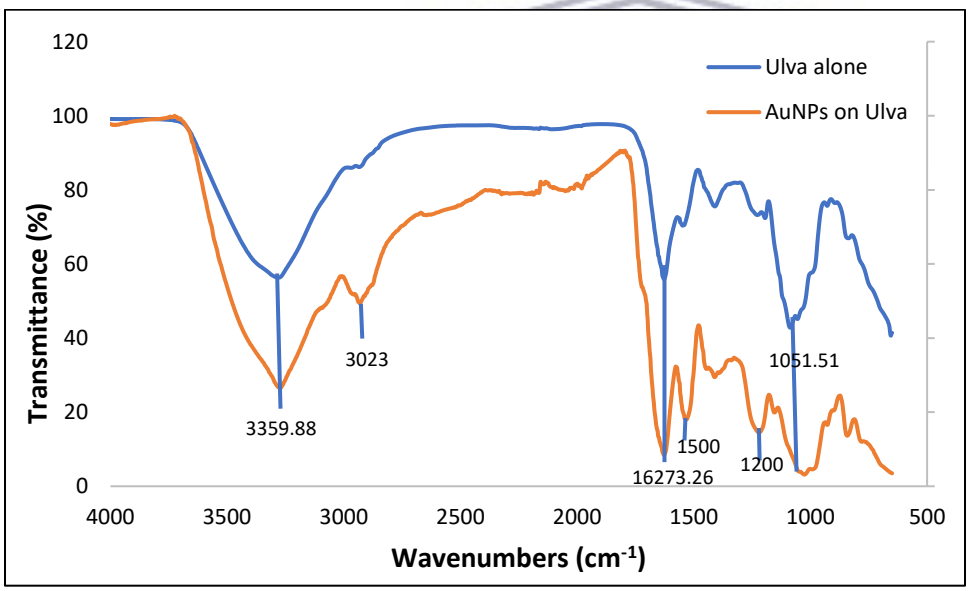

Figure 4.11: FTIR spectra of the powdered *Ulva* before (Ulva alone) and after the biosynthesis of AuNPs (AuNPs on *Ulva*).

4.3.2.6. Thermogravimetric analysis (TGA)

The TGA curves of *Ulva* alone and that for the AuNP embedded in the *Ulva* leaf are shown in Figure 4.12. Four events of mass loss were observed for both TGA curves. The first stage two

stages of mass loss were observed firstly in the region of 30 to 120 ºC with the second stage seen between 120 and 250 ºC and this may have been attributed due to loss of volatile and water components (Martins *et al.*, 2015). At these two stages of mass loss it can be observed that the *Ulva* alone lost a higher percentage at all stages compared to the *Ulva* coated with AuNPs. The third mass loss stage occurred between 450 ºC where both curves overlapped and 800 ºC where again overlapped, albeit unexpectedly. It can be noted that at this stage the mass of *Ulva* coated with AuNPs was a little higher than that of *Ulva* alone. This may have been caused by the degradation of the materials (Martins *et al.*, 2015). The overlap observed at 450 ºC shows that *Ulva* alone presents higher thermal stability as compared to the one supporting the AuNPs. Carbon is expected to decompose at approximately 500 ºC, and thus it was assumed that all of the seaweed would have been consumed at this stage. The fact that a 100% mass loss was not observed, could be due to the presence of sea salt (NaCl and KCl) in the seaweed sample. It was expected that it would be possible to calculate the mass of Au embedded in the seaweed, but this was not feasible.

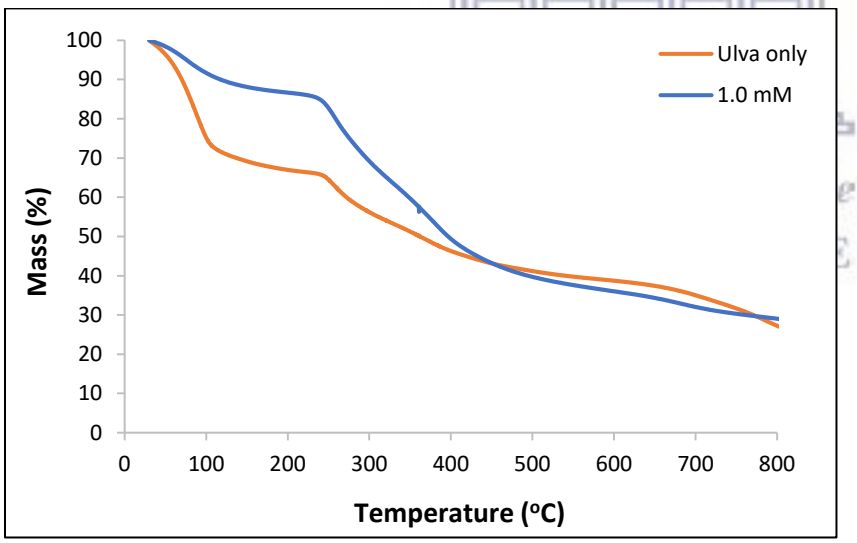

Figure 4.12: TGA curves obtained for the Ulva seaweed alone and that of the AuNPs supported on *Ulva*.

4.4 Conclusion

This study has shown that *Ulva* can be used as an efficient, green synthetic factory to produce AuNPs. *Ulva* presented a unique ability for the intracellular formation of AuNPs which were also revealed to form on the surface of the *Ulva* thallus. The synthesis procedure is ideal due to its eco-friendly nature, eliminating the disadvantages associated with conventional physical and chemical methods. These biosynthesized NPs are expected to have variety of applications such as catalytic activities as well as biomedical applications.

Chapter 5 Catalytic activity of the AuNPs supported on *Ulva lactuca*

Summary

This chapter presents some background on the catalytic ability of the gold nanoparticles (AuNPs) for the reduction of 4-nitrophenol (4-NP) to 4-aminophenol (4-AP) as a model reaction. This is followed by an assessment of the gold nanoparticles supported on *Ulva* (as a solid support) synthesized in this study as a catalyst.

5.1. Introduction

AuNPs have attracted an extensive amount of interest in nanotechnology and material science due to their unique catalytic, optical, biological, medical, magnetic and electronic properties which make them applicable in different fields such as catalysis (Yu *et al.*, 2016), sensors (Rana *et al.*, 2016), biomedicine (Liu *et al.*, 2015; Joseph *et al.*, 2014), fluorescence imaging (Zhang *et al.*, 2015), surface-enhanced Raman scattering (SERS) (Xie *et al.*, 2014), electronics and photonics (Luechinger *et al.*, 2008).

The exploration of gold nanocatalysts for several reactions became a hot research topic in the late 1980's when Haruta and colleagues discovered that AuNPs were effective in the catalysis of low-temperature oxidation of CO (Haruta *et al.*, 1987). However, naked (or bare) AuNPs usually aggregate or dissolve during the catalytic reaction, which, understandably, gradually reduces their initial catalytic activities, or the catalytic function fades after several cycles. In recent years, the anchoring of AuNPs on, or into, a number of solid supports such as polymers (Percebom *et al.*, 2016; Quan *et al.*, 2016; Zyuzin *et al.*, 2016), metal oxides (Korotcenkov *et al.*, 2016; *Zhao et al.*, 2015), silica (Laveille *et al.*, 2016), carbon materials (Lozano-Martı´n *et al.*, 2015; Simenyuk *et al.*, 2015) and biomaterials (Wei and Lu 2012) has been successfully used to overcome this problem.

The exploitation of the catalytic properties of coinage metal NPs such as AuNPs, AgNPs and CuNPs in the reduction of nitro-containing, aromatic environmental pollutants (such as nitrobenzene or 4-NP) to less harmful, or even useful by-products, was vital because of the simplicity and low cost (given that the reduction procedure takes place in water at room temperature). 4-NP is a pollutant frequently found in wastewater, often originating as an end-product in the degradation of pesticides such as parathion and nitrofen (Marais *et al.,* 2006), from industrial plants used in paper manufacturing processes, in pharmaceutical companies and dye industries (Li *et al.,* 2007; Gupta *et al.,* 2014). 4-aminophenol (4-AP) is a crucial compound in the synthesis of painkillers, antipyretic drugs and as corrosion inhibitors (Panigrahi *et al.,* 2014). The reduction of the toxic 4-NP by $NaBH_4$ to produce 4-AP requires the use of a catalyst and one with enhanced abilities is therefore desired.

Prahdan *et al*. (2002) reported on the catalytic reduction of 4-NP using $NaBH_4$ in the presence of AgNPs as catalysts, while AuNPs have also been used in the catalytic reduction of 4-NP using $NaBH_4$ (Fedorczyk *et al.,* 2015; Sharma *et al.,* 2007). It has been previously demonstrated that the reduction of 4-NP by $NaBH_4$ does not proceed without the addition of NPs which act as a catalyst. However, upon addition of AuNPs, the reaction proceeds easily (Pradhan *et al.,* 2001). An electron transfer mechanism is responsible for the reaction and it takes place between the 4-NP, the $NaBH_4$ and the NPs (Chang and Chen, 2009).

This reaction was chosen as the model reaction since it is fast, clean and can be easily monitored in real-time following the addition of AuNPs to the mixture. The reaction is observed by the decrease of the 4-NP absorption peak at 400 nm and the appearance of 4-AP peak at 298 nm over time using UV-vis spectroscopy. The use of a much higher concentration of $NaBH_4$ compared to that of 4-NP shows that the reduction rate is independent of $NaBH_4$ (Lee *et al.,* 2007). Thus, this process is regarded as standard test reaction to investigate the catalytic activity of differently synthesized NPs which can vary in size and shape (Zhao *et al.,* 2015b; Fedorczyk *et al.,* 2015).

Although there are only a few reports of AuNPs embedded in biomaterials such as *Sesbania drummondi* (Sharma *et al.,* 2007), there is no report of AuNPs embedded uniformly on *Ulva.*

Therefore, the synthesis of AuNPs embedded on surface of *Ulva* with good catalytic activity and high stability will be a good inclusion to research the ability of *Ulv*a as a biosupport. Herein, we report on the catalytic function of AuNPs embedded on *Ulva* for the reduction of 4-nitrophenol in the presence of $NaBH_4$.

5.2. Chemicals

$HAuCl_4$, $NaBH_4$ and 4-nitrophenol (4-NP) were all purchased from Sigma Aldrich and used as received. All aqueous solutions were prepared with MilliQ water (18 mΩ, Millipore).

5.3. Methodology

5.3.1. Catalytic experiments

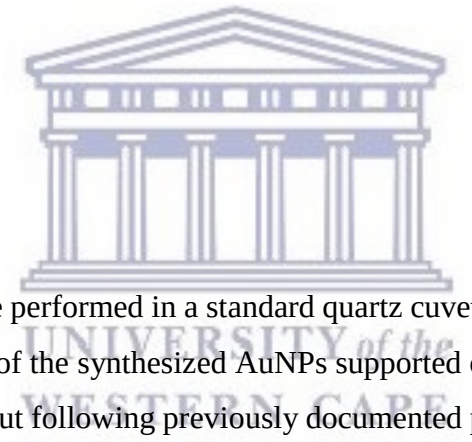

The catalytic experiments were performed in a standard quartz cuvette with an optical path length of 1 cm. The catalytic activity of the synthesized AuNPs supported on *Ulva* in the reduction of 4-NP using $NaBH_4$ was carried out following previously documented protocols (Quites *et al.*, 2017; Sharma *et al.*, 2007) with minor modifications. The AuNPs bound to *Ulva* were firstly cryoground in liquid nitrogen to obtain a very fine powder. An amount of 500 µL of freshly prepared aqueous $NaBH_4$ (0.88 mM) was added to 25 mL of four different concentrations of 4-NP (0.75, 1.0, 1.50 and 2.0 mM) in a 50 mL centrifuge tube, resulting in a colour change from light yellow to deep yellow. Subsequently, 20 mg of the AuNP powder supported on *Ulva* was added. Following sonication, 100 µL aliquots of the reaction mixture were removed every 30min for 2 h, thereafter every 4 h and were diluted with 2.9 mL of water and the decolourization monitored using a UV-vis spectrophotometry.

5.4. Results and discussion

5.4.1. Catalytic reduction of 4-NP

The spectrum of a neutral aqueous solution of 4-NP (at 1.5 mM) showed a strong absorption peak with a λ_{max} at 316 nm (Figure 5.1; peak A). Upon the addition of the $NaBH_4$ (0.88 mM), the colour of the solution changed from a light yellow to a deep yellow and bubbles were formed in solution (due to H_2 gas liberation). These observations all indicate transformation of the 4-NP into the 4-nitrophenolate ions (Quites *et al.*, 2017; Fedorczyk *et al.*, 2015), together with a resultant red shift in the absorption band to longer wavelengths at λ_{max} = 400 nm (Figure 5.1; peak B) (Panigrahi *et al.*, 2007; Pradhan *et al.*, 2002).

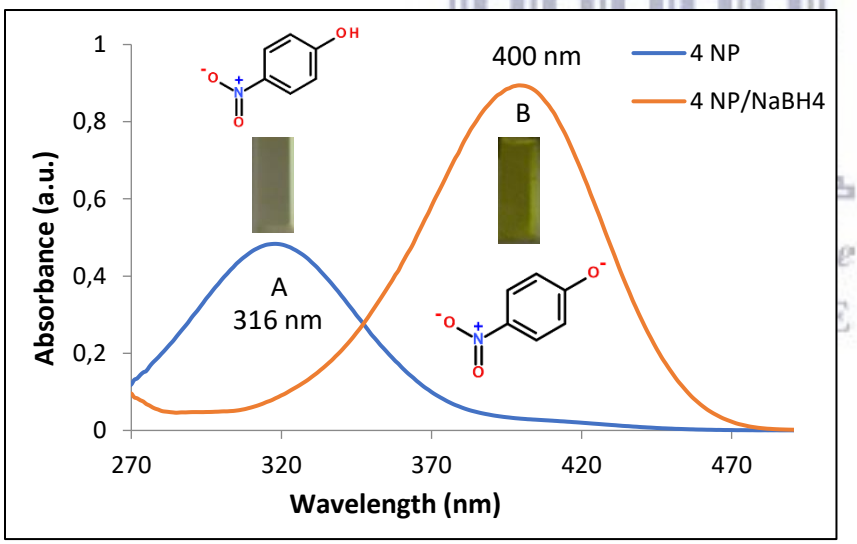

Figure 5.1: UV-vis absorption spectra of an aqueous solution of 4-NP (peak A) and of the 4-nitrophenolate ions (peak B) produced upon the addition of $NaBH_4$ to 4-NP.

Addition of the AuNPs resulted in a decrease in the 4-nitrophenolate absorption peak with the appearance and growth of a small peak at 298 nm at approximately 60 min, as can be seen in Figure 5.2 (A-D), indicating formation of the 4-AP (Sharma *et al.*, 2007; Zhao *et al.*, 2015; Hayakawa *et*

al., 2003). Since different concentrations of 4-NP (0.75, 1.0, 1.5 and 2.0 mM) were used with a constant concentration of AuNPs (20 mg) and $NaBH_4$ (0.88 mM), it is important to note the difference in the size of the 4-AP peak at 298 nm as well as how quickly it formed. It is also important to monitor how rapid the 4-NP peak at 400 nm was reduced. At lower concentrations of 4-NP (i.e. 0.75 mM), the development of the peak at 298 nm appeared much bigger with a much higher absorbance followed by that of 1.0, 1,5 and 2.0 mM respectively. This suggests that an increase in the concentration of 4-NP results in a decrease in the concentration of 4-AP concentration using the Beer-Lambert Law. Alternatively, the nitrophenolate absorption at 400 nm, appeared to be reduced much more quickly at a concentration of 0.75 mM compared to other higher concentrations. The 0.75 mM [NP] solution was almost completely reduced since the nitrophenolate absorbance peak is almost zero, while as the 4-NP concentration is increased, the 4-NP is not reduced as much.

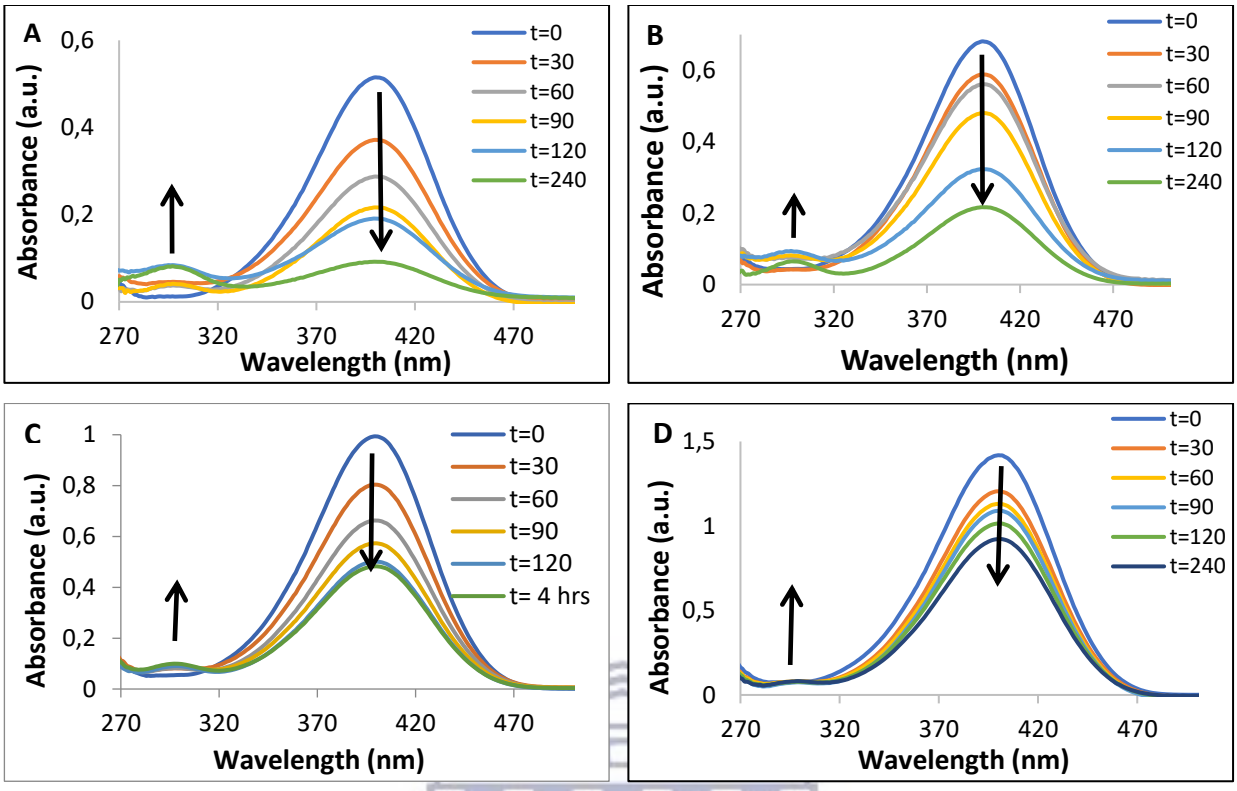

Figure 5.2: Time (in minutes) dependent UV-vis absorption spectra for the reduction of the 4-nitrophenol and for the gradual development of 4-AP over 4 h. Conditions: (A) [4-nitrophenol] = 0.750 mM (B) [4-NP] = 1.0 mM, (C) [4-NP] = 1.50 mM and (D) [4-NP] = 2.0 mM. Concentration of [$NaBH_4$] = 0.88 mM and quantity of AuNPs = 20 mg.

It is important to note that the intensity of the absorbance peak corresponding to 4-AP is much smaller in comparison to that of 4-nitrophenolate peak and this may be due to very low extinction coefficient (2582 M^{-1} cm^{-1}) of the 4-AP compound at λ = 298 nm (Ferdorczyk *et al.*, 2015) compared to 4 nitrophenolate ions which have an extinction coefficient of 1.76×10^4 M^{-1} cm^{-1} at λ = 400 nm. Thus, it is not possible to compare the relative intensities of these peaks offhand to give an indication of the quantities present for each component.

Two control reactions were used in this study. Figure 5.3 illustrates the UV-vis absorption spectra obtained for the reduction of the 4-NP in the absence of any *Ulva* material alone or AuNPs supported on *Ulva*. It became apparent that the reaction does not proceed in the absence of a catalyst (in this case the AuNPs) which agrees with other studies (Chang and Chen, 2009; Prahadan

et al., 2001; Fedorczyk *et al.*, 2015; Sharma *et al.*, 2007). This suggests that the AuNPs supported on the *Ulva* served as a catalyst for the reduction and is required for the reaction to proceed (Chang and Chen, 2009; Prahadan *et al.*, 2001; Fedorczyk *et al.*, 2015; Sharma *et al.*, 2007). A second control reaction (Figure 5.4) was carried out, where 20 mg of *Ulva* without AuNPs were added to the reaction mixture and similar results were obtained, showing that the reaction cannot proceed without AuNPs and that the *Ulva* alone is not responsible for the reduction.

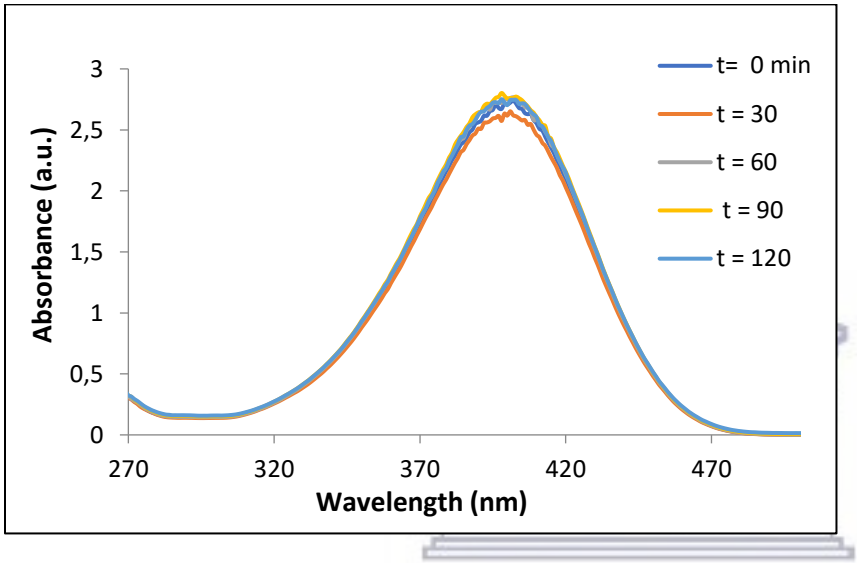

Figure 5.3: Time dependent UV-vis absorption spectra for the attempted reduction of the 4-nitrophenolate ions with $NaBH_4$ in the absence of *U. lactuca* or AuNPs (in water). The legend given is time in minutes.

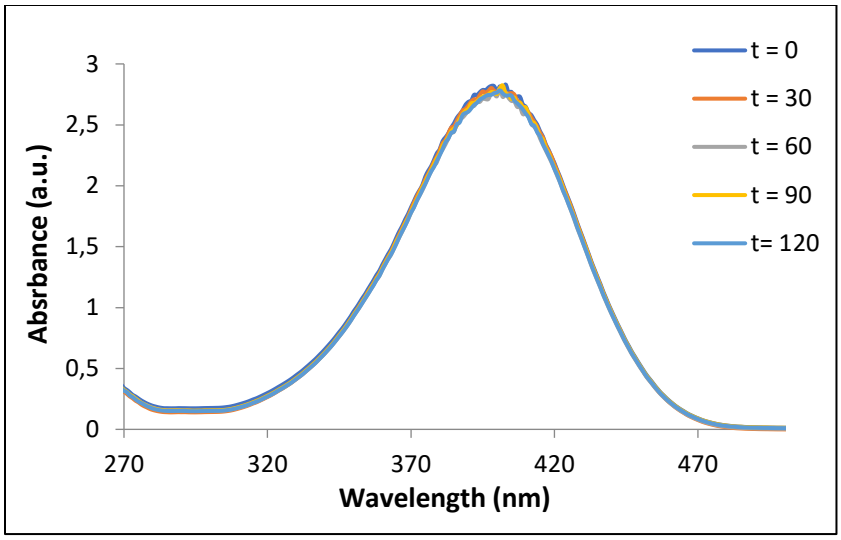

Figure 5.4: Time dependent UV-vis absorption spectra for the attempted reduction of the 4-nitrophenolate ions with $NaBH_4$ using *Ulva* without AuNPs (in water). The legend given is time in minutes.

5.4.2. Determination of rate constants for the reduction of 4-NP

Figure 5.2 shows the absorption spectral changes observed during the reduction of 4-NP at 30 min intervals using the AuNPs supported on *Ulva* as a support. Figures 5.3 and 5.4 further show that it is the AuNPs which are responsible for the catalytic activity and that *Ulva* acts simply as a support and does not interfere with the AuNPs' ability to catalyze the reduction.

A plot of the 4-NP concentration versus reaction time is shown in Figure 5.5 and the kinetic data obtained is listed in Table 5.1. The linearity of the plots obtained from $\ln(C_o/C)$ vs. time indicates that this reaction follows first order kinetics. The data shows that with an increase in concentration of 4-NP, the rate of 4-NP reduction generally stayed the same, while a decrease in k_{obs} was observed with an increase in 4-NP concentration. The half-lives for the reaction were found to increase with an increase in concentration of 4-NP, indicating the efficiency of the AuNPs is greater at lower concentrations of 4-NP. It is apparent from these data (and the R^2 values obtained) that at a concentration of 2.0 mM, the efficiency of the AuNPs in reducing 4-NP is reaching a

threshold. Due to time constraints, reduction reactions at lower concentrations (than 0.75 mM) of 4-NP were not assessed.

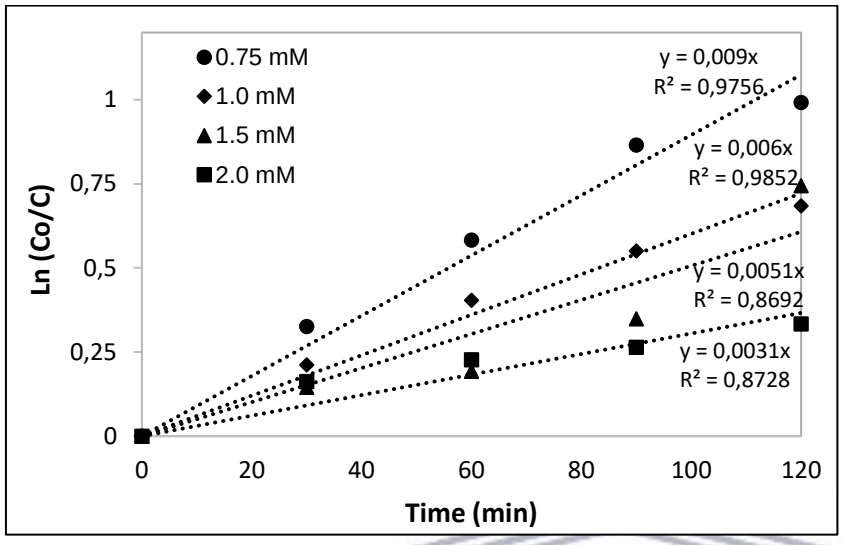

Figure 5.5: A Plot of ln(C_o/C) versus reaction time for the reduction of 4-NP at four different concentrations (i.e. 0.75, 1.0, 1.5 and 2.0 mM).

Table 5.1: Comparison of the rate constants, initial rate and half-lives obtained for 4-NP (at 0.75, 1.0, 1.5, 2.0 mM) in the presence of 20 mg of AuNPs and 0.88 mM $NaBH_4$.

[4NP] / x 10^{-3} mol.L^{-1}	***k*obs**	**Initial rate / x10^{-6} mol.L^{-1}.min^{-1}**	**Half-life/min**
0.75	0.0090	6.75	77
1.0	0.0060	6.00	116
1.5	0.0051	7.65	136
2.0	0.0031	6.20	224

5.4. Conclusions

The AuNPs synthesized using live *Ulva*, were shown to be efficient in carrying out the reduction of 4-nitrophenol using $NaBH_4$ particularly at lower concentrations of 4-NP. The study showed that

it was indeed the AuNPs that were responsible for the successful reduction of 4-NP as shown by the decrease in the λ_{max} of the 4 nitrophenolate ions at 400 nm, together with the successful formation of 4-AP by the appearance of the characteristic absorption peak at 298 nm using UV-vis spectroscopy. The catalyst could be viewed as an organic–inorganic hybrid system in which AuNPs are encapsulated in a *U. lactuca* as a matrix.

Chapter 6 Conclusions and future work

6.1. Conclusions

Growing concern for the environment, together with the outstanding properties associated with nanoparticles has led to the intensive development of green synthetic methods for these nanomaterials. The first step in this study involved the screening of the several aqueous extracts from a variety of green, red and brown algae to gauge their capacity to make gold nanoparticles. Eleven aqueous extracts were screened, including that of the green seaweed *Ulva lactuca*. Only three of the eleven aqueous extracts which were from brown algae shown to produce AuNPs and these extracts were all obtained from brown algae. As it has been indicated that in this may have been due to the presence of certain water soluble reductant species in the brown algae, while the green and red algae in the study do not have. A future question will be to answer is "What are they?" The total antioxidant and total reducing power contents, as well as the DPPH radical scavenging abilities for these extracts were determined and related to their ability to produce the NPs, as previously shown by Mmola *et al*. (2016).

UV-vis spectroscopy revealed the development of the characteristic SPR band for AuNPs at ~540 nm and the absorbance used to determine the rate of AuNP formation for these NPs. The zeta potential measurements of SB2014 AuNPs was very close to zero (-1.36 mV) while those of NDK100 and NDK130 were a highly negative with values of -27.8 and -23.2 mV. The colour changed from pink to blue which showed that they were not too stable in water and therefore it would be necessary to improve their stability by addititon of a capping agent in the future. HRTEM was used to image the samples and the AuNPs were found to be of various shapes and sizes including spheres, rods and triangles, with sizes ranging from 20 nm to 200 nm.

Thus, a green, eco-friendly, one-step synthesis of AuNPs using algal aqueous extracts as reducing agents at room temperature and pressure conditions was developed. The process was deemed to

be energy efficient, the reagent wastage was kept to a minimum with real time monitoring and no unnecessary ancillary materials or auxiliary derivatives were employed since only the metal salt and aqueous extracts (which functioned as both the reducing and capping agent) were employed. This is in keeping with some of the twelve principles of green chemistry. These AuNPs may find use in various biomedical applications, since the NPs produced are biocompatible and they may be further loaded with an active pharmaceutical ingredient such as an anticancer agent. Furthermore, the polysaccharides which are likely capping the NPs are loosely bound to the nanoparticle surface via hydrogen bonding, making these NPs potentially useful in catalysis.

The serendipitous discovery of a green synthetic method for AuNP synthesis using a live marine green seaweed *Ulva lactuca* followed this initial study. The formation of AuNPs was at first visually observed with a change in solution colour from yellow and to a deep pink colour, which was confirmed by monitoring the SPR band using UV-vis spectroscopy. UV-vis spectroscopy showed that the production of AuNPs commenced in solution after 30 min as observed by an increase in absorbance at the SPR band of AuNPs at 550 nm, and a shoulder at 660 nm, up until 120 min, when a decrease in the maximum absorbance was observed at both wavelengths. It became apparent that after some of the AuNPs were formed in solution, these NPs were then taken up the live *Ulva* too. This accounted for the decrease observed in the absorbance observed. The amount of gold remaining in the solution after addition of *Ulva* was quantified using ICP-AES, which revealed that the *Ulva* rapidly depletes the heavy metal from solution (100% in 90 min). This is in keeping with previous studies which observed that *Ulva* is efficient in heavy metal bioremediation. HRTEM coupled to energy dispersive X-ray (EDX) spectroscopy and selected area electron diffraction (SAED) was used to determine average particle size, morphology, elemental composition and crystallinity of the AuNPs formed initially in solution. The images revealed AuNPs which were mostly spherical, with the occasional triangular shape, with sizes ranging between 9 and 30 nm on day 7. Additionally, HRTEM was also used to determine the site of formation of the AuNPs on and in the *Ulva* leaf and cells. HRTEM, FESEM and XPS revealed that the AuNP formation takes place on the surface of the *Ulva* thallus, while the TEM images further revealed that the AuNPs were located consistently in the chloroplasts and around the cell walls. The oxidation state of the Au on the surface of the *Ulva* thallus was determined to be in its

metallic state (i.e. Au(0)) using XPS, while the reflections in the XRD spectra showed the AuNPs embedded in the *Ulva* to be in an fcc crystalline phase, with an average particle size of ~10 nm. This study has shown that *Ulva* can be used as an efficient, green synthetic biofactory to produce AuNPs. *Ulva* has presented a unique ability for the intracellular formation of AuNPs which were also revealed to form on the surface of the *Ulva* thallus too.

The catalytic ability of the as-synthesized AuNPs supported on the *U. lactuca* seaweed were subsequently assessed using a model reaction i.e. the reduction of 4-nitrophenol (4-NP) 4-aminophenol. The AuNPs supported on *Ulva* were successful in reducing the toxic 4-nitrophenol to the less toxic, industrially useful intermediate, 4-aminophenol (4-AP). The AuNPs supported on *Ulva lactuca* demonstrated excellent catalytic activity in the reduction of 4-NP by $NaBH_4$ especially at lower concentrations of 4-NP, as shown by the rapid decrease in the nitrophenolate absorption band at 400 nm and the appearance of new absorption band at 298 nm, revealing formation of the 4-aminophenol. The study demonstrates that, although it is preferred that the capping agent is loosely bound on the NP surface for catalytic applications, the AuNPs supported on the Ulva seaweed can still find some purpose.

The synthetic procedures involved in this study are therefore ideal due to its eco-friendly nature, eliminating the disadvantages associated with conventional physical and chemical methods. These biosynthesized NPs are expected to have variety of applications such as catalytic activities as well as biomedical applications.

6.2. Future work

The synthesis of AuNPs using the live seaweed brings about the question of how the nanoparticles are produced by the seaweed. It is clear that the gold metal salt is taken up by the seaweed since it is toxic and it is therefore reduced to it's the metallic state (which is non-toxic). The AuNPs formed on the *Ulva* thallus surface, in the chloroplasts and cell walls of *Ulva*, and it is therefore important to isolate the various cellular components to confirm the mechanism of formation of the AuNPs.

The biomatrix supported AuNPs showed good catalytic activity in the reduction of 4-NP which is a common environmental pollutant found in wastewater. A full evaluation of the kinetics of the reaction remain to be determined together with whether the catalyst could be reused or recycled. The catalyst could be also be considered in the catalysis of some other environmentally hazardous compounds such in the oxidation of carbon monoxide to CO_2. Additionally, the AuNPs formed within the solution could also be tested for some biomedical applications upon incorporation of biologically active components as well.

References

Aaron J, de la Rosa E, Travis K, Harrison N, Burt J, José-Yacamán M & Sokolov K (2008). Polarization microscopy with stellated gold nanoparticles for robust, in-situ monitoring of biomolecules. *Optics express;* **16(3):**2153-2167.

Abd El Baky HH, El-Baroty GS, Ibrahim AE & El Baz FK (2014). Cytotoxicity, antioxidants and antimicrobial activities of lipids extracted from some marine algae. *J. Aquacult. Res. Dev;* **5(7):**1-5.

Ahmad A, Senapati S, Khan MI, Kumar R, Ramani R, Srinivas V & Sastry M (2003). Intracellular synthesis of gold nanoparticles by a novel alkalotolerant actinomycete *Rhodococcus* species. *Nanotechnol;* **14**:824–825.

Ai J, Biazar E, Jafarpour M, Montazeri M, Majdi A, Aminifard S, Zafari M, Akbari HR & Rad HG (2011). Nanotoxicology and nanoparticle safety in biomedical designs. *Int j nanomed*; **6:**1117–1127.

Akhtar MS, Panwar, J & Yun YS (2013). Biogenic synthesis of metallic nanoparticles by plant extracts. *ACS Sustain Chem. Eng;* **1:**591–602**.**

Ale MT, Mikkelsen JD & Meyer AS (2011). Important determinants for fucoidan bioactivity: a critical review of structure-function relations and extraction methods for fucose-containing sulfated polysaccharides from brown seaweeds. *Mar Drugs*; **9:**2106–2130.

Alivisatos AP (1996). Perspectivdes on the physical chemistry of semiconductor nanocrystals. *J Phys Chem*; **100:**13226–13239.

Allafchian AR, Mirahmadi-Zare SZ, Jalali SAH, Hashemi SS & Vahabi MR (2016). Green synthesis of silver nanoparticles using *Phlomis* leaf extract and investigation of their antibacterial activity. *J. Nanostructure Chem*; **6**:129–135.

Amendola V& Meneghetti M (2009). Size Evaluation of Gold Nanoparticles by UV−vis Spectroscopy. *J. Phys. Chem;* 113**(11):**4277–4285.

Anastas PT & Warner JC (1998). Green Chemistry: Theory and Practice. Oxford, UK: *Oxford University Press***.**

Ankamwar B (2010). Biosynthesis of gold nanoparticles (green-gold) using leaf extract of *Terminalia catappa*. *J Chem;* **7:**1334–1339.

Aromal SA, Vidhu VK & Philip D (2012). Green synthesis of well-dispersed gold nanoparticles using *Macrotyloma uniflorum*. *Spectrochim Acta A Mol Biomol Spectrosc*; **85:**99–104.

Arunachalam KD, Annamalai SK & Hari S (2013). One-step green synthesis and characterization of leaf extract-mediated biocompatible silver and gold nanoparticles from *Memecylon umbellatum*. *Int j nanomed;* **8:**307–1315.

Asmathunisha N & Kathiresan K (2013). A review on biosynthesis of nanoparticles by marine organisms. *Colloids Surf. B: Biointerfaces;* **103**:283–28.

Bankar A, Joshi B, Kumar AR & Zinjarde S (2010). Banana peel extract mediated synthesis of gold nanoparticles. *Colloids Surf B Biointerf*; **80:**45–50.

Baudot C, Tan CM & Kong JC (2010). FTIR spectroscopy as a tool for nano-material characterization. *Infrared Phys Technol*; **53:**434–438.

Bearden JA (1967). X-ray Wavelengths. *Rev. Mod. Phys;* **39:**78- 124.

Bhumkar DR, Joshi HM, Sastry M & Pokharkar VB (2007). Chitosan reduced gold nanoparticles as novel carriers for transmucosal delivery of insulin. *Pharm. Res;* **24:**1415–1426.

Bolton JJ & Stegenga H (2002). Seaweed species diversity in South Africa. *Afr. J. Marine Sci;* **24(1)**:9-18.

Bolton JJ, Robertson-Andersson DV, Shuuluka D & Kandjengo L (2009). Growing *Ulva* (Chlorophyta) in integrated systems as a commercial crop for abalone feed in South Africa: a SWOT analysis. *J Appl Phycol;* **21:**575–583.

Borchert H, Shevchenko EV, Robert A, Mekis I, Kornowski A, Grübel G & Weller H (2005). Determination of nanocrystal sizes: a comparison of TEM, SAXS, and XRD studies of highly monodisperse CoPt3 particles. *Langmuir;* **21(5):**1931-6.

Bozˇanic DK, Luyt AS, Trandafilovic LV & Djokovic V (2013). Glycogen and gold nanoparticle bioconjugates: controlled plasmon resonance via glycogen-induced nanoparticle aggregation. *RSC Adv;* **3:**8705- 8713.

Bradford MM (1976). A rapid and sensitive method for the quantitation of microgram quantities of protein utilizing the principle of protein-dye binding. *Anal Biochem;* **72:**248–254.

Brar SK & Verma M (2011). Measurement of nanoparticles by light-scattering techniques. *TrAC Trends Anal Chem;* **30:**4–17.

Brayner R, Ferrari-Iliou R, Brivois N, Djediat S, Benedetti M & Fiévet F (2006). Toxicological impact studies based on *Escherichia coli* bacteria in ultrafine ZnO nanoparticles colloidal medium. *Nano Lett;* **6:**866–870.

Brust M, Walker M, Bethell D, Schiffrin DJ & Whyman RJ (1994). Synthesis of thiol derivatised gold nanoparticles in a two-phase liquid – liquid system. *Chem Soc Chem Commun;* **7:**801–802.

Cai W, Shin DW, Chen K, Gheysens O, Cao Q, Wang SX, Gambhir SS & Chen X. (2006). Peptide-labeled near-infrared quantum dots for imaging tumor vasculature in living subjects. *Nano Lett*; **6:**669–676.

Cai W, Chen K, Li ZB, Gambhir SS & Chen X (2007). Dual-function probe for PET and near-infrared fluorescence imaging of tumor vasculature. *J Nucl Med;* **48:**1862–1870.

Cai W, Hsu AR & Li ZB (2007b). Are quantum dots ready for in vivo imaging in human subjects? *Nanoscale Res Lett;* **2:**265–281.

Cai W & Chen X (2007). Nanoplatforms for targeted molecular imaging in living subjects. *Small;* **3:**1840–1854.

Cai W & Chen X (2008). Multimodality imaging of tumor angiogenesis. *J Nucl Med;* **49:**113S–128S.

Cai W, Gao T, Hong H & Sun J (2008). Applications of gold nanoparticles in cancer nanotechnology. *Nanotechnol. Sci. Appl;* **8(1):**17–32.

Chaikin Y, Kedem O, Raz J, Vaskevich A & Rubinstein I (2013). Stabilization of Metal Nanoparticle Films on Glass Surfaces Using Ultrathin Silica Coating. *Anal. Chem;* **85(21):**10022–10027.

Chandran SP, Chaudhary M, Pasricha R, Ahmad A & Sastry M (2006). Synthesis of gold nanotriangles and silver nanoparticles using *Aloevera* plant extract. *Biotechnol Progress*; **22:**577–583.

Chang YC & Chen DH (2009). Catalytic reduction of 4-nitrophenol by magnetically recoverable Au nanocatalyst. *J. Hazard. Mater;* **165:**664-669.

Cantor CR & Schimmel PR (1980). Techniques for the study of biological structure and function. San Francisco: *W. H. Freeman*.

Cao X, Ye Y & Liu S (2011). Gold nanoparticle-based signal amplification for biosensing. *Anal. Biochem;* **417(1):**1–16.

Chandrasekharan N & Kamat PV (2000). Improving the photoelectrochemical performance of nanostructured TiO_2 films by adsorption of gold nanoparticles. *J Phys Chem B;* **104:**10851–10857.

Chauhan A & Chauhan P (2014). Powder XRD Technique and its Applications in Science and Technology. *Anal Bioanal Tech;* **5(212)**:1-5.

Chen W, Cai W, Zhang L, Wang G & Zhang L (2001). Sonochemical processes and formation of gold nanoparticles within pores of mesoporous silica. *J. Colloid Interface Sci;* **238:**291–295.

Chen S & Yang Y (2002). Magnetoelectrochemistry of gold nanoparticle quantized capacitance charging. *J Am Chem Soc;* **124:**5280– 5281.

Chen R, Du Y, Xing W & Xu N (2006). The Effect of Titania Structure on Ni/TiO_2 Catalysts for p-Nitrophenol Hydrogenation. *Chin. J. Chem. Eng;* **14:**665–669.

Chen ZH, Jie JS, Luo LB, Wang H, Lee CS & Lee ST (2007). Applications of silicon nanowires functionalized with palladium nanoparticles in hydrogen sensors. *Nanotechnol*; **18:**1–5.

Chen YH, Tsai CY, Huang PY, **Chang MY, Cheng PC, Chou CH, Chen DH, Wang CR, Shia AL & Wu C L** (2007b). Methotrexate conjugated to gold nanoparticles inhibits tumor growth in a syngeneic lung tumor model. *Mol Pharm;* **4:**713–722.

Cioc RC, Ruijter E & Orru RVA (2014). Multicomponent reactions: advanced tools for sustainable organic synthesis. *Green Chem;* **16**:2958-2975.

Coats AW & Redfern JP (1963). Thermogravimetric analysis. A review. *Analyst*; **88**: 906-924.

Coccia F, Tonucci L, Bosco D, Bressan M & d'Alessandro N (2012). One pot synthesis of lignin-stabilized platinum and palladium nanoparticles and their catalytic behaviours in oxidation and reduction reactions. *Green Chem;* **14:**1073–1078**.**

Copertino MS, Tormena T & Seeliger U (2009). Biofiltering efficiency, uptake assimilation rates of *Ulva clathrata* (Roth) *J. Agardh* (Chlorophyceae) cultivated in shrimp aquaculture waste water. *J Appl Phycol;* **21:**31–45.

Corbett JF (1999). An histological review of the use of dye precursors in the formulation of commercial oxidation hair dyes. *Dyes Pigments*; **41:**127-136.

Costa S, Crespo D, Henriques BMG, Pereira E, Duarte AC & Pardal MA (2011). Kinetics of Mercury Accumulation and Its Effects on *Ulva lactuca* Growth Rate at Two Salinities and Exposure Conditions. *Water Air Soil Pollut*; **217:**689–699.

Crossley ML (1922). The Chemistry of Intermediates. *Ind. Eng. Chem;* **14:**802–804.

Dahl JA, Maddux BLS & Hutchison JE (2007). Toward greener nanosynthesis. *Chem. Rev.* 2007, **107:**2228-2269.

Dann SE (2002). Reactions and Characterization of Solids. 1st ed. *Polestar Wheatons Ltd*, Exeter: *Royal Society of Chemistry;* 10.

Darcy-Vrillon B (1993). Nutritional aspects of the developing use of marine macroalgae for the human food industry. *Int J Food Sci Nutr;* **44:**S23–S35.

Das RK, Gogoi N & Bora U (2011). Green synthesis of gold nanoparticles using *Nyctanthes arbortristis* flower extract. *Bioprocess Biosyst Eng;* **34:**615–619.

Dhas ST, Kumar GV, Abraham SL, Karthick V & Govindaraju K (2012). *Sargassum myriocystum* mediated biosynthesis of gold nanoparticles. *Spectrochim. Acta, Part A*; **99**(**15):** 97–101.

Douglas KR & Tyla SF (2010). Transmission electron microscopy of cartilage and bone. *Methods in Cell Biology;* **96:**443-473.

Drummond IW & Bryson RMD (1996) Spatial Resolution in X-Ray Photoelectron Spectroscopy. *Phil. Trans R Soc;* **354:**2667-268.

Dujardin E, Peet C, Stubbs G, Culver JN & Mann S (2003)**.** Organization of Metallic Nanoparticles Using *Tobacco Mosaic Virus* Templates. *Nano. Lett*; **3**:413-417.

Elavazhagan T & Arunachalam KD (2011). *Memecylon edule* leaf extract mediated green synthesis of silver and gold nanoparticles. *Int j nanomed;* **6:**1265–1278.

Esumi K, Isono R & Yoshimura T (2004). Preparation of PAMAM− and PPI−Metal (Silver, Platinum, and Palladium) Nanocomposites and Their Catalytic Activities for Reduction of 4-Nitrophenol. *Langmuir;* **20:**237–243.

Eustis S, Hsu HY & El-Sayed MA (2005). Excitation in colloidal solutions. A proposed molecular mechanism. *J Phys Chem B;* **109(11):**4811–4815.

FAO (2004). The State of the World Fisheries and Aquaculture. FAO, Rome.

Fedorczyk A, Ratajczak J, Kuzmych O, Skompska M (2015). Kinetic studies of catalytic reduction of 4-nitrophenol with $NaBH_4$ by means of Au nanoparticles dispersed in a conducting polymer matrix. *Solid State Electrochem;* **19(9)**: 2849–2858.

Feldheim DL & Colby A Jr (2002). Metal Nanoparticles: Synthesis, Characterization, and Applications. *CRC Press;* Boca Raton, FL.

Ferrari M (2005). Cancer nanotechnology: opportunities and challenges. *Nat Rev Cancer;* **5:**161–171.

Fourie AM (1994). Tank culturing of *Gracilaria verrucosa* for use as a food source for abalone. MSc Dissertation. University of Port Elizabeth, Port Elizabeth, South Africa

Freeman RG, Grabar KC, Allison KJ, Bright RM, Davis JA, Guthrie AP, Hommer MB, Jackson MA, Smith PC, Walter DG & Natan MJ (1995). Self-assembled metal colloid monolayers: an approach to SERS substrates. *Science;* **267:**1629–1632.

French RA, Jacobson AR, Kim B, Isley SL, Penn RL & Baveye PC (2009). Influence of ionic strength, pH, and cation valence on aggregation kinetics of titanium dioxide nanoparticles. *Environ Sci Technol*; **43:**1354–1359.

Frens G (1973). Controlled nucleation for the regulation of the particle size in monodisperse gold suspensions. *Nature;* **241:**20–22.

Galbraith CG & Galbraith JA (2011). Super-resolution microscopy at a glance. *J Cell Sci;* **124:**1607-1611.

Gardea-Torresdey JL, Parsons JG, Gomez E, Peralta-Videa J, Troiani HE, Santiago P & Yacaman JM (2002). Formation and growth of Au nanoparticles inside live alfalfa plants. *Nano Lett;* **2:**397–401.

Ghodake G & Lee DS (2011). Biological synthesis of gold nanoparticles using the aqueous extract of the brown algae *Laminaria japonica. J. Nanoelectron Optoe;* **6:**1–4.

Ghosh SK, Mandal M, Kundu S, Nath S & Pal T (2004).Bimetallic Pt–Ni nanoparticles can catalyze reduction of aromatic nitro compounds by sodium borohydride in aqueous solution. *Appl. Catal A;* **268:**61–66.

Gherbawy YA, Shalaby IM, Abd El-sadek MS, Elhariry HM & Banaja AA (2013). The anti-fasciolasis properties of silver nanoparticles produced by *Trichoderma harzianum* and their improvement of the anti-fasciolasis drug triclabendazole. *Int J Mol Sci;* **14**:21887–21898.

Giddings TH (2003). Freeze-substitution protocols for improved visualization of membranes in high-pressure frozen samples. *J. of Microscopy*; **212:**53-61.

Giusti L (2001). Heavy metal contamination of brown seaweed and sediments from the UK coastline between the Wear river and the Tees river. *Enviro Internat;* **26**:275-286.

Global Market Insights (2016) https://globenewswire.com/news-release/2016/04/21/831351/0/en/Gold-Nanoparticles-Market-Size-to-exceed-USD-8-Billion-by-2022-Global-Market-Insights-Inc.html

Goldstein JI, Newbury DE, Echlin P, Joy DC, Romig Jr AD, Lyman CE, Fiori C & Lifshin E (1992). Scanning Electron Microscopy and X-ray Microanalysis.2nd ed. *Plenum Press:* New York*;* 820.

Goettmann F, Moores A, Boissière C, Le Floch P & Sanchez C (2005). A Selective Chemical Sensor Based on the Plasmonic Response of Phosphinine-Stabilized Gold Nanoparticles Hosted on Periodically Organized Mesoporous Silica Thin Layers. *Small;* **1(6):**636–639.

Goodsell DS (2004). Bionanomedicine in action. In Bionanotechnology: Lessons from Nature. *John Wiley & Sons Inc;* Hoboken, NJ, USA.

Golding CG, Lamboo LL, Beniac DR & Booth TF (2016). The scanning electron microscope in microbiology and diagnosis of infectious disease. *Sci. Rep;* **6(26516):**1-8.

Govindaraju K, Kiruthiga V, Kumar VG & Singaravelu G (2009). Extracellular synthesis of silver nanoparticles by a marine alga, *Sargassum wightii Greville* and their antibacterial effects. *J Nanosci Nanotechnol;* **9:**5497–5501.

Grodzinski P, Silver M & Molnar LK (2006). Nanotechnology for cancer diagnostics: promises and challenges. *Expert Rev Mol Diagn*; **6:**307–318.

Guo S & Wang E (2007). Synthesis and electrochemical applications of gold nanoparticles. *Anal. Chim. Acta;* **29:**181–192.

Gupta VK, Atar N, Yola ML, Ustundag Z & Uzun L (2014). A novel magnetic Fe@Au core-shell nanoparticles anchored graphene oxide recyclable nanocatalyst for the reduction of nitrophenol compounds. *Water Re*s; **48:**210–217.

Guzzinati G, Clark L, Béché A, Juchtmans R , Van Boxem R, Mazilu M & Verbeeck J (2015). Prospects for versatile phase manipulation in the TEM: Beyond aberration correction. *Ultramicroscopy*; **151:**85–93.

Hanada N, Hirotoshi E, Chikawa T, Akiba E & Fujii H (2008). SEM and TEM characterization of magnesium hydride catalyzed with Ni nano-particle or Nb_2O_5. *J. Alloy Comp;* **450:**395-399.

Haruta M, Kobayashi T, Sano H & Yamada N (1987). Novel gold catalysts for the oxidation of carbon monoxide at a temperature far below 0°C. *Chem Lett;* **16:**405–408.

Haruta M & Daté M (2001). Advances in the catalysis of Au nanoparticles. *Appl Catal A General;* **222:**427–437.

Hayakawa K, Yoshimura T & Esumi K (2003) Preparation of gold–dendrimer nanocomposites by laser irradiation and their catalytic reduction of 4-nitrophenol. *Langmuir;* **19:**5517–5521.

Hayat MA (2000). Principles and Techniques of Electron Microscopy: BiologicalApplications, 4th ed. *Cambridge University Press;* Cambridge.

Herizchi R, Abbasi E, Milani M & Akbarzadeh A (2014). Current methods for synthesis of gold nanoparticles. *Artif Cells Nanomed Biotechnol;* **3:**1–7.

Hind AR, Bhargava SK & McKinnon A (2001). At the solid/liquid interface: FTIR/ATR—the tool of choice. *Adv Colloid Interface Sci;* **93:**91–114.

Hinrichsen E (2007). Introduction to Aquaculture in the Western Cape: Edition 1. Division of Aquaculture, Stellenbosch University Report. Republic of South Africa, Provincial Government of the Western Cape, Department of Environmental Affairs and Development Planning, Cape Town.

Howe JM, Mori H & Wang ZL (2008). In situ high-resolution transmission electron microscopy in the study of nanomaterials and properties. *Mat Res Bull;* **33(2):**115–121.

Hrapovic S, Liu Y, Male KB & Luong JHT (2004) Electrochemical biosensing plateform using platinum nanoparticles and carbon nanotubes. *Anal Chem;* **76:**1083–1088.

Hulkoti NI & Taranath TC (2014). Biosynthesis of nanoparticles using microbes—A review. *Colloids Surf B Biointerf;* **121**:474–483.

Hu M, Chen J, Li ZY, Au L, Hartland GV, Li X, Marquez M & Xia Y (2006). Gold nanostructures: engineering their plasmonic properties for biomedical applications. *Chem Soc Rev;* **35:**1084–1094.

Huang M & Hieftje GM (1989). Simultaneous measurement of spatially resolved electron temperatures, electron number densities and gas temperatures by laser light scattering from the ICP. *Spectrochim Acta B;* **44(8):**739–749.

Huang H & Yang X (2004). Synthesis of polysaccharide-stabilized gold and silver nanoparticles: a green method. *Carbohydr Res;* **339(15):**2627–2631.

Huang, D, Liao F, Molesa S, Redinger & Subramanian V (2003). Plastic-compatible low resistance printable gold nanoparticle conductors for flexible electronics. *Journal of the Electrochemical Society;* **150:**G412–G417.

Huang CJ, Chiu PH, Wang YH, Chen KL , Linn JJ & Yang CF (2006). Electrochemically controlling the size of gold nanoparticles. *J Electrochem Soc;* **153:**D193-D198.

Huang J, Li Q, Sun D, Lu Y, Su Y, Yang X, Wang H, Wang Y, Shao W, He N, Hong J & Cuixue Chen C (2007). Biosynthesis of silver and gold nanoparticles by novel sundried *Cinnamomum camphora* leaf. *Nanotechnol;* **18:**1-11.

Huang X, Jain PK, El-Sayed IH & El-Sayed MA (2007b). Gold nanoparticles: interesting optical properties and recent applications in cancer diagnostics and therapy. *Nanomed;* **2:**681–693.

Huennekens FM (1994). The methotrexate story: a paradigm for development of cancer chemotherapeutic agents. *Adv Enzyme Regul;* **34:**397–419.

Hunter RJ (2001). Foundations of colloid science. 2nd ed. Oxford: *Clarendon Press*.

Ibrahim WM, Hassan AF, Azab YA (2016). Biosorption of toxic heavy metals from aqueous solution by *Ulva lactuca* activated carbon. *EJB App Sci;* **3:**241–249.

Inbakandan D, Venkatesan R & Khan SA (2010). Biosynthesis of gold nanoparticles utilizing marine sponge *Acanthella elongata* (Dendy, 1905). *Colloids Surf B Biointerf;* **81:**634–639.

Jain D, Daima HK, Kachhwahaa S & Kotharia SL (2009). Synthesis of plant-mediated silver nanoparticles using papaya fruit extract and evaluation of their anti-microbial activities. Digest. *J Nanomater Biostruct*; **4(4)**:723-727.

Jain N, Bhargava A, Majumdar S & Panwar J (2011). Extracellular biosynthesis and characterization of silver nanoparticles using *Aspergillus flavus* NJP08: A mechanism prospective. *Nanoscale*; **3:**635–641.

Jain N, Bhargava A, Tarafdar JC, Singh SK & Panwar J (2013). A biomimetic approach towards synthesis of zinc oxide nanoparticles. *Appl. Microbiol.Botechnol*; **97**: 859–869.

James JZ, Lucas D & Koshland CP (2012). Gold nanoparticle films as sensitive and reusable elemental mercury sensors. *Environ Sci Technol;* **4; 46(17):**9557–9562.

Jana S, Ghosh SK, Nath S, Pande S, Praharaj S, Panigrahi S, Basu S, Endo T & Pal T (2006). Synthesis of silver nanoshell-coated cationic polystyrene beads: a solid phase catalyst for the reduction of 4-nitrophenol. *Appl. Catal A;* **313:**41–48.

Jones MR, Osberg KD, Macfarlane RJ; Langille MM & Mirkin CA. (2011). Templated techniques for the synthesis and assembly of plasmonic nanostructures. *Chem Revs;* **111:**3736-3827.

Jiang J, Oberdorster G & Biswas P (2009). Characterization of size, surface charge, and agglomeration state of nanoparticle dispersions for toxicological studies. *J. Nanopart. Res;* **11**(1):77–89.

Jiao G, Yu G, Zhang J & Ewart HS (2011). Chemical Structures and Bioactivities of Sulfated Polysaccharides from Marine Algae. *Mar Drugs;* **9:**196-223.

Johal MS (2011). Understanding nanomaterials. *CRC Press:* Boca Raton, FL.

Joseph D, Tyagi N, Geckeler C & Geckeler KE (2014). Protein coated pH-responsive gold nanoparticles: microwave-assisted synthesis and surface charge-dependent anticancer activity. *Beilstein J Nanotechnol;* **5:**1452–1462.

Kalishwaralal K, Deepak VV, Pandian SRK , Kottaisamy M, Kanth SB , Kartikeyan B & Gurunathan S (2010). Biosynthesis of silver and gold nanoparticles using *Brevibacterium casei*. *Col Surf B Biointerf;* **77:**257–262.

Kamat PV, Flumiani M & Hartland GV (1998). Picosecond dynamics of silver nanoclusters. Photoejection of electrons and fragmentation. *J. Phys. Chem. B;* **102**: 3123–3128.

Kamat PV (2002). Photophysical, Photochemical and Photocatalytic Aspects of Metal Nanoparticles *J. Phys. Chem.* **106:**7729–7744.

Kannan RRR, Arumugam R, Ramya D, Manivannan K & Anantharaman P (2013). Green synthesis of silver nanoparticles using marine macroalga *Chaetomorpha linum*. *Appl. Nanosci;* **3:**229–233.

Kantam ML Chakravarti R, Pal U, Sreedhar B & Bhargava S (2008). Nanocrystalline Magnesium Oxide-Stabilized Palladium(0): An Efficient and Reusable Catalyst for Selective Reduction of Nitro Compounds. *Adv. Synth. Catal;* **350:**822–827.

Kariis H, Westermark G, Persson I & Liedberg B (1998). Infrared Spectroscopic and Temperature-Programmed Desorption Studies of Dimethylphenylphosphine Adsorbed on the Coinage Metals. *Langmuir;* **14:**2736-2743.

Kazarian SG & Chan KL (2006). Applications of ATR–FTIR spectroscopic imaging to biomedical samples. *Biochim Biophys Acta*; **1758:**858–867.

Kelly MA (2003). Analysing Insulators with XPS and AES, in: D. Briggs, J.T. Grant (Eds.) Surface Analysis by Auger and X-ray Photoelectron Spectroscopy, *IM Publications*, Chichester; 191-210.

KimLing J, Maier M, Okenve B, Kotaidis V, Ballot H & Plech A (2006). Turkevich method for gold nanoparticle synthesis revisited. *J Phys Chem B;* **110:**15700–15707.

Knoll M & Ruska E (1932). Contribution to geometrical electron optics (in German). *Annalen der Physik;* **5**:607-661.

Korotcenkov G, Brinzari V & Cho B (2016). Conductometric gas sensors based on metal oxides modified with gold nanoparticles: a review. *Microchim Acta;* **183:**1033–1054.

Koteswari P, Krishna SR, Reddy VP & Nasaru LM (2011). Formulation and preparation of felodipine nanoemulsion. *Asian J. Pharm. Clin. Res;* 4:116–117.

Kreibig U & Vollmer M (1995). Optical Properties of Metal ClustersSpringer Series in Material Science. *Springer-Verlag*. . Berlin: 25.

Krolikowoska A, Kudelski A, Michota A & Bukowska J (2003). SERS studies on the structure of thioglycolic acid monolayers on silver and gold. *Surf Sci;* **532:**227–232.

Kulkarni N & Muddapur U (2014). Biosynthesis of Metal Nanoparticles: A Review. *J Nanotech;* **2014**:1-8.

Kumar A, Mandal S, Selvakannan PR, Parischa R, Mandale & Sastry M (2003). Investigation into the interaction between surface-bound alkylamines and gold nanoparticles. *Langmuir*; **19:**6277–6282.

Kumar A, Murugesan S, Pushparaj V, Xie J, Soldano C, John G, Nalamasu O, Ajayan PM & Linhardt RJ (2007). Conducting organic – metallic composite submicrometer rods based on Ionic liquids. *Small*; **3:**429–433.

Kumar JIN, Oommen C & Kumar RN (2009). Biosorption of Heavy Metals from Aqueous Solution by Green Marine Macroalgae from Okha Port, Gulf of Kutch, India. *J. Agric. & Environ. Sci;* **6(3):**317-323.

Kumar KP, Paul W & Sharma CP (2011). Green synthesis of gold nanoparticles with *Zingiber offi cinale* extract: characterization and blood compatibility. *Proc Biochem;* **46:**2007–2013.

Kumar KM, Mandal BK, Sinha M & Krishnakumar V (2012). *Terminalia chebula* mediated green and rapid synthesis of gold nanoparticles. *Spectrochim Acta A Mol Biomol Spectrosc;* **86:**490–494.

Kuge K, Arisawa M, Aoki N & Hasegawa A (2000). Preparation of gelatin layer film with gold clusters in using photographic film. *Jpn J Appl Phys;* **39:**6550-6554.

Kuppusamy P, Yusoff MM, Maniam GP & Govindan N (2014). Biosynthesis of metallic nanoparticles using plant derivatives and their new avenues in pharmacological applications – An updated report. *Saudi Pharm J*; **24(4**):473-484.

Kuppusamy P, Ichwan JAS, Parine NR, Yusoff MM, Maniam GP & Govindan N (2015). Intracellular biosynthesis of Au and Ag nanoparticles using ethanolic extract of *Brassica oleracea L.* and studies on their physicochemical and biological properties. *J. Environ. Sci*; **29**:151-157.

Kruse N & Chenakin S (2011). XPS characterization of Au/TiO2 catalysts: Binding energy assessment and irradiation effects. *Applied Catalysis A: General*; **391:**367–376.

Lahaye M (1991). Marine-algae as sources of fibers—determination of soluble and insoluble dietary fiber contents in some sea vegetables. *J Sci Food Agric;* **54:**587–594.

Lahaye M & Ray B (1996). Cell-wall polysaccharides from the marine green alga *Ulva rigida* (Ulvales, Chlorophyta)-NMR analysis of ulvan oligosaccharides. *Carbohydr Res;* **283:**161–173.

Lahaye M, Brunel M & Bonnin E (1997). Fine chemical structure analysis of oligosaccharides produced by an ulvan-lyase degradation of the water-soluble cell-wall polysaccharides from *Ulva* sp. (Ulvales, Chlorophyta). *Carbohydr Res;* **304:**325–333.

Lahaye M & Robic A (2007). Structure and functional properties of ulvan, a polysaccharide from green seaweeds. *Biomacromol;* **8:**1765–1774.

Laveille P, Guillois K, Tuel A, Petit C, Basset JM & Caps V (2016). Durable PROX catalyst based on gold nanoparticles and hydrophobic silica. *Chem Commun;* **52:**3179–3182.

Lavanya R & Veerappan N (2011). Antibacterial potential of six seaweeds collected from gulf of mannar of southeast coast of India. *Adv Biol Res;* **5:**8-44.

Lee KY, Hwang J, Lee YW, Kim J & Han SW (2007). One-step synthesis of gold nanoparticles using azacryptand and their applications in SERS and catalysis. *J. Colloid Interface Sci;* **316:**476-481.

Lee HJ, Lee G, Jang NR, Yun J.H, Song JY & Kim BS (2011). Biological synthesis of copper nanoparticles using plants extract. *Nanotechnol;* **1:**371–374.

Levec J & Pintar A (1995). Catalytic oxidation of aqueous solution of organics. An alternative method for removal of toxic pollutants from wastewater. *Catal. Today;* **24:**51-58.

LewisOscar F, Bakkiyaraj D, Nithya C & Thajuddin N (2014). Deciphering the diversity of microalgal bloom in wastewater—an attempt to construct potential consortia for bioremediation. *JCPAM;* **3(2):**92–96.

Li YP, Cao HB, Liu CM & Zhang Y (2007). Electrochemical reduction of nitrobenzene at carbon nanotube electrode. *J Hazard Mater;* **148:***158*–163.

Li C, Li D, Wan G, Xu J & Hou W (2011). Facile synthesis of concentrated gold nanoparticles with low size-distribution in water: temperature and pH controls. *Nanoscale Res Lett;* **6:**1–10.

Li WR, Xie XB, Shi QS, Duan SS, Ouyang YS & Chen YB (2011b). Antibacterial effect of silver nanoparticles on *Staphylococcus aureus*. *Biometals;* **24:**135–141.

Li L & Zhang Z (2016). Biosynthesis of Gold Nanoparticles Using Green Alga *Pithophora oedogonia* with Their Electrochemical Performance for Determining Carbendazim in Soil. *Int. J. Electrochem. Sci;* **11:**4550 – 4559

Liebig F, Sarhan RM, Prietzel C, Reinecke A & Koetz J (2016). Green gold nanotriangles: synthesis, purification by polyelectrolyte/micelle depletion flocculation and performance in surface-enhanced Raman scattering. *RSC Adv;* **6**:33561-33568.

Link S & El-Sayed MA (1999). Size and temperature dependence of the plasmon absorption of colloidal gold nanoparticles. *J Phys Chem B;* **103:**4212–4217.

Liss KD, Bartels A, Schreyer A & Clemens H (2003). High-Energy X-rays: A tool for Advanced Bulk Investigations in Materials Science and Physics. *Textures Microstruct;* **35:**219-252.

Liu H & Webster TJ (2007). Nanomedicine for implants: a review of studies and necessary experimental tools. *Biomaterials;* **28:**354–369.

Liu ZL, Deng JC, Deng JJ & Li FF (2008).s Materials Science and EngineeringB-Advanced Functional Solid-State Materials; Fabrication and photocatalysis of CuO/ZnO nano-composites via a new method. *Mat Sci Eng B;* **150:**99-104.

Liu G, Li Q, Ni W, Zhang N, Zheng X, Wang Y, Shao D & Tai G (2015). Cytotoxicity of various types of gold-mesoporous silica nanoparticles in human breast cancer cells. *Int J Nanomed;* **10:**6075–6087.

Loo C, Lowery A, Halas N, West J & Drezek R (2005). Immunotargeted nanoshells for integrated cancer imaging and therapy. *Nano Lett;* **5:**709–711.

Lopez N, Janssens TVW, Clausen BS, Xu Y, Mavrikakis M, Bligaard T & Nørskov JK (2003). On the origin of the catalytic activity of gold nanoparticles for low-temperature CO oxidation. *J. Catal;* **223:**232–235.

Lowery AR, Gobin AM, Day ES, **Halas NJ & West JL** (2006). Immunonanoshells for targeted photothermal ablation of tumor cells. *Int J Nanomed;* **1:**149–154.

Lozano-Martı´n MC, Castillejos E, Bachiller-Baeza B, Rodri-guez-Ramos I & Guerrero-Ruiz A (2015). Selective 1,3-butadiene hydrogenation by gold nanoparticles on novel nanocarbon materials. *Catal Today;* **249:**117–126.

Lu Y, Mei Y, Drechsler M & Ballauff M (2006). Thermosensitive core–shell particles as carriers for Ag nanoparticles: modulating the catalytic activity by a phase transition in networks. *Angew Chem Int Ed;* **45:**813-816.

Lu R, Xu L, Ge Z, Li R, Xu J, Yu L & Chen K (2016). Improved Efficiency of Silicon Nanoholes/Gold Nanoparticles/Organic Hybrid Solar Cells via Localized Surface Plasmon Resonance. *Nanoscale Res. Lett.;* **11(160):**1-7.

Luechinger NA, Athanassiou EK & Stark WJ (2008). Graphene stabilized copper nanoparticles as an air-stable substitute for silver and gold in low-cost ink-jet printable electronics. *Nanotechnology;* **19:**445201.

Mafune F, Kohno J, Takeda Y & Kondow T (2001). Formation of gold nanoparticles by laser ablation in aqueous solution of surfactant. *J Phys Chem B*; **105:**5114–5120.

Mahdavi M, Namvar F, Ahmad MB & Mohamad R (2013). Green biosynthesis and characterization of magnetic iron oxide (Fe_3O_4) nanoparticles using seaweed (*Sargassum muticum*) aqueous extract. *Molecules;* **18(5):**5954-5964.

Mahmoud MA, Saira F & El-Sayed MA (2010). Experimental Evidence For The Nanocage Effect In Catalysis With Hollow Nanoparticles. *Nano Lett;* **10(9):**3764-3769.

Makarov VV, Love AJ, Sinitsyna OV, Makarova SS, Yaminsky IV, Taliansky ME & Kalinina NO (2014). Green Nanotechnologies: Synthesis of Metal Nanoparticles Using Plants. *Acta naturae*; **6(1)**:35-44.

Malta E-J, Draisma S & Kamermans P (1999). Free-floating *Ulva lactuca* in the southwest Netherlands: species or morphotypes? A morphological, molecular and ecological comparison. *Eur J Phycol;* **34(5):**443-454.

Manivasagan P & Kim SK (2015). Biosynthesis of Nanoparticles Using Marine Algae: A Review, in Marine Algae Extracts: Processes, Products, and Applications (eds S.-K. Kim and K. Chojnacka), Wiley-VCH Verlag GmbH & Co. KGaA, Weinheim, Germany. doi: 10.1002/97835276 79577.ch17.

Maneveldt GW, Chamberlain YM & Keats DW (2008). A catalogue with keys to the non-geniculate coralline algae (*Corallinales*, Rhodophyta) of South Africa. *SA J Botany*; **74:**555–566.

Manchu N, Melpha Y & James JE (2014). Phytochemical investigation of three species of *Ulva* from Rasthacaud Coast, Tamil Nadu. *India J Chem and Pharm Res;* **6(8):**570-574.

Manna A, Chen P , Akiyama H, Wei T, Tamada K & Knoll W (2003). Optimized Photoisomerization on Gold Nanoparticles Capped by Unsymmetrical Azobenzene Disulfides. *Chem. Mater;* **15(1):**20–28.

Marais E, Klein R, Antunes E & Nyokong T (2006). Photocatalysis of 4-nitrophenol using zinc phthalocyanine complexes. *J. Mol. Catal. A: Chem*. **261:**36–42.

Martins AF, Facchi SP, Monteiroa JP, Nocchi SR, Silva CT, Nakamura CV, Girotto EM, Rubira AF & Muniz AC (2015). Preparation and cytotoxicity of N,N,N-trimethyl chitosan/alginate beads containing gold nanoparticles. *Int J Biol Macromol;* **72:**466-471.

Mata YN, Torres, Blázquez ML, Ballester A, González F & Munoz JA (2009). Gold(III) biosorption and bioreduction with the brown alga *Fucus vesiculosus*. *J Hazard Mater;* **166**:612–618.

Matus KJM, Hutchison JE, Peoples R, Rung S & Tanguay RL (2011). Green Nanotechnology Challenges and Opportunities. *ACS green chemistry institute.*

Maye MM, Luo J, Han L, Kariuki N, Rab Z, Khan N, Naslund HR & Zhong C (2004). Gold and alloy nanoparticle catalysts in fuel reaction. *Prept Pap Am Chem Soc Div Fuel Chem;* **49(2)**:938-939.

McDonald KL (2009). A review of high-pressure freezing preparation techniques for correlative light and electron miccroscopy of the same cells and tissues. *J. Microscopy;* **235:**273-281.

McClenathan DM, Wetzel WC, Lorgea SE & Hieftje GM (2006). Effect of the plasma operating frequency on the figures of merit of an inductively coupled plasma time-of-flight mass spectrometer. *J Anal At Spectrom;* **21**:160-167.

Mehrparvar AH, Davari MH, Mollasadeghi A, Vahidi MR, Mostaghaci M, Bahaloo M & Shokouh P (2013). Hearing Loss due to Carbon Monoxide Poisoning. *Case Reports Otolaryngol;* **2013:**1-3.

Mehta SK and Gaur JP (2005). Use of algae for removing heavy metal ions from wastewater: progress and prospects. *Crit Rev Biotechnol;* **25:**113–152.

Menard LD, Gao SP, Xu H, Twesten RD, Harper AS, Song Y, Wang G, Douglas AD, Yang JC, Frenkel AI, Nuzzo RG & Murray RW (2006). Sub-Nanometer Au Monolayer-Protected Clusters Exhibiting Molecule-like Electronic Behavior: Quantitative High-Angle Annular Dark-Field Scanning Transmission Electron Microscopy and Electrochemical Characterization of Clusters with Precise Atomic Stoichiometry. *J Phys Chem B;* **110:**12874-12883.

Mescher AL (2009). *Juenquira's* basic histology. 12th Ed. Columbus, OH: *McGraw-Hill Companies Inc;* 480.

Meyers MA, Mishra A & Benson DJ (2006). Mechanical properties of nanocrystalline materials. *Prog Mater Sci*; **51:**427–556.

Mitsudome T & Kaneda K (2013). Gold nanoparticle catalysts for selective hydrogenations. *Green Chem;* **15:**2636-2654.

Mittal AK, Chisti YY & Banerjee UC (2013). Synthesis of metallic nanoparticles using plant extracts. *Biotechnol Adv;* **31:**346–356.

Mlambo M, Mdluli PS, Shumbula P, Mpelane S, Moloto N, Skepu A & Tshikhudo R (2013). Synthesis and characterization of mixed monolayer protected gold nanorods and their Raman activities. *Mat Res Bull;* **48:**4181–4185.

Mmola M, Roes-Hill ML, Kim Durrell K, Bolton JJ, Sibuyi N, Meyer ME, Beukes DR & Antunes E (2016). Enhanced Antimicrobial and Anticancer Activity of Silver and Gold Nanoparticles Synthesised Using *Sargassum incisifolium* Aqueous Extracts. *Molecules;* 1-22. doi:10.3390/molecules21121633

Mtolera MSP & Semesi AK (1996). Antimicrobial Activity of Extracts from Six GreenAlgae from Tanzania. *Curr. Trends Marin Bot. East Afr. Region;* 211-217.

Mocellin S & Nitti D (2008). TNF and cancer: the two sides of the coin. *Front Biosci;* **13:**2774–2783.

Moghaddam AB, Namvar F, Moniri M, Tahir P, Azizi & Mohamad R (2015). Nanoparticles Biosynthesized by Fungi and Yeast: A Review of Their Preparation, Properties, and Medical Applications. *Molecules*; **20**:16540-16565.

Mohomed K (2016). Thermogravimetric analysis (TGA) Theory and Applications. www.tainstruments.com/wp-content/uploads/CA-2016-TGA.pdf.

Moulder JF, Stickle WF, Sobol PE & Bomben KD (1992). Handbook of X-ray Photoelectron Spectroscopy. *PerkinElmer Corporation, Physical Electronics Division*. United States of America.

Mukherjee P, Senapati S, Mandal D, Ahmad A, Khan MI, Kumar R & Sastry M (2002). Extracellular synthesis of gold nanoparticles by the fungus *Fusarium oxysporum*. *Chem. Bio. Chem*; **3**:461–463.

Mulvaney P (1996). Surface Plasmon Spectroscopy of Nanosized Metal Particles. *Langmuir;* **12(3):**788–800.

Murphy CJ & Jana NR (2002). Controlling the Aspect Ratio of Inorganic Nanorods and Nanowires. *Adv. Mater;* **14:**80-82.

Murphy CJ, Sau TK, Gole AM, Orendorff CJ, Gao J, Gou L, Hunyadi SE & Li T (2005). Anisotropic Metal Nanoparticles: Synthesis, Assembly, and Optical Applications. *J Phys Chem B*; **109:**13857-13870.

Muse JO, Carducci CN, Stripeikis JD, Tudino MB, Ferna´ndez FM (2005). A link between lead and cadmium kinetic speciation in seawater and accumulation by the green alga *Ulva lactuca*. *Environ Pollut;* **141:**126-130

Mutter J, Naumann J, Schneider R, Walach H & Haley B (2005). Mercury and autism: Accelerating Evidence? *Neuroendocrinol Lett;* **26(5):**439–446.

Nakanishi K, Nishijima M, Nishimura M, Kuwano K & Saga N (1996). Bacteria that induce morphogenesis in *Ulva pertusa* (chlorophyta) grown under axenic conditions. *J. Phycol;* **32:**479-482.

Nanowerk (2014). Centre for Green Nanotechnology launched in South Africa. http://www.nanowerk.com/nanotechnology-news/newsid=36651.php

Narayanan K & Sakthivel N (2008). *Coriander* leaf mediated biosynthesis of gold nanoparticles. *Mater Lett;* **62:**4588–4590.

Navarro JRG, Frédéric L, Cepraga C, Micouin G, Favier A, Chateau D, Charreyre M, Lanoë P, Monnereau C, Chaputa F, Marotte S, Leverrier Y, Marvel J, Kamada K, Andraud C, Baldeck PL & Parola S (2013). Nanocarriers with ultrahigh chromophore loading for fluorescence bio-imaging and photodynamic therapy. *Biomaterials;* **34:**8344–8351.

Neori A, Chopin T, Troell M, Buschmann AH, Kraemer GP, Halling C, Shpigel M & Yarishet C (2004). Integrated aquaculture: rationale, evolution and state of the art emphasizing seaweed biofiltration in modem mariculture. *Aquaculture* **231:**361–391.

Nikolaisen L, Jensen PD, Bech KS, Dahl J, Busk J, Brødsgaard T, Rasmussen MB, Bruhn A, Bjerre A , Bangsøe Nielsen HB, Albert KR, Ambus P, Kadar Z, Heiske S, Sander B & Schmidt ER (2011). Energy Production from Marine Biomass (*Ulva lactuca*). PSO Project No. 2008-1-0050. *Danish Technological Institute,* Denmark.

Nikoobakht B & El-Sayed MA (2003). Preparation and Growth Mechanism of Gold Nanorods (NRs) Using Seed-Mediated Growth Method. *Chem Mater*; **15:**1957-1962.

Njagi EC, Huang H, Stafford L, Genuino H, Galindo HM & Collins JB (2011). Biosynthesis of iron and silver nanoparticles at room temperature using aqueous *sorghum bran* extracts. *Langmuir;* **27:**264–271.

Noruzi M, Zare D, Khoshnevisan K & Davoodi D (2011): Rapid green synthesis of gold nanoparticles using *Rosa* hybrid petal extract at room temperature. *Spectrochimica Acta Part A*; **79(5)**:1461–1465.

Ojea-Jiménez I, Bastús NG & Puntes V (2011). Influence of the sequence of the reagents addition in the citrate-mediated synthesis of gold nanoparticles. *J Phys Chem C;* **115:**15752–15757.

Orbaek A & Barron AR (2014). ICP-AES analysis of nanoparticles. (http://www.oercommons.org/courses/icp-aes-analysis-of-nanoparticles/view).

Ortiz J, Romero N, Robert P, Araya J, Lopez-Hernandez J, Bozzo C, **Navarrete E, Osorio A & Rios A** (2006). Dietary fiber, amino acid, fatty acid and tocopherol contents of the edible seaweeds *Ulva lactuca* and *Durvillaea antarctica*. *Food Chem;* **99:**98–104.

Oumaskour K, Boujaber N, Etahiri S & Assobhei O (2012). Screening of antibacterial and antifungal activities in green and brown algae from the coast of Sidi Bouzid (El Jadida, Morocco). *Afr J Biotechnol;* **11:**16831-16837.

Pacheco S, Medina M, Valencia F & Tapia J (2006). Removal of Inorganic Mercury from Polluted Water Using Structured Nanoparticles. *J. Environ. Eng;* **132(3):**342-349.

Pal S, Tak YK & Song JM (2007). Does the antibacterial activity of silver nanoparticles depend on the shape of the nanoparticle? A study of the gram-negative bacterium *Escherichia coli*. *Appl. Environ. Microbiol;* **73(6):**1712–1720.

Panigrahi S, Basu S, Praharaj S, Pande S, Jana S, Pal A, Ghosh SK & Pal T (2007). Synthesis and size-selective catalysis by supported gold nanoparticles—study of heterogeneous and homogeneous catalytic process. *J Phys Chem C;* **111:**4596–4605.

Parial D, Patra HK, Dasgupta AK & Pal R (2012) Screening of different algae for green synthesis of gold nanoparticles. *Eur. J. Phycol;* **47(1)**:22–29.

Parida UK, Bindhani BK & Nayak P (2011). Green synthesis and characterization of gold nanoparticles using onion (*Allium cepa*) extract. *World J Nano Sci Eng*; **1:**93– 98.

Park JW, Benz CC & Martin FJ (2004). Future directions of liposome-and immunoliposome-based cancer therapeutics. *Semin Oncol;* **31:**196–205.

Park JH, Lim YT, Park OO, Kim JK, Yu J & Kim YC (2004b). Polymer/Gold Nanoparticle Nanocomposite Light-Emitting Diodes: Enhancement of Electroluminescence Stability and Quantum Efficiency of Blue-Light-Emitting Polymers. *Chem Mater;* **16(4):**688–692.

Parker HL, Rylott EL, Hunt AJ, Dodson JR, Taylor AF, Bruce NC & Clark JH (2014). Supported Palladium Nanoparticles Synthesized by Living Plants as a Catalyst for Suzuki-Miyaura Reactions. *PLOS One*; **9(1):** e87192 (6 pages).

Patri A, Dobrovolskaia M, Stern S, McNeil S & Amiji M (2006). Nanotechnology for cancer therapy. Preclinical characterization of engineered nanoparticles intended for cancer therapeutics. *CRC Press*: Boca Raton, FL; 105-138.

Patungwasa W & Hadak JH (2008). pH tunable morphology of the gold nanoparticles produced by citrate reduction. *Mater Chem Phys;* **108:**45–54.

Pedersen MF & Borum J (1996). Nutrient control of algal growth in estuarine waters. Nutrient limitation and the importance of nitrogen requirements and nitrogen storage among phytoplankton and species of macroalgae. *Mar. Ecol. Prog. Ser;* **142**:261–272.

Peng ZA & Peng XG (2002). Nearly Monodisperse and Shape-Controlled CdSe Nanocrystals via Alternative Routes: Nucleation and Growth. *J Am Chem Soc;* **124(13):**3343–3353.

Peng X, Manna L, Yang W, Wickham J, Scher E, Kadavanich A & Alivisatos AP (2000). Shape control of CdSe nanocrystals. *Nature*; **404(6773):**59-61.

Percebom AM, Giner-Casares JJ, Claes N, Bals S, Loh W, Luis M & Liz-Marza´n LM (2016). Janus gold nanoparticles obtained via spontaneous binary polymer shell segregation. *Chem Commun;* **52:**4278–4281.

Percival E & McDowell RH (1967). Chemistry and Enzymology of Marine Algal Polysaccharides; *Academic Press*: New York, NY, USA, 219.

Perevedentseva E, Cai PJ, Chiu YC & Cheng CL (2010). Characterizing protein activities on the lysozyme and nanodiamond complex prepared for bio applications. *Langmuir* **27:**1085–1091.

Perez J, Bax L & Escolano C (2005). Roadmap Report on Nanoparticles*; Willems & Van Den Wildenberg*: Barcelona, Spain.

Peto G, Molnar GL, Pasxti Z, Geszti O, Beck A & Guczi L (2002). Electronic structure of gold nanoparticles deposited on SiOx/Si (100). *Mater Sci Eng C;* **19:**95–99.

Philip D (2010). Rapid green synthesis of spherical gold nanoparticles using *Mangifera indica* leaf. *Spectrochim Acta A Mol Biomol Spectrosc;* **77:**807–810.

Philip D, Unni C, Aromal SA & Vidhu VK (2011). *Murraya Koenigii* leaf assisted rapid green synthesis of silver and gold nanoparticles. *Spectrochim Acta A Mol Biomol Spectrosc;* **78:**899–904.

Pollini M, Paladini F, Catalno M, Taurino A, Licciulli A, Maffezzoli A & Sannio A (2011). Antibacterial coatings on haemodialysis catheters by photochemical deposition of silver nanoparticles. *J. Mater. Sci. Mater. Med;* **22:**2005–2012.

Pons T, Uyeda HT, Medintz IL & Mattoussi H (2006). Hydrodynamic dimensions, electrophoretic mobility, and stability of hydrophilic quantum dots. *J Phys Chem B*; **110:**20308–20316.

Ponnuchamy K & Jacob AJ (2016). Metal nanoparticles from marine seaweeds – A Review. *Nanotechnology Reviews.* ISSN (Online) 2191-9097, DOI: 10.1515/ntrev-2016-0010 ISSN (Print): 2191-9089.

Pradhan N, Pal A & Pal T (2001). Catalytic Reduction of Aromatic Nitro Compounds by Coinage Metal Nanoparticles. *Langmuir*; **17:**1800–1802.

Pradhan N, Pal A & Pal T (2002). Silver nanoparticle catalyzed reduction of aromatic nitro compounds. *Colloids Surf A;* **196:**247– 257.

Praharaj S, Nath S, Ghosh SK, Kundu S & Pal T (2004). Immobilization and Recovery of Au Nanoparticles from Anion Exchange Resin: Resin-Bound Nanoparticle Matrix as a Catalyst for the Reduction of 4-Nitrophenol. *Langmuir;* **20**:9889-9892.

Prasad KS, Patel H, Patel T, Patel K & Selvaraj K (2012). Biosynthesis of Se nanoparticles and its effect on UV-induced DNA damage. *Colloids Surf B Biointerf;* **103:**261–266.

Prasad BSN & Padmesh TVN (2014). Seaweed (*Sargassum ilicifolium*) assisted green synthesis of palladium nanoparticles. *IJSER;* **5(3):**2229-5518.

Pimprikar PS, Joshi SS, Kumar AR, Zinjarde SS & Kulkarni SK (2009). Influence of biomass and gold salt concentration on nanoparticle synthesis by the tropical marine yeast *Yarrowia lipolytica* NCIM 3589. *Colloids Surf B Biointerf;* **74:**309–16.

Priyadharshini RI, Prasannaraj G, Geetha N & Venkatachalam P (2014). Microwave-Mediated Extracellular Synthesis of Metallic Silver and Zinc Oxide Nanoparticles Using Macro-Algae (*Gracilaria edulis*) Extracts and Its Anticancer Activity Against Human PC3 Cell Lines. *Biotechnol. Appl. Biochem*; **174**:2777–2790.

Provasoli L & Pintner IJ (1980). Bacteria induced polymorphism in axenic laboratory strain of *Ulva lactuca* (Chlorophyceae). *J. Phycol;* **16:**196-201.

Puntes VF, Krishnan KM & Alivisatos AP (2001). Colloidal Nanocrystal Shape and Size Control: The Case of Cobalt. *Science;* **291:**2115-2117.

Puvanakrishnan P, Park J, Chatterjee D, Krishnan S & Tunnel JW (2012). In vivo tumor targeting of gold nanoparticles: Effect of particle type and dosing strategy. *Int j nanomed.;* **7:**1251–1258.

Qian H, Pretzer LA, Velazquez JC, Zhao Z & Wong MS (2013). Gold nanoparticles for cleaning contaminated water. *J Chem Technol Biotechnol;* **88(5):**735-741.

Quan X, Peng CW, Dong J & Zhou J (2016). Structural properties of polymer-brush-grafted gold nanoparticles at the oil–water interface: insights from coarse-grained simulations. *Soft Matter;* **12:**3352–3359.

Quites FJ, Azevedo CKS, Alves EPP, Germino JC, Vinhas RCG, Richard Landers R, Terezoa AJ & Atvars TDZ (2017). Ag Nanoparticles-Based Zinc Hydroxide-Layered Hybrids as Novel and Efficient Catalysts for Reduction of 4-Nitrophenol to 4-Aminophenol. *J. Braz. Chem. Soc;* **28(01):** 106-115. http://dx.doi.org/10.5935/0103-5053.20160152.

Raghunandan D, Basavaraja S, Mahesh B, Balaji S, Manjunath SY & Venkataraman A (2009). Biosynthesis of stable polyshaped gold nanoparticles from microwave-exposed aqueous extracellular anti-malignant guava (*Psidium guajava*) leaf extract. *Nano Biotechnol;* **1(4):**34–41.

Rajathi AA, F, Parthiban C, Kumar GV & Anantharaman P (2012) Biosynthesis of antibacterial gold nanoparticles using brown alga, *Stoechospermum Marginatum* (Kutzing). *Spectrochim Acta A Mol Biomol Spectrosc*; **99:**166–173.

Rajasulochana P, Dhamotharan R, Krishnamoorthy P & Murugesan S (2009). Antibacterial activity of the extracts of marine red and brown algae. Marsland Press. *J Am Sci;* **5(3):**20-25.

Rajesh S, Raja DP, Rathi J & Sahayaraj K (2012). Biosynthesis of silver nanoparticles using *Ulva fasciata* (Delile) ethyl acetate extract and its activity against *Xanthomonas campestris* pv. *malvacearum*. *J. Biopestic;* **5:**119–128.

Rajeshkumar S, Malarkodi C, Gnanajobitha G, Paulkumar K, Mahendran Vanaja M, Kannan C & Annadurai G (2013). Seaweed-mediated synthesis of gold nanoparticles using *Turbinaria conoides* and its characterization. *J Nanostruct Chem*; **3**:1-7.

Ramakrishna M, Babu DR, Gengan RM, Chandra S, Rao GN (2015). Green synthesis of gold nanoparticles using marine algae and evaluation of their catalytic activity**.** *J Nanostruct Chem;* DOI 10.1007/s40097-015-0173-y.

Rana D, Jamwal D, Katoch A, Thakur P & Kalia S (2016). Eicosyl ammoniums elicited thermal reduction alleyway towards gold nanoparticles and their chemo-sensor aptitude. *Analyst;* **141:**2208–2217.

Rauwel P, Küünal S, Ferdov S & Rauwel E (2015). A review on the green synthesis of silver nanoparticles and their morphologies studied via TEM. *Adv Mater Sci Eng;* 682749: 9.

Raven PH, Evert RF & Eichhorn SE (2005). Biology of Plants, Seventh edition. New York, *W.H. Freeman and Company;* 231.

Reetz MT & Helbig W (1994). Size-selective synthesis of nanostructured transition metal clusters. *J Am Chem Soc;* **116:**7401–7402.

Reetz MT, Helbig W, Quaiser SA, Stimming U, Breuer N & Vogel R (1995). Visualization of surfactants on nanostructured palladium clusters by a combination of STM and high resolution TEM. *Science;* **267:**367–369.

Rizhi C, Yan D, Weihong X & Nanping X (2007). Effect of alumina particle size on Ni/A12O3 catalysts for p-nitrophenol hydrogenation. *Chin. J. Chem. Eng;* **15:**884–888.

Robertson-Andersson DV (2007). Biological and economical feasibility studies of using seaweeds *Ulva lactuca* (chlorophyta) in recirculation systems in abalone farming. PhD Dissertation, University of Cape Town, South Africa.

Robertson-Andersson DV, Potgieter M, Hansen J, Bolton JJ, Troell M, Anderson RJ, Halling C, Probyn T (2008). Integrated seaweed cultivation on an abalone farm in South Africa. *J Appl Phycol;* **20:**579–595.

Robertson-Andersson DV, Wilson DT, Bolton JJ, Anderson RJ & Maneveldt GW (2009). Rapid assessment of tissue nitrogen in cultivated *Gracilaria gracilis* (Rhodophyta) and *Ulva lactuca* (Chlorophyta). *Afr J Aquatic Sci;* **34(2):**169-172.

Robic A, Bertrand D, Sassi JF, Lerat Y & Lahaye M (2009). Determination of the chemical composition of ulvan, a cell wall polysaccharide from *Ulva* spp. (Ulvales, Chlorophyta) by FTIR and chemometrics. *J Appl Phycol;* **21:**451–456.

Rode CV, Vaidya MJ & Chaudhari RV (1999). Synthesis of p-Aminophenol by Catalytic Hydrogenation of Nitrobenzene. *Org. Process Res. Dev;* **3:**465−470.

Rodriguez-Sanchez L, Blanco MC & Lopez-Quintela MA (2002). Electrochemical synthesis of silver nanoparticles. *J Phys Chem B;* **104:**9683–9688.

Romero CE, Li Y, Bilirgen H, Sarunac N & Levy EK (2006). Modification of boiler operating conditions for mercury emissions reductions in coal-fired utility boilers. *Fuel;* **85:**204–212.

Rosenauer A, Krause FF, Müller K, Schowalter M & Mehrtens (2014). Conventional Transmission Electron Microscopy Imaging beyond the Diffraction and Information Limits. *Phys Rev Lett;* **113:**96-101.

Ruska E & Knoll M (1931)**.** Die magnetische Sammelspule für schnelle Elektronenstrahlen (The magnetic collection coil for fast electron beams). *Z. Tech. Phys.* **12:**389-448.

Saha S, Subrata A, Kundu S, Basu S & Pal T (2009). Photochemical Green Synthesis of Calcium-Alginate-Stabilized Ag and Au Nanoparticles and Their Catalytic Application to 4-Nitrophenol Reduction. *Langmuir;* **26(4):**2885–2893.

Sangeetha N & Saravanan K (2014). Biogenic Silver Nanoparticles using Marine Seaweed (*Ulva lactuca*) and Evaluation of its Antibacterial activity. *J Nanosci. Nanotechnol*; **2**:2279–0381.

Sapsford KE, Tyner KM, Dair BJ, Deschamps JR & Medintz IL (2011). Analyzing nanomaterial bioconjugates: a review of current and emerging purification and characterization techniques. *Anal Chem;* **83:**4453–4488.

Saritha K, Mani AE, Priyalaxmi M & Patterson J (2013). Antibacterial Activity and Biochemical Constituents of Seaweed *Ulva lactuca. GJ Pharmacol*; **7(3):**276-282.

Sastry M, Ahmad A, Khan MI & Kumar R (2003). Biosynthesis of metal nanoparticles using fungi and actinomycete. *Curr Sci*; **85:**162–170**.**

Saxena A, Tripathi RM, Zafar F & Singh P (2010).) Joint Committee on Powder Diffraction Standards. Diffraction Data File: JCPDS (File No. 04–0783). *International Center for Diffraction Data.* Swarthmore PA.

Schaaff TG, Shafigullin MN, Khoury JT, Vezmar I, Whetten RL, Cullen WG, First PN, Gutierrez-Wing C, Ascensio J & Jose-Yacaman MJ (1997). Isolation of Smaller Nanocrystal Au Molecules: Robust Quantum Effects in Optical Spectra. *J Phys Chem B;* **101:**7885-7891.

Scheuer PJ (1990). Some marine ecological phenomena: chemical basis and biomedical potential. *Science;* **248:**173-177.

Seah MP, Gilmore IS & Beamson G (1998). XPS: Binding Energy Calibration of Electron Spectrometers 5ÈRe-evaluation of the Reference Energies. *Surf Interface Anal*; **26:**642-649.

Senapati S, Syed A, Moeez S, Kumar A & Ahmad A (2012). Intracellular synthesis of gold nanoparticles using alga *Tetraselmis kochinensis*. *Mater Lett;* **79:**116–118.

Sepeur S (2008). Nanotechnology: Technical Basics and Applications. *Vincentz Network GmbH & Co KG*, Hannover.

Shah M, Fawcett D, Sharma S , Tripathy SK & Poinern GEJ (2015). Green Synthesis of Metallic Nanoparticles via Biological Entities. *Materials*; **8:**278–7308.

Shang L, Wang Y, Jiang J & Dong S (2007). pH-Dependent protein conformational changes in albumin: gold nanoparticle bioconjugates: a spectroscopic study. *Langmuir;* **23:**2714–2721.

Shankar SS, Rai A, Ahmad A & Sastry M (2004). Rapid synthesis of Au, Ag, and bimetallic Au core – Ag shell nanoparticles using Neem (*Azadirachta indica*) leaf broth. *J Colloid Interface Sci;* **275:**496–502.

Shankar SS, Rai A, Ankamwar B, Singh A, Ahmad A & Sastry M (2004b). Biological synthesis of triangular gold nanoprisms. *Nat Mater;* **3:**482–488.

Shahverdi AR, Shakibaie M & Nazari P (2011). Basic and Practical Procedures for Microbial Synthesis of NanoparticlesMetal Nanoparticles in Microbiology. Berlin Heidelberg; 177–195.

Sharma BK (2000). Instrumental Methods of Chemical Analysis. *Krishna Prakashan Media*, Meerut, India, 514.

Sharma NC, Sahi SV, Nath S, Parsons JG, Gardea-Torresdey JL & Pal T (2007). Synthesis of Plant-Mediated Gold Nanoparticles and Catalytic Role of Biomatrix-Embedded Nanomaterials. *Environ. Sci. Technol;* **41**:5137-5142.

Sharma A, Sharma S, Sharma K, Chetri SPK, Vashishtha A, Singh P, Kumar R, Rathi B & Agrawal R (2016). Algae as crucial organisms in advancing nanotechnology: a systematic review. *J Appl Phycol;* **28:**1759–1774.

Sheeba JM & Thambidurai S (2009). Extraction, characterization, and application of seaweed nanoparticles on cotton fabrics. *J. Appl. Polym. Sci;* **113(4):**2287–2292.

Shem PM, Sardar R & Shumaker-Parry JS (2009). One-step synthesis of phosphine-stabilized gold nanoparticles using the mild reducing agent 9-BBN. *Langmuir;* **25:**13279-13283.

Shenhar R & Rotello VM (2003). Nanoparticles: Scaffolds and Building Blocks. *Acc. Chem. Res;* **36(7):**549–561.

Shetty G, Kedall C, Shepherd N, Stone N & Barr H (2006). Raman spectroscopy: elucidation of biochemical changes in carcinogenesis of oesophagus. *Brit. J. Cancer;* **94:**1460-1464.

Shiny PJ, Mukherjee A & Chandrasekaran N (2014). Haemocompatibility assessment of synthesised platinum nanoparticles and its implication in biology. *Bioprocess Biosyst Eng;* **37(6)**:991-997.

Shirley DA (1972). High-Resolution X-ray Photoemission Spectrum of the Valence Bands of Gold. *Phys. Rev. B;* **5:**4709- 4714.

Siddhanta AK, Mody KH, Ramavat BK, Chauhan VD, Garg HS, Goel AK, Doss MJ, Srivastava MN, Patnaik GK & Kamboj VP (1997). Bioactivity of marine organisms: Part VIII-Screening of some marine flora of western coast of India. *Indian J. Exp. Biol;* **35:**638-643.

Simenyuk GY, Zakharov YA, Pavelko NV, Dodonov VG, Pugachev VM, Puzynin AV, Manina TS, Barnakov CN & Ismagilov ZR (2015). Highly porous carbon materials filled with gold and manganese oxide nanoparticles for electrochemical use. *Catal Today;* **249:**220–227.

Singaravelu G, Arockiamaryc JS, Kumarb VG & Govindaraju K (2007). A novel extracellular synthesis of monodisperse gold nanoparticles using marine alga, *Sargassum wightii* Greville. *Colloids Surf B Biointerf*; **57**:97–101.

Singh M, Kalaivani R, Manikandan S, Sangeetha N & Kumaraguru AK (2013). Facile green synthesis of variable metallic gold nanoparticle using *Padina gymnospora*, a brown marine macroalga. *Appl. Nanosci.;* **3(2)**:145–151.

Skakle J (2005). Application of X-ray powder diffraction in Material Chemistry. *Chem. Soc*; **5:**252-262.

Skoog DA, Holler FJ & Crouch SR (2007). Principles of Instrumental Analysis. Sixth Edition, *Thomson Brooks*, USA.

Smit AJ (1997) Optimising *Gracilaria verrucosa* production in a laboratory based culture system. MSc Dissertation, University of Port Elizabeth, Port Elizabeth, South Africa.

Smitha SL, Philip D & Gopchandran KG (2009). Green synthesis of gold nanoparticles using *Cinnamomum zeylanicum* leaf broth. *Spectrochim Acta A Mol Biomol Spectrosc*; **74:**735–739.

Smoluchowski V (1917). Versuch einer mathematischen Theorie der Koagulationskinetik kolloider Lo¨sungen. Z *Phys Chem;* **XCII:** 129-168.

Sobol M (2010). Comparasion methods of high-pressure freezing and automated freeze-substitution of suspension cells combined with LR-White embedding. *Histochem Cell Bio;* **134(6):**631-641.

Soisuwan S, Warisnoicharoen W, Lirdprapamongkol K & Svasti J (2010). Eco-friendly synthesis of fucoidan-stabilized gold nanoparticles. *Am. J. Appl. Sci.*, **7(8):**1038–1048.

Song YZ, Li X, Song Y, Cheng ZP, Zhong H, Xu JM, Lu JS, Wei CG, Zhu AF, Wu FY & Xu J (2013). Electrochemical synthesis of gold nanoparticles on the surface of multi-walled carbon nanotubes with glassy carbon electrode and their application. *Russ J Phys Chem A;* **87:** 74–79.

Sridhar S & Rengasamy R (2012). The effects of Seaweed Liquid Fertilizer of *Ulva lactuca* on Capsicum annum. *Algol Stud;* **138:**75–88.

Stanglmair C, Scheeler SP & Pacholski C (2014). Seeding Growth Approach to Gold Nanoparticles with Diameters Ranging from 10 to 80 Nanometers in Organic Solvent. *Eur J Inorg Chem;* **2014(23):**3633–3637.

Strasser P, Koh S, Anniyev T, Greeley J, More K, Yu C, Liu Z, Kaya S, Nordlund D, Ogasawara H, Toney MF & Nilsson A (2010). Lattice-strain control of the activity in dealloyed core–shell fuel cell catalysts. *Nat Chem;* **2:**454–460.

Steyn PP (2000). A comparative study of the production and suitability of two *Ulva* species as abalone fodder in a commercial mariculture system. M. Sc. Dissertation. University of Port Elizabeth, South Africa.

Sujitha MV & Kannan S (2013). Green synthesis of gold nanoparticles using Citrus fruits *Citrus limon, Citrus reticulata and Citrus sinensis* aqueous extract and its characterization. *Spectrochim Acta A Mol Biomol Spectrosc*; **102:**15–23.

Swinehart DF (1962). The Beer-Lambert Law. *J Chem Educ;* **39(7):**333-335.

Sykora D, Kasicka V, Miksik I, Rezanka P, Zaruba K, Matejka P & Kral V (2010). Applications of gold nanoparticles in separation sciences. *J. Sep. Sci;* **30:**372–387.

Tamuly C, Hazarika M, Borah SCh, Das MR & Boruah MP (2013). In situ biosynthesis of Ag, Au and bimetallic nanoparticles using *Piper pedicellatum* C.D.C., green chemistry approach. *Colloids Surf B Biointerf*; **1:**627–634.

Taskin E, Ozturk M, Taskin E & Kurt O (2007). Antibacterial activities of some marine algae from the Aegean Sea (Turkey). *Afr J Biotechnol;* **6(24):**2746-2751.

Thakkar KN, Mhatre SS & Parikh RY (2010). Biological synthesis of metallic nanoparticles. *Nanomed. Nanotechnol. Biol. Med*; **6:**257–262.

Thorek DL, Chen AK, Czupryna J & Tsourkas A (2006). Superparamagnetic iron oxide nanoparticle probes for molecular imaging. *Ann Biomed Eng;* **34:**23–38.

Tian L, Tadepalli S Fei M, Morrissey JJ, Kharasch ED & Singamaneni S (2015). Off-Resonant Gold Superstructures as Ultrabright Minimally Invasive Surface-Enhanced Raman Scattering (SERS) Probes. *Chem Mater;* **27:**5678−5684.

Tikhonov NA, Arkhangelsky IV, Belyaev SS & Matveev AT (2009). Carbonization of polymeric nonwoven materials. *Thermochimica Acta;* **486:**66–70.

Tobwala S, Fan W, Hines CJ, Folk WR & Ercal N (2014). Antioxidant potential of *Sutherlandia frutescens* and its protective effects against oxidative stress in various cell cultures. *BMC Complement Altern Med*; **14:**271.

Tong L, Zhao Y, Huff TB, Hansen MN, Wei A & Cheng JX (2007). Gold nanorods mediate tumor cell death by compromising membrane integrity. *Adv Mater*; **19:**3136–3141.

Torres-Chavolla E, Ranasinghe RJ & Alocilja EC (2010). Characterization and functionalization of biogenic gold nanoparticles for biosensing enhancement. *IEEE Trans. Nanobiotechnol;* **9**:533–538.

Treguer M, Cointet C, Remita H, Khatouri J, Mostafavi M, Amblard J & Belloni J (1998). Dose rate effects on radiolytic synthesis of gold– silver bimetallic clusters in solution. *J Phys Chem B*; **102:**4310–432.

Troell M, Rönnback P, Halling C, Kautsky N & Buschmann A (1999). Ecological engineering in aquaculture: use of seaweeds for removing nutrients from intensive mariculture. *J Appl Phycol;* **11:**89–97.

Troell M, Halling C, Neori A, Chopin T, Buschmann AH, Kautsky N, Yarish C (2003). Integrated mariculture: asking the right questions. *Aquaculture;* **226:**69–90.

Troell M, Robertson-Andersson D, Anderson RJ, Bolton JJ, Maneveldt G, Hallinge C & Probyn T (2006). Abalone farming in South Africa: an overview with perspectives on kelp resources, abalone feed, potential for on-farm seaweed production and socio-economic importance. *Aquacualture;* **257:**266-281.

Trono Jr GC (1999). Diversity of the seaweed flora of the Philippines and its utilization. *Hydrobiologia;* **398(399):**1-6.

Tsagkamilis P, Danilidis D, Dring MJ & Katsaros C (2010). Removal of phosphate by the green seaweed Ulva lactuca in a small-scale sewage treatment plant (Ios Island, Aegean Sea, Greece). *J Appl Phycol;* 22, 331–339.

Turkevich J, Stevenson PC & Hillier J (1951). Nucleation and growth process in the synthesis of colloidal gold. *Discuss Faraday Soc;* **11:**55–75.

Vaidya MJ, Kulkarni SM & Chaudhari RV (2003). "Synthesis of p-aminophenol by catalytic hydrogenation of p-nitrophenol". *Org. Process Res. Dev;* **7:**202–208.

van Horssen R, Ten Hagen TL & Eggermont AM (2006). TNF-alpha in cancer treatment: molecular insights, antitumor effects, and clinical utility. *Oncol;* **11:**397–408.

Veith GM, Lupini AR, Pennycook SJ, Ownby GW & Dudney NJ (2005). Nanoparticles of gold on γ -Al_2O_3 produced by dc magnetron sputtering. *J. Cat;* **231:**151–158.

Vijayan SR, Santhiyagu P, Singamuthu M, Ahila NK, Jayaraman R & Ethiraj K (2014). Synthesis and characterization of silver and gold nanoparticles using aqueous extract of seaweed, *Turbinaria conoides*, and their antimicrofouling activity. *Scientific World J;* Article ID 938272, 10 pages; http://dx.doi.org/10.1155/2014/938272.

Vijayaraghavana K, Mahadevana A, Sathishkumar M, Pavagadhi S & Balasubramanianan R (2011). Biosynthesis of Au(0) from Au(III) via biosorption and bioreduction using brown marine alga *Turbinaria conoides*. *Chem Eng J;* **167:**223–227.

Vinod VTP, Saravanan P, Sreedhar B, Devi DK & Sashidhar RB (2011). A facile synthesis and characterization of Ag, Au and Pt nanoparticles using a natural hydrocolloid gum kondagogu (*Cochlospermum gossypium*). *Colloids Surf B Biointerf;* **83:**291–298.

Visaria RK, Griffin RJ, Williams BW, Ebbini ES, Paciotti GF, Song CW & Bischof JC (2006). *Enhancement* of tumor thermal therapy using gold nanoparticle-assisted tumor necrosis factor-alpha delivery. *Mol Cancer Ther;* **5:**1014–1020.

Visaria R, Bischof JC, Loren M, Williams B, Ebbini E, Paciotti G & Griffin R (2007). Nanotherapeutics for enhancing thermal therapy of cancer. *Int J Hyperthermia*; **23:**501–511.

Visha P, Nanjappan K, Selvaraj P, Jayachandran S, Elango A & Kumaresan G (2015). Biosynthesis and Structural Characteristics of Selenium Nanoparticles using Lactobacillus Acidophilus Bacteria by Wet Sterilization Process. *J. Adv. Vet. Anim. Res;* **4(1**):178-183.

Vivek M, Kumar PS, Steffi & Sudha S (2011) Biogenic silver nanoparticles by *Gelidiella acerosa* extract and their antifungal effects. *Avicenna J. Med. Biotechnol;* **3**(3):143–148.

Volkert AA, Subramaniam V & Haes AJ (2011). Implications of citrate concentration during the seeded growth synthesis of gold nanoparticles. *Chem Commun*; **47:**478–480.

Wald J (2010). Evaluatiestudie naar mogelijkheden voor grootschalige zeewierteelt in het zuidwestelijke Deltagebied, in het bijzonder de Oosterschelde. Final Thesis. Wageningen UR, Lelystad, the Netherlands.

Wang ZL (1998). Structural Analysis of Self-Assembling Nanocrystal Super lattices. *Advan Mater;* **10:**13-30.

Wang ZL (2000). Transmission Electron Microscopy of Shape-Controlled Nanocrystals and Their Assemblies. *J. Phys. Chem. B;* **104:**1153-1175.

Wang C & Yu C (2013). Detection of chemical pollutants in water using gold nanoparticles as sensors: a review. *Rev Anal Chem*; **32(1):**1–14.

Wei H & Lu Y (2012). Catalysis of gold nanoparticles within lysozyme single crystals. *Chem Asian J;* **7:**680–683**.**

West PR, Ishii S, Naik GV, Emani NK, Shalaev VM & Boltasseva A (2010). Searching for better plasmonic materials. *Laser Photonics Res;* **4:**795–808.

Winey M, Meehl JB, O'Toolea ET & Giddings TH Jr. (2013). Conventional transmission electron microscopy. *Mol Biol Cell;* **25:**319-323.

Xie J, Lee JY, Wang DI & Ting YP (2007). Silver nanoplates: from biological to biomimetic synthesis. *ACS Nano*; **1(5):**429–439.

Xie HN, Lin Y, Mazo M, Chiappini C, Sa´nchez-Iglesias A, Liz- Marza´n LM & Stevens MM (2014). Identification of intracellular gold nanoparticles using surface-enhanced Raman scattering. *Nanoscale;* **6:**12403–12407.

Xu X, Stevens M and Corte MB (2004). In situ precipitation of gold nanoparticles onto glass for potential architectural applications. *Chem Mater*; **16:**2259–2266.

Yaich H, Garna H, Besbes S , Paquot M, Blecker C, Attia H (2011). Chemical composition and functional properties of Ulva lactuca seaweed collected in Tunisia. *Food Chem*; **128**:895–901.

Yasantha A, Lee KW, Kim SK & Jeon YJ (2007). Anticoagulant activity of marine green and brown algae collected from Jeju Island in Korea. *Bioresource Technol*; **98:**1711-1716.

Yu J, Xu D, Guan HN, Wang C, Huang LK & Chi DF (2016). Facile one-step green synthesis of gold nanoparticles using *Citrus maxima* aqueous extracts and its catalytic activity. *Mater Lett*; **166:** 110–112.

Yunus IS, Harwin, Kurniawan A, Adityawarman D & Indarto A (2012). Nanotechnologies in water and air pollution treatment. *Enviro Technol Rev;* **1(1)**:136–148.

Zabetakis K, Ghann WE, Kumar S & Daniel M (2012). Effect of high gold salt concentrations on the size and polydispersity of gold nanoparticles prepared by an extended turkevich-frens method. *Gold Bull;* **45:**203–211.

Zhang H (2002). Transmission electron microscopy for the semiconductor industry. *Micron;* **33**:517-525**.**

Zhang G & Wang DY (2008). Fabrication of Heterogeneous Binary Arrays of Nanoparticles via Colloidal Lithography. *J. Am. Chem. Soc*. **130:**5616–5617.

Zhang Z & Wu Y (2010). Investigation of the $NaBH_4$ -induced aggregation of Au nanoparticles. *Langmuir;* **26:**9214–9223.

Zhang L, Feng Q, Wang J, Zhang S, Ding B, Wei Y, Dong M, Ryu J, Yoon T, Shi X, Sun J & Jiang X (2015). Microfluidic Synthesis of Hybrid Nanoparticles with Controlled Lipid Layers: Understanding Flexibility-Regulated Cell? Nanoparticle Interaction. *ACS Nano;* **9(10)**:9912–9921.

Zhang J, Li C, Zhang X, Huo S, Jin S, An FF, Wang X, Xue X, Okeke CI, Duan G, Guo F, Zhang X, Hao J, Wang PC, Zhang J & Liang XJ (2015). In vivo tumor-targeted dualmodal fluorescence/CT imaging using a nanoprobe coloaded with an aggregation-induced emission dye and gold nanoparticles. *Biomaterials;* **42**:103–111.

Zhao Y, Mann MD, Pavlish JH, Mibeck BF, Dunham GE & Olson ES (2006). Application of Gold Catalyst for Mercury Oxidation by Chlorine. *Environ*. *Sci. Technol;* **40(5):**1603–1608.

Zhao P, Li N & Astruc D (2013). State of the art in gold nanoparticle synthesis. *Coord Chem Rev;* **257:**638– 665.

Zhao G, Xin-Ping W, Chai R, Zhang Q, Gong X, Huang J & Yong L (2015). Tailoring nano-catalysts: turning gold nanoparticles on bulk metal oxides to inverse nano-metal oxides on large gold particles. *Chem Commun;* **51:**5975–5978.

Zhao P, Feng X, Huang D,Yang G & Astruc D (2015b). Basic concepts and recent advances in nitrophenol reduction by gold- and other transition metal nanoparticles. *Coord Chem Rev;* **287:**114–136.

Zharov VP, Mercer KE, Galitovskaya EN, Smeltzer MS (2006). Photothermal nanotherapeutics and nanodiagnostics for selective killing of bacteria targeted with gold nanoparticles. *Biophys J;* **90:**619–627

Zyuzin MV, Honold T, Carregal-Romero S, Kantner K, Karg M & Parak WJ (2016). Influence of temperature on the colloidal stability of polymer-coated gold nanoparticles in cell culture media. *Small;* **12:**1723–1731.